Accuracy-Speed Relationships of a Robotic Filament Winding Cell

by

Seng-Kum Chan

#484783

Thesis submitted to the School of Graduate Studies

in partial fulfilment of the requirements for the degree of

Master of Applied Science

in

Mechanical Engineering

Ottawa-Carleton Institute for

Mechanical and Aeronautical Engineering

University of Ottawa

Ottawa, Ontario

Canada

1994

ISBN 0-612-15596-X

UNIVERSITÉ D'OTTAWA
UNIVERSITY OF OTTAWA

Dedicated to my mother

Lee Oi Pan

Abstract

This thesis describes the background research and the development of a robot based filament winding cell. The cell was implemented using an industrial robot (ASEA IRB 6/2) and an in-house mandrel drive mechanism, both being coordinated by a personal computer. Filament winding is a process in which continuous fibres are placed on a rotating mandrel to cover the entire surface, under controlled tension forming a composite component. Traditionally, filament winding is carried out on multi-axis numerically controlled lathe-like machines. There are two major parts in this research. The first part deals with the cell control structure theory and the second deals with the experimental validation of the control structure. Communication protocols, user interface software, control hardware specifications and procedures are elaborated in detail. To simplify the experimental work, a highly automated robotic control software program was written. This program, reduces the complexities of operating the robot and ensure accurate repeatable results. The applications program was based upon on an expert system approach. The factors studied were the speed versus the accuracy, the accuracy of the payout eye position, the effects of the segment's length and winding speed used for the approximation of the fibre path. Validation of the control theory is tested experimentally using a simple cylindrical mandrel in various configurations and an asymmetrical S-mandrel.

Acknowledgements

I would like to express my gratitude to my supervisors, Dr. A. Fahim and Dr. M. Munro, for their guidance and assistance.

I am grateful to the National Science and Engineering Research Council and the University of Ottawa for their financial support.

Many people have contributed to making this research enjoyable. I would especially like to thank my father, brothers, and sisters for their support during my studies. Without naming them, I appreciate the friends in graduate studies, administration and the work shop staff of the Mechanical Engineering Department.

Table of Contents

List of Figures

List of Tables

Glossary

Aramid	- A generic name for a class of synthetic organic fibres called aromatic polyamide fibres.
AutoCAD	- Computer Aided Design (CAD) Software package from AutoDesk.
COM1	- The RS232 communication port 1 of the personal computer.
.DXF	- The data file format that the AutoCAD uses for storing the drawing information. It is used for transferring drawing information into other application programs.
Geodesic Path	- These are stable paths. When a fibre is placed between two points on a frictionless surface, the fibre will always shift to find the lowest energy or stable position depending on the geometry.
Half duplex	- Communication protocol denoting, the case where only one party of the communication link can transmit at one time.

Harmonic drive - A gear system, consists of three concentric parts: an inner elliptical wave generator, a flexspline, and an outer rigid circular spline. The teeth of the nonrigid flexspline and the rigid circular spline are in continuous engagement at the apogees of the ellipse, but are disengaged at the perigees, where they are misaligned by half a tooth. The flexspline has two less teeth than the circular spline. When the elliptical wave generator is turned through one revolution, the flexspline moves relative to the circular spline by a distance of two teeth.

Host Computer - The computer that initiated the transmission link.

Payout Eye - The location where the fibre exit from the winding machine on to the mandrel surface.

Poly-line - A line type in AutoCAD. The line width is adjustable and can be used with other segments to form a smooth curve.

Slave Computer - This denotes the computer that is currently receiving data or command information.

CHAPTER 1

INTRODUCTION

The first application of filament winding using steel wire was done in the middle ages to increase the burst strength of a cannon [1]. The earliest recorded use of a modern filament winding process was for the fibreglass rocket nozzle of the X248 solid rocket motor by Hercules, Inc. in 1948. In 1989, there were over 1000 filament winding machines located throughout the world [2]. The equipment varied from a modified lathe to a custom microprocessor controlled multi-axis system. During the same time there have been advances in the fibres and matrices that have been used in manufacturing of composite materials.

1.1: Composite Material

Many modern components require complex combination of properties, such as low density, high strength, high stiffness, corrosion and impact resistance. Composite materials represent a relatively low cost means of obtaining these properties which are virtually impossible to obtain in single phase materials.

Composites are multi-phase materials that have a combination of properties that are superior to each of the component phase. These materials are usually composed of two phases; the matrix, and the dispersed phase (Figure 1.1).

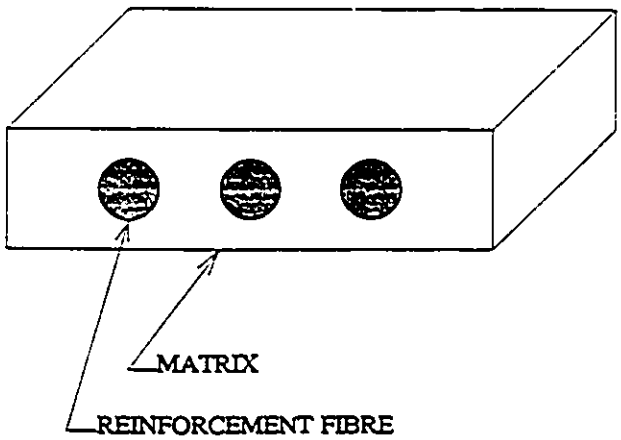

Figure 1.1: Fibre Reinforced Composite Material

The properties of the composite depends on the properties of the constituent phases, volume fractions, the shape and orientation of the dispersed phase [3].

There are three types of microscopic composites.

(1) Dispersion Strengthened

- the matrix phase has very fine particles with diameters between 0.01 and 0.1 μm. Particle volume fractions up to 15%.

(2) Particle Reinforced

- the particle size is larger (>1 μm in diameter) and particle

volume fraction is between 20-40%.

(3) Fibre Reinforced

- the microstructural shape has a large length to diameter ratio. Typical diameters are in 10-12 μm with fibre volume fractions up to 70% (for unidirectional fibre orientation).

The matrix is used for binding the fibres together, thus acting as the medium by which external loads are transferred and distributed to the fibres. It also helps to protect the fibres from abrasion and harsh environments. The matrix and the interface (between the fibre and the matrix) provide the main contributions to the toughness of the composite material. The most common types of polymeric matrices are polyester, epoxy, phenolic, silicon and nylon resins.

Since critical surface flaws are proportional to the fibre surface area, small diameter fibres are inherently stronger than bulk material. Fibres have high strength, low stiffness, low toughness and are brittle. Therefore, they are used for resisting the applied forces in the composite materials. Fibres are classified by their diameters:

(1) Whisker

These are very thin single crystals that have extremely large length to diameter ratios. They have superior strengths due to the high degree of crystalline perfection. Whiskers are difficult to manufacture and as a result very expensive. Common whiskers are graphite, silicon carbide, silicon nitride and aluminum.

(2) Fibre

Fibres have smaller length to diameter ratios than whiskers and typically include such materials as nylon, carbon or graphite, aramids, glass, boron, and aluminum oxide. They are used in pressure vessels, chemical storage tanks, and sports equipment.

(3) Wire

These fibres have a larger diameter to length ratios than fibres or whiskers. They are used to provide added strength in tires, rocket nozzles, and many pressure vessels. The wires are typically made from steel, molybdenum, and tungsten.

The strength of the composite depends on its ability to transmit loads from the matrix to the fibre. This depends on fibre length and the fibre-matrix interfacial bond. Increasing the fibre length will result in a higher reinforcement of the matrix. Short fibre reinforced composite materials are generally used in commercial applications requiring improved multi-directional properties. Continuous fibre reinforced composite materials are used in high strength and stiffness applications as found in the aerospace, military, and the sports equipment markets.

Fibre orientation also influences the strength of the composites. Continuous and aligned fibres give highly directional strength but poor transverse strengths. Short randomly oriented fibre composites have more uniform properties.

Some major advantages of modern composites are:

1) high strength.

2) high stiffness.

3) low weight.

4) low thermal expansion.

5) excellent chemical resistance.

This thesis will deal primarily with the manufacturing of composite materials, composed of continuous aligned fibres and formed using a winding technique.

1.2: Filament Winding

Filament winding is a process for placing continuous resin-impregnated reinforcing fibres on a rotating mandrel surface in a specified geometric pattern to achieve specific mechanical properties. A filament winding machine consists of fibre supply spools, fibre tensioner, resin impregnator, fibre delivery eye, and the mandrel drive unit (Figure 1.2). During the winding process the fibres are supplied from one or more spools. These fibres are impregnated with resin and dispersed throughout the delivery eye to the filament path on the rotating mandrel.

When the winding is completed, the matrix is cured generally in an oven. After curing, the mandrel is generally removed to leave the fibre reinforced composite shell. Filament winding is an economical, medium capital cost process that can be adapted to

fabricate a variety of shapes and size of components.

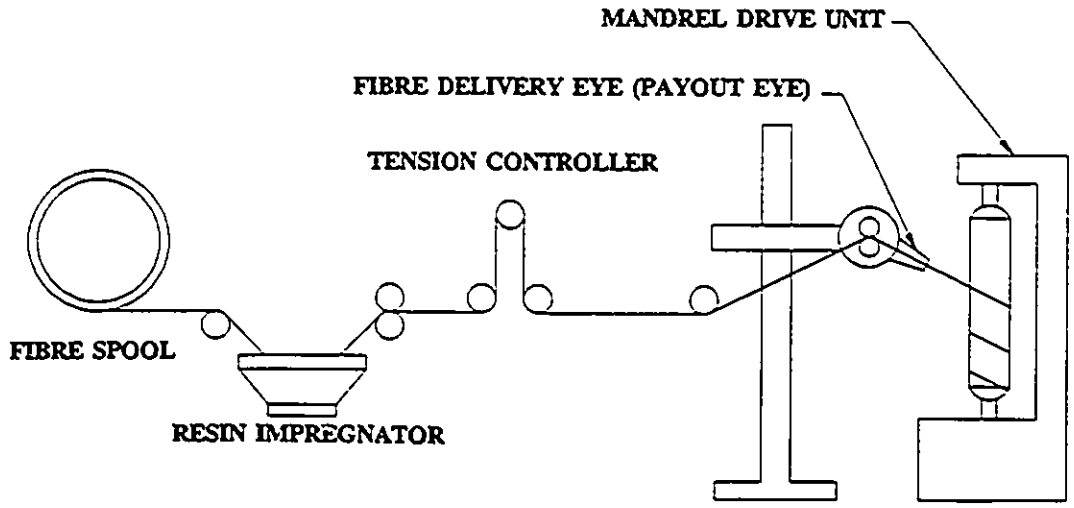

Figure 1.2: Filament Winding Machine

Traditionally, the winding machine was a modified lathe with the cutting tool replaced by a fibre delivery eye. As with lathes, mechanical gearing was used to position the fibre delivery eye. These machines produce simple geometry components such as pressure vessels, cylindrical tubes, and rocket motor casings.

As part shapes or winding patterns became more complex, the delivery eye positioning required higher degrees of flexibility. This characteristic was achieved by using flexible machines with many independent axes such as the computer numerically controlled machines or a robotic manipulator. These machines can produce complex shapes such as turbine blades, pipe tees, elbows, robotic arms, and sports equipment.

The process of winding has been simplified with the availability and advancements of economical computer technology. Parameters such as resin temperature, fibre tension, fibre breakage, etc. can be controlled using computers in real time. The computer has enabled alternative methods to "Teach-in" (where the filament delivery eye is guided through its motion by an operator) by off-line simulation or by programming of the machine's memory. Another benefit is that the same computer can be used for determining the fibre paths off-line necessary to cover the entire mandrel surface. These paths can be modified at any time by the designer to suit the product requirements. The strength and stiffness of the components can be readily analyzed by finite element programs after the simulation but before manufacture. This eliminates production waste and assures consistent component quality.

Manufacturers are now selecting machines that reduce overall production costs and that are multi-faceted. Using robots can help reduce the cost of production due to their flexibility, accuracy and repeatability. They can execute complex payout eye positions and be programmed through an external computer on or off-line. They can also perform other tasks such as loading/unloading of mandrels, drilling, trimming and painting of composite components.

1.3: Robots

In the early 1960's the first industrial robot was introduced by George Devol of Unimation Incorporated [4]. The principal goal was to build a machine that was flexible enough to do variety of tasks automatically and that could be easily reprogrammed. If the components or processes change, the robot could accommodate its new job without costly retooling.

A robot is a reprogrammable, multi-functional manipulator designed to move material, tools, parts, or specialized devices through variable programmed motions for the performance of a variety of tasks that are independent of direct human control [4]. Numerical controlled machines are not considered as robots because they lack sufficient versatility.

1.3.1: Elements of Robot

The four features of a robot are (a) mechanical structure, (b) actuators, (c) control system, and (d) tooling.

(1) Mechanical Structure

The mechanical structure consists of a central pedestal and appendages. Usually the base is stationary but often the base rides along a track or rail to facilitate relocation to a different work cell. The base can be mounted on the floor or on the ceiling of the

shop. A ceiling mounted robot is called a gantry robot.

The robot arms are made from mechanical links connected with prismatic or revolute joints (Figure 1.3).

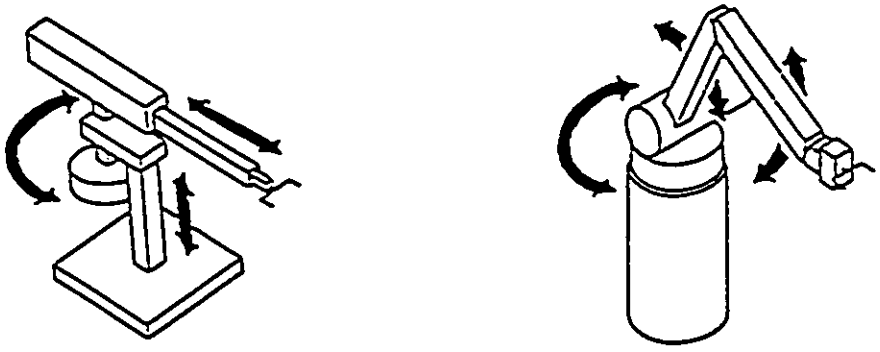

Prismatic Joint **Revolute Joint**

Figure 1.3: Typical Robot Joints [5]

As many as six degrees of freedom (six independent ways to position) maybe required to orient the end effector to any point in the robot working volume. The first three degrees of freedom are required for positioning the end effectors to a given location. The remaining degrees of freedom are used for orienting the end effector. The workspace of a robot depends on the robot configuration. The four basic configurations are (a) Cartesian, (b) cylindrical, (c) polar and (d) revolute. Figure 1.4 shows the basic robot configurations and respective workspaces.

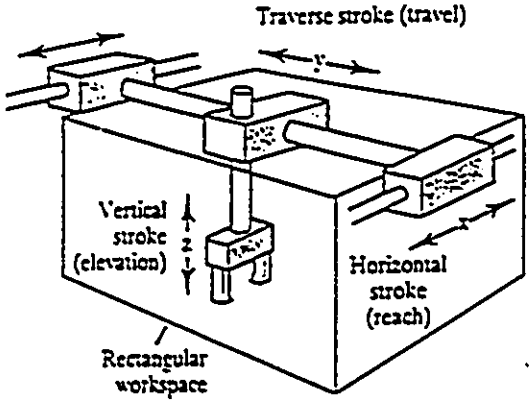

(a) Cartesian

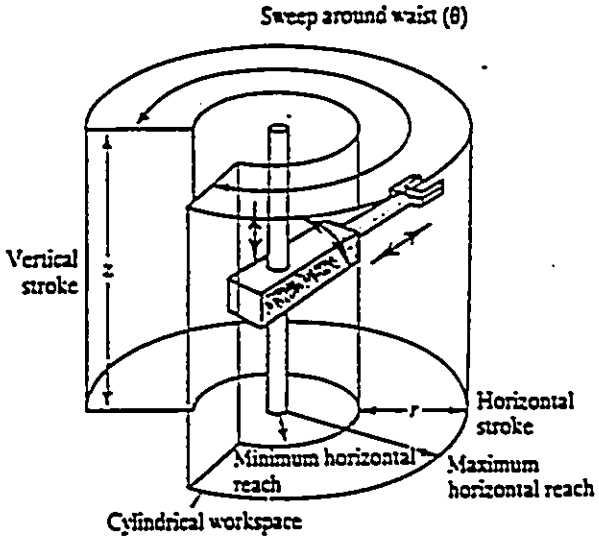

(b) Cylindrical

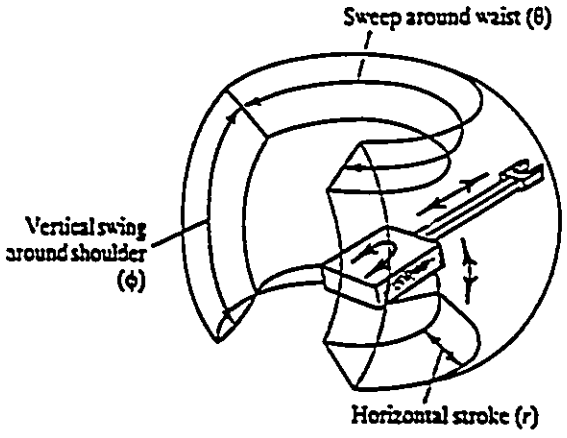

(c) Polar

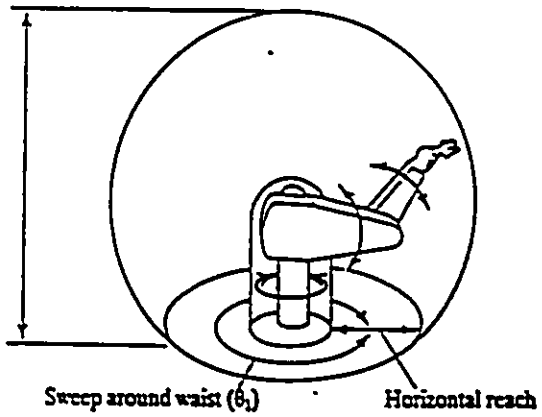

(d) Revolute

Figure 1.4: Basic Robot Configurations and Workspace [5]

The Cartesian configuration (Figure 1.4 (a)) uses only prismatic joints and thus defines a rectangular workspace. The cylindrical configuration (Figure 1.4 (b)) is a modified form of a Cartesian configuration with a revolute joint in place of a waist joint. This configuration defines a cylindrical workspace. If the shoulder joint is replaced by a revolute joint, a polar configuration (Figure 1.4 (c)) is formed. It defines a spherical thick shell workspace. Lastly, if all the joints were replaced by revolute joints, the revolute configuration (Figure 1.4 (d)) is formed. This robot defines a complex thick-walled spherical shell[5].

(2) Actuators

There are three types of actuators for robots:

a) Pneumatic actuators

Pneumatic actuators use pneumatic cylinders that can be extended or retracted with the extension and retraction positions being controller by mechanical stop. This type of actuator is used in pick and place robots where no path control is required[5]. Some advantages are: (a) low cost, (b) high speed, (c) clean operation, (d) no fire hazard, (e) actuator can be stalled without damage and (f) low maintenance and (g) high reliability. Some disadvantages are: (a) reduced accuracy due to compressibility of air, (b) noisy, (c) air filters may be required, and (d) very limited positional

control.

b) Hydraulic actuators

Hydraulic actuators use hydraulic cylinders that can be extended or retracted depending on the differential pressure between the two chambers. The volume of fluid let into the chamber controls the distance the cylinder moves. The ability to control the pressure of the two chambers simultaneously allows positional control with very little overshoot. Some advantages are: (a) large lift capacity, (b) moderate speeds, (c) very good servo control, (d) self-lubrication, (e) fast response, (f) use in flammable areas and (g) smooth operation in low speeds. Some disadvantages are: (a) very costly, (b) high maintenance due to wearing of seals, and (c) high pressures fluid requirements [5].

c) Electrical actuators

Electrical actuators use stepper motors and direct current motors. The stepper motors are driven by a series of electrical pulses. In its simplest form a stepper motor consists of stator and rotor. The stator is made of two separate coils which have a magnetic field offset angularly by half a rotor pole. A rotating magnetic field is generated by the alternating series of electrical pulses. The rotor, which is polarized with alternating north and south poles, aligns

itself with the magnetic field, and rotates with it [5]. Thus, each pulse will turn the rotor through a single fixed step. A direct current motors use similar components as in stepper motor. The stator is either made from a wound coil or permanent magnet. A commutator is a cylinder with copper contact placed in the periphery. When these copper contacts are connected with the carbon brushes, a distortion in the magnetic field between the rotor and stator results. This resultant torque turns the rotor. Some advantages are: (a) high accuracy, (b) high speed, (c) inexpensive, and (d) fast response. Some disadvantages are: (a) low torque at minimum revolution per minute, (b) poor accuracy due to gear backlash, (c) unsuitable for flammable areas, (d) over heating under stalled conditions, and (e) requirement of a positive locking system when power is removed.

(3) Control System

A robot controller performs three essential functions:

(1) storing, sequencing, and positioning of data to memory.

(2) initiating and stopping manipulator motion at any given point.

(3) interacting with the external environment.

The controller consists of hardware and software elements and can be mechanical,

pneumatic, or electrical. Electrical controllers can be numerical controllers or computers. The controller must be programmed to execute the desired motion profile. Its memory can be programmed using the following methods:

(1) manually installing a sequence program.

(2) "Teach-in" physically leading the robot through a desire sequence of motion.

(3) using a machine input control through a computer terminal.

(4) Tooling

Tools are usually attached to the end of the robot arm. Depending on the applications, and on the role of the robot in the process, the tool can be a gripper, a drill, a spray gun, a welding head, or a host of other tools. These end effectors are either electrically or pneumatically controlled. Multifaceted robots can have interchangeable tools and provision for automatic engagement and disengagement of such tools.

1.3.2: Robot Classification

Robots are classified by the nature of the application and controller as follows:

(1) The purpose of the pick and place robot is to pick up objects and to move them to desired locations. This function is used in loading/unloading, palletizing, stacking and material handling. At these desired points a robot can

perform various tasks such as spot welding, gluing, drilling, or deburring. This method requires only the end point information be given.

(2) The continuous path control robot controller is given all the information about the initial point and the path between the end points. In addition, the speed and the acceleration must also be supplied for the robot. This method produces a smooth path. This type of robot controller can be used for spray painting, seam welding, cutting and inspection.

1.3.3: Suitability of a Robot for Filament Winding

For a simply shaped mandrel, such as a cylindrical pipe, only two degrees of freedom are required to guide the fibre. One degree of freedom is used for rotating the mandrel and the other is for translating the payout eye parallel to the axis of the mandrel. This can be achieved by using the traditional modified lathe winding machines.

A six degrees of freedom robotic cell is required to wind a mandrel with a complex shape. Five degrees of freedom are for the robot manipulator and the sixth degree of freedom is for the rotation of the mandrel. The robot base provides the degree of freedom for the yaw motion. Two degrees of freedom are used for the motion of the two links. The last two degrees of freedom form the pitch and roll motions of the wrist.

The advantages for using a robot in filament winding are as follows [6]:

(1) robots can perform other tasks, such as loading and unloading of

mandrels and inspection.

(2) robotic filament winders are less expensive than some conventional winders.

(3) the maximum winding speed of a robot is higher than a conventional winding machine in some situations.

The disadvantages are as follows [6]:

(1) robot winding accuracy is lower than a conventional winding machine.

(2) it may be difficult to synchronize an off the shelf robot with a mandrel drive unit that has not been designed to work together.

These last three points are addressed in detail in the thesis.

1.4: Problem Definition

A robot with an auxiliary mandrel drive unit existed at the University of Ottawa at the beginning of the thesis. Simple shapes had been filament wound using this elementary winding cell. In this configuration an Apple computer was used as the pulse generator for the stepper motor drive of the auxiliary mandrel. Control between the robot and mandrel drive was through an output port of the robot. Payout eye positions were entered manually into the robot memory. This setup was acceptable for winding very simple shapes; however, a more sophisticated approach was required for complex axis-symmetric and asymmetric mandrels.

The objective of this thesis was to develop a complete control structure for a robotic composite filament winding cell and to then study the accuracy and repeatability of the cell for simple cylindrical and an asymmetrical S-mandrel. The fibre paths of the S-mandrel were generated by an existing program called TRIASYM, by E. Bernard [7]. Bernard used the computer algorithm to determine the fibre paths for any asymmetrical mandrel. The control structure of the cell consists of both hardware and software elements. The hardware element contains the robot, robot computer and mandrel drive. A control algorithm for the robot controller and the mandrel is first generated. Secondly, an interface for sending data files into the robot memory and executing the data file at random or sequentially is implemented. The third step will be to code a control software with user friendly menus on a personal computer with a utility software to extract data from the AutoCAD drawing files to produce payout eye paths. Experiments are then conducted to evaluate the accuracy and repeatability of the winding cell for axis-symmetric, offset axis-symmetric, axis-asymmetric and S-mandrels.

1.5: Overview of Thesis

This thesis is divided into five parts: (a) introduction, (b) literature review, (c) control structure, (d) experimental procedures, results and discussion, and (e) conclusions. Chapter 1, the introduction, presented the basic information on composite materials, robots, and filament winding. Chapter 2, the literature review, elaborates on the past and

current research in the field of filament winding. Chapters 3 to 5, the control structure, examine the basis behind the theory, hardware, and software required in the developed robotic winding cell. Chapter 6, the procedures, results and discussions, describes the technique to verify the control structure. It reveals the accuracy and repeatability of the robotic winding cell and sources of errors are discussed. Chapter 7, states the conclusions and the recommendations for the developed robotic filament winding cell.

CHAPTER 2

LITERATURE REVIEW

This chapter will discuss the past and current filament winding machines as well as a brief description of filament winding path prediction techniques.

In the past, the filament winding process was carried out using a modified lathe. The payout eye of this machine was translated using mechanical components (gears, sprockets, cams and chains, etc...). This limited the machine to the winding of simply shaped mandrels. Therefore, new types of machines were required to produce complex shape components. Two popular types of winding machines are the computer numerically controlled (CNC) winding machine and a robotic filament winding machine. Winding machines have now evolved from simple lathes to complex flexible machines.

Presently, the geodesic and non-geodesic fibre paths for complex shaped mandrels are being predicted using a number of approaches. These theoretical fibre paths are generated in explicit or numerical iteration form. These fibre paths are then used for determining the payout eye and the mandrel rotational positions.

2.1: Review of Filament Winding Path Prediction Techniques

One of the advantages of components produced with filament winding, is to cover a mandrel using individual fibre bundles. Since the fibres are wound under tension onto the mandrel surface, the fibres may not stay in the chosen position or direction. Thus, a stable path must be found for the fibres to prevent them from shifting on the mandrel surface. Two approaches to achieving a stable path are mechanical keying and by considering surface friction between the fibre and the mandrel surface. Mechanical keying utilizes pins, tags or some form of anchoring mechanism to confine the fibre on the desired path.

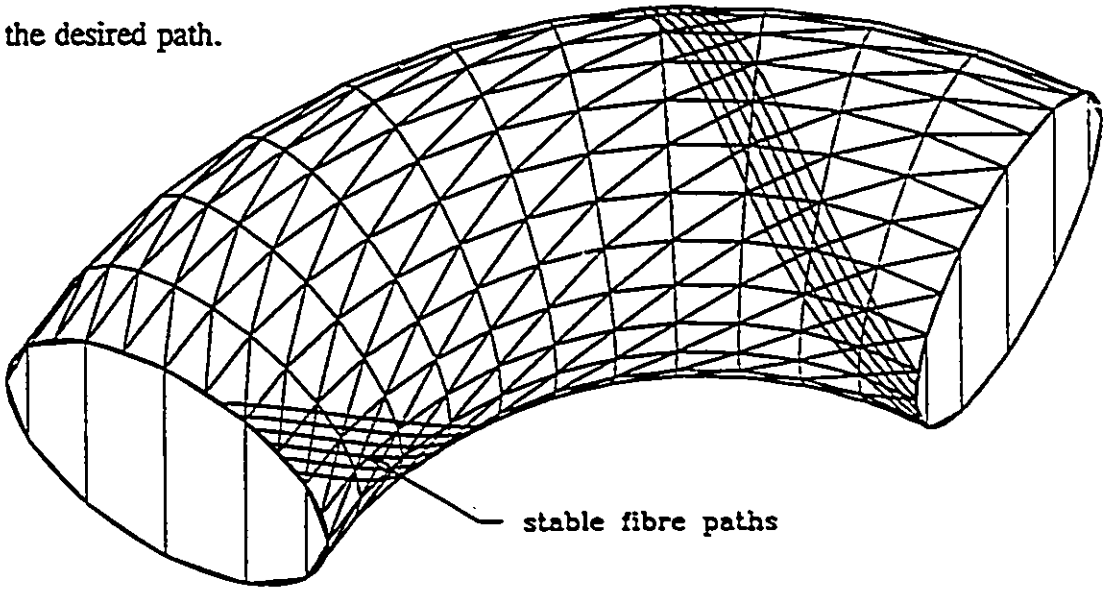

Figure 2.1: Geodesic Paths on a Mandrel [7]

A stable path can also result from using the geometrical shape of the mandrel and the surface coefficient of friction. When the coefficient of friction is not considered, i.e., equal to zero, the stable path will rely solely on the geometrical shape of the mandrel. This will produce a geodesic path (Figure 2.1). The principle behind the geodesic path

is the fibre will always move to find the lowest energy or stable position on a frictionless surface. Non-geodesic paths are generated when the surface friction is considered. The entire mandrel surface can be covered with the combination of the geodesic and non-geodesic paths.

The two principle methods used for predicting stable paths are the geometric and the mathematical. The geometric method uses vector algebra for finding the filament paths. A geodesic path of a simple mandrel shape of standard geometries such as cones and cylinders can be found by creating developed surfaces where the geodesic path is a straight line. The geodesic path for a sphere is the great circle. When the mandrel is a complex axis-symmetric geometry, an approximation can be made by dividing the mandrel into a series of truncated cones and cylinders. As described before, these shapes can be developed and the geodesic on their development is a straight line [7]. Another approach is to use triangular patches to define the mandrel surface where the geodesic path is found for each patch. Middleton et. al. [8], incorporated the triangular patches method and a utility program to generate control data into a software program called CADFIL. This program was restricted to axis-symmetric mandrels. Bernard [7] extended the triangular method to axis-asymmetric mandrels and produced a software program called TRIASYM. Both authors concluded that triangulation method can be used for any shaped mandrel and produced solutions faster than solving the mathematical equations defining the geometry. However, the disadvantages of the triangular patch method are low accuracy and the large memory requirements for the data [7,8].

The mathematical method uses initial value and second order differential equations [6,9] which requires numerical solution for complex shape geometries. In this method, the starting point and direction are the only required data to predict a stable path. Wells, et. al. [9], used a software program called SYSTRID which found the fibre paths by a piecewise solution of a second order differential equations. This program will generate solutions until the fibre path on the mandrel has reached a surface discontinuity. A similar software program called Computer Aided Filament Winding of Asymmetric Shapes using Robots (CAWAR) was used by Scholliers [6]. This method produces high accuracy dependent only on the integration steps used in the calculation.

2.2: Filament Winding with CNC Machines

The simplest Computerized Numerical Control (CNC) filament winding machines have two axes (Figure 2.2). One axis is used to rotate the mandrel and the other to translate the payout eye carriage. More axes can be added as indicated in Figure 2.3. These axes are typically controlled by a microprocessor based control system which are capable of controlling both linear and nonlinear motion of the payout eye.

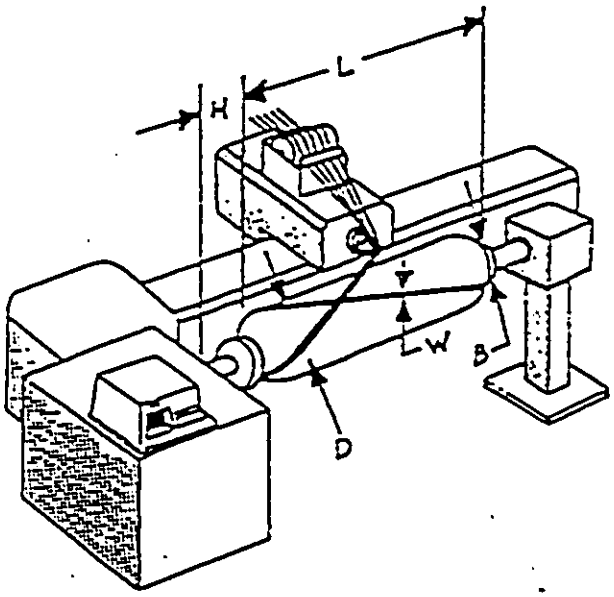

Figure 2.2: Typical Helical Winding Pattern CNC Machine [10]

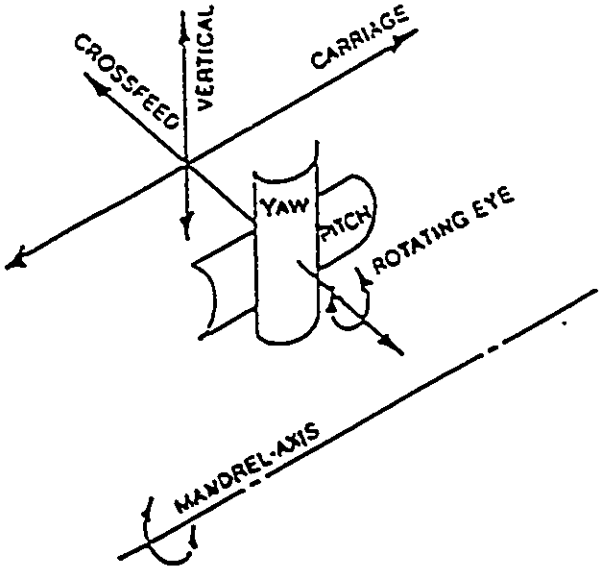

Figure 2.3: Typical Axes of Computer-Controlled Helical Winding Machine [10]

The payout eye and mandrel positions can be programmed either in the "Teach-in" method or down loaded from an external computer. The "Teach-in" method requires a trained experienced operator to wind a complex geometry mandrel.

The second approach i.e. using an external computer to calculate the fibre paths has been used by a number of researchers. Stewart [11] used CADFIL to generate the control data for the FANUC CNC filament winding machine. Similarly, Middleton [12] utilized the data from CADFIL for a three degrees of freedom CNC filament winding machine. Boey [13] produce an economical CNC filament winding machine which contained a BALDOR smart controller card that can be program externally. Similarly, Olofsson [14] used a four degrees of freedom winding machine with an external computer controller to study the wet winding of thick-walled cylinders. He also considered collision avoidance between the payout eye and the mandrel.

2.3: Filament Winding with Multi-axis Robots

A robotic filament winding cell is very similar in its basic function to the traditional Computer Numerically Controlled (CNC) winding machine. However, robots are more flexible than a CNC machine. A robot can easily move a relatively light payload through a complex motion and can be easily programmed to repeat such task. Robots can also perform a host of other tasks such as drilling, trimming, painting, and loading/unloading of mandrels. A robotic filament winder is less expensive, faster (in some situations) and more easily adaptable than a conventional filament winder [10].

A robotic filament winding cell consists of a robot and mandrel driver or support (Figure 2.4). Usually, the robot has five degrees of freedom and the mandrel has one degree of freedom [10,12,15,16]. Six degrees of freedom robots with a stationary mandrel were also used in filament winding [6,17,18]. Bubeck [15] and Seereeam [16] at Automated Dynamics Corporation used a Robotic Winding System (ROWS) consisting of a five degree of freedom gantry type Unimate 6000 series robot with a stationary mandrel. Munro [10] used a five degree of freedom ASEA IRB 6/2 industrial robot with a rotating vertically mounted mandrel. Middleton [12] developed a flexible manufacturing winding cell with five degree of freedom FANUC S1 robot with a horizontally mounted mandrel drive. Scholliers [6], and Hummler [17] used a six degree of freedom Unimation PUMA 762 with a horizontally mounted mandrel drive. Hence, a robotic filament winding cell typically has at least six degrees of freedom.

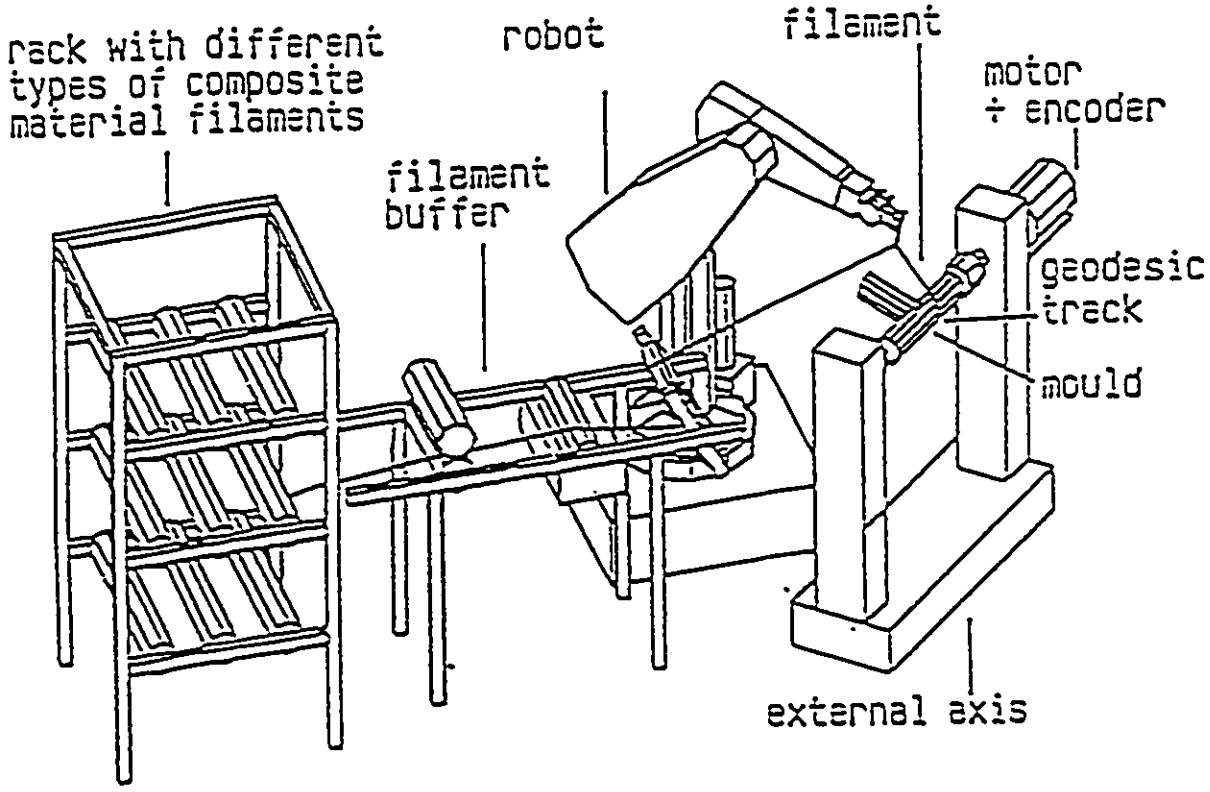

Figure 2.4: Robotic Filament Winding Machine [6]

The robot and mandrel drive controller have generally been programmed from an external source such as a microcomputer [6,10,15]. The control data was generated using software such as CADFIL or SYSTRID. This data was used by the controller to manipulate the robot and the mandrel in unison. Bubeck [15] used the DEC PDP 11

controller to control the robot while Munro [10] utilized the controller provided by ASEA.

Fibres are supplied from a creel system during the winding process. These fibres are tensioned prior to existing the payout eye. The tension can be applied through many forms such as pneumatic or electrical brakes [10]. Munro [10] used an electric brake to applied tension to the fibres where the fibres were supplied from a fibre spool, mounted on the output arm of the robot.

Robotic filament winding was carried out by many researchers [6,10,12,15,16,17,18]. All the researchers found favourable results from using the robotic filament winding cell. These results provided support for the development of an advanced robotic filament winding cell, as described in the next three chapters.

CHAPTER 3

ROBOTIC FILAMENT WINDING MACHINE THEORY

3.1: Filament Paths Generation

For this project the geodesic paths for the S-shaped mandrel surface were obtained using a simulation program called TRIASYM [7]. This program uses the AutoCAD work environment. Custom commands (macros) were incorporated in the AutoCAD menu.

A spine model of the mandrel was first generated using poly-lines. The spine model was carefully generated to reproduce the fibre path from engineering drawings or by tracing the mandrel. The mandrel surface geometry was created using the specified cross-sectional radius and a number of facets to define the circumference. The mandrel surface was then approximated with triangular patches. Using the triangular meshed mandrel surface, many desired fibre paths can be produced depending on the initial setting such as the wind angle and the starting position on the circumference.

After generating the fibre paths, they may be viewed using AutoCAD. If the paths do not satisfy the desired requirements or a collision between the mandrel and payout eye is found, the process can be repeated with different initial settings.

3.2: Payout Eye Position

Filament winding is a process where continuous fibres are placed on a desired path. Since the fibres are not directly deposited on the mandrel (similar to a cutting tool on a lathe) the payout eye position becomes a critical element in the winding accuracy. The payout eye must follow the mandrel without colliding and must accurately position the fibre on the desired fibre path. The payout eye position needs to be tangent to the mandrel surface and at a specific fibre winding angle. The primary disadvantage to this technique is the tow distance that the payout eye must maintain between the mandrel surface and the payout eye to avoid collisions. The effect on the fibre placement due to errors in the payout eye position is minimal as the distance from the payout eye to the mandrel increases; however, a longer tow distance will result in longer winding times due to larger payout eye movements. The continuous fibres are placed on the mandrel surface by using a tow distance that will minimize the winding time and ensure adequate collision avoidance.

The calculations of payout eye position are based on the assumption that any smooth curve can be represented by an infinite number of linear segments. Smaller segments result in higher accuracy. The theoretical model produced a continuous fibre path. Since the robot needs points to describe the path, the continuous path is divided into equal length segments. The segment length will depend on the definition of mandrel geometry. If the mandrel is of a complex geometry, segment length has to be kept small to maintain good definition of the mandrel surface. In the model, the mandrel was

assumed to be made up of many circular cross-sections. Each cross-section location coincides with the end point of the segments. From these cross-sections, the angles (θ) that make the robot tangent to the end points of the segment can be determined (Figure 3.1). In each cross-section, TRIASYM gave the values of offset distance between the rotational centre of the mandrel drive unit and the mandrel centroid (R), mandrel radius (r), and the end point coordinate reference system (X',Y',Z') at the mandrel centroid. Figure 3.1 shows that the robot is situated directly in front of the mandrel drive unit (on the X axis) with a distance of b. The mandrel rotates about the rotational centre of the mandrel drive unit with an offset distance of R. The mandrel drive unit has a coordinate system of X,Y,Z located at the rotational centre and the mandrel has a relative coordinate system of X',Y',Z' located at the mandrel centroid. The X' axis always lies along the direction of R. The mandrel centroid is defined by (x,y,z) and the end point on the mandrel surface is denoted by (X,Y,Z). Figure 3.1 indicates a typical situation where the mandrel has been rotated an angle of θ to make the robot become tangent to the end point of the segment (direction of r becomes perpendicular to the direction of a).

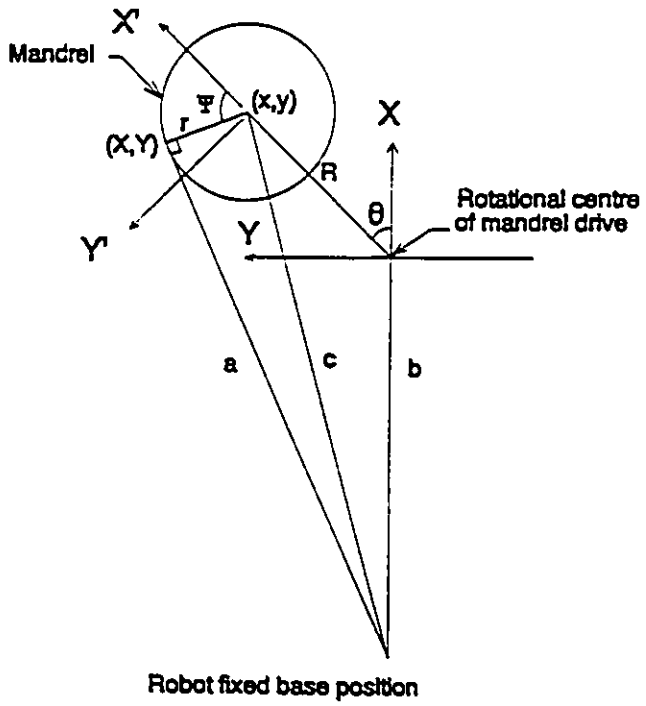

Figure 3.1: Tangent Position on the Mandrel Surface

The following development shows the equations used in finding the tangent angle (θ). With reference to Figure 3.1, the program TRIASYM produces a file of X' and Y' which are the coordinates of points on the mandrel surface with respect to centroid of the mandrel cross-section. The angle Ψ hence obtained from these information as follows:

$$\Psi = \arctan\left(\frac{Y'}{X'}\right) \tag{3.1}$$

The mandrel centroid for a given cross-section relative to the rotational centre of the mandrel drive unit is given by:

$$x = R\cos(\theta) \tag{3.2}$$

$$y = R\sin(\theta) \tag{3.3}$$

The position of the point on the mandrel surface relative to the rotation centre of the mandrel drive unit is given by Equations 3.4 and 3.5 as follows:

$$X = x + r\cos(\Psi+\theta) \tag{3.4}$$

$$Y = y + r\sin(\Psi+\theta) \tag{3.5}$$

The distance c between the robot fixed base position to the mandrel centroid can be expressed as:

$$\begin{aligned} c^2 &= (x+b)^2 + y^2 \\ &= r^2 + (X+b)^2 + Y^2 \end{aligned} \tag{3.6}$$

Substituting Equations 3.1 to 3.5 in Equation 3.6 gives the tangent angle of the robot end effector to the end point on the mandrel surface as follows:

$$\theta = \arccos\left(\frac{-r - R\cos(\Psi)}{b}\right) - \Psi \tag{3.7}$$

The difference between two successive θ values give the angle of rotation of the mandrel between the beginning of a segment on the mandrel surface and the end of the segment.

Once the tangent angle (for the robot to a point on the mandrel surface) is calculated, the payout eye position must be modified to maintain the desired wind angle (Figure 3.2). Figure 3.2 shows that the mandrel has the same coordinate system as in

Figure 3.1. The payout eye position is calculated by translating from the end point coordinate (X2',Y2',Z2'). The point (X1',Y1',Z1') is the previous tangent point on the fibre path. The variable *offset* represents the distance between the payout eye and the mandrel surface.

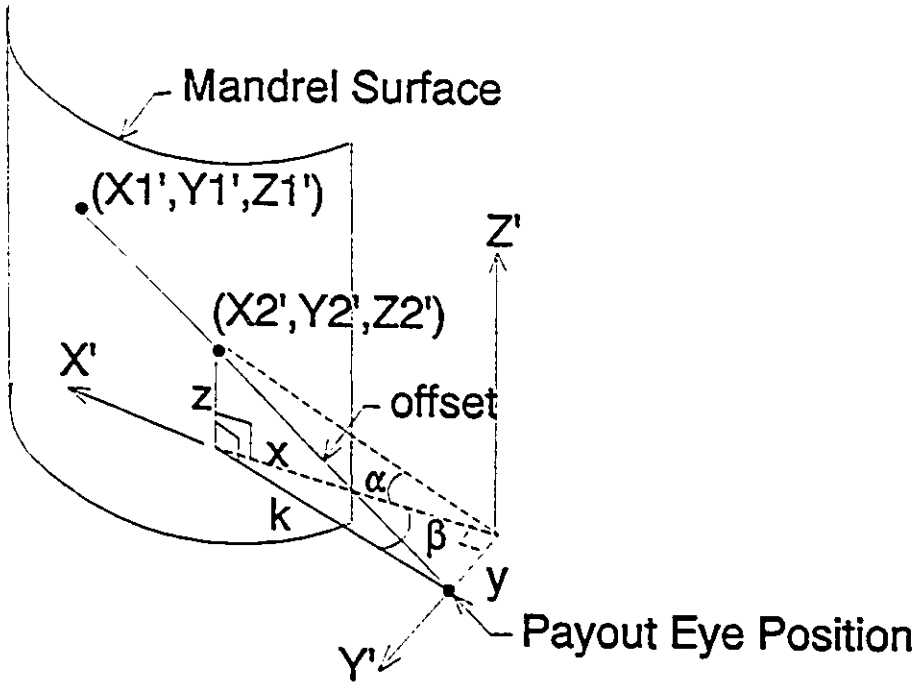

Figure 3.2: Angle of Fibre to the Mandrel Surface

The following is the development for finding the distance that the payout eye has to translate. Equations 3.8 and 3.9 denote two angles that are needed to calculate the relative position of the payout eye to the tangent point on the mandrel surface (Figure

3.2).

$$\alpha = \arctan\left(\frac{Z_2' - Z_1'}{X_2' - X_1'}\right) \tag{3.8}$$

$$\beta = \arctan\left(\frac{Y_2' - Y_1'}{X_2' - X_1'}\right) \tag{3.9}$$

The α angle, in Equation 3.8, represents the angle in the X'-Z' plane (Figure 3.2). It is used for finding the distance to translate in the Z' direction. The β angle, in Equation 3.9, in the X'-Y' plane, is used for translating the payout eye tangent to the previously laid fibre position (Figure 3.2). Figure 3.2 shows that the x value is defined by Equation 3.10.

$$x = k\cos(\beta) \tag{3.10}$$

Equation 3.11 defines the variable k using the Pythagoras theorem (Figure 3.1).

$$k = \sqrt{\text{offset}^2 - (x\tan(\alpha))^2} \tag{3.11}$$

Substituting Equation 3.11 into the Equation 3.10 and rearranging gives x as follows:

$$x = \frac{\text{offset}}{\sqrt{\frac{1}{\cos^2(\beta)} + \tan^2(\alpha)}} \tag{3.12}$$

The variables y and z can then be found with respect to x, β, and α as follows:

$$y = x \tan(\beta) \tag{3.13}$$

$$z = x \tan(\alpha) \tag{3.14}$$

The above variables x, y and z represent the distance that has to be added to the tangent point (X2',Y2',Z2') on the mandrel surface to obtain the correct payout eye position (Figure 3.2).

CHAPTER 4

ROBOTIC FILAMENT WINDING MACHINE HARDWARE

4.1: Experimental Apparatus

The robotic filament winding cell makes use of hardware that is described in the following sections. The items described in section 4.1.1 to 4.1.6 existed previously [19]. Items 4.1.7 and 4.1.8 were added as part of this study.

4.1.1: ASEA IRB 6/2 Five Degree of Freedoms Industrial Robot

The ASEA IRB 6/2, manufactured in Sweden (Figure 4.1), is a five degrees of freedom industrial robot. It is a revolute robot with a stationary base pedestal and has two rigid rectangular box links to form the manipulator. At the end of the robot arm, there is a wrist attachment for end effectors. The wrist joint has pitch and roll but not yaw motion. Servomotors drive the arms using harmonic drives and linkages. The maximum speed of the robot with arm extended is 2300 mm/s, and 630 mm/s with arm retracted. The rated capacity of the ASEA IRB 6/2 is 6 kg.

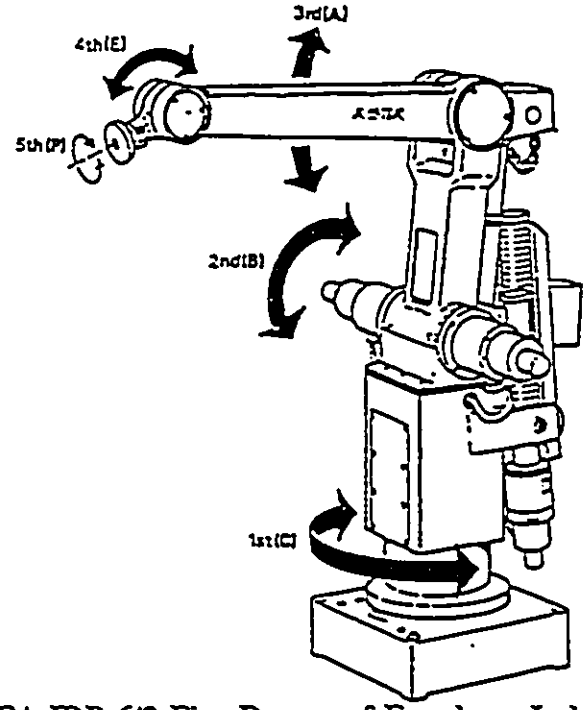

Figure 4.1: ASEA IRB 6/2 Five Degree of Freedoms Industrial Robot [20]

4.1.2: ASEA Robot Computer

The robot computer supervises all the motor drive units and is capable of storing data files (Figure 4.2). The robot computer can control up to five drive motors and oversee six inputs/outputs electrical signals [20]. It has a pendant with a keypad and a joystick to jog the robot manipulator. A disc drive was provided for storing programs from the robot memory onto a diskette. The robot computer has 6 kilobytes of main memory space that could store 470 plain positioning instructions or 300 positioning instructions and 200 control instructions. The positioning instructions were made up of point coordinate, velocity, and movement modes, which were used for moving the robot manipulators. The control instructions are used for controlling the gripper or external devices. The robot computer can be programmed by using the "Teach-in" mode, or from

data files on a diskette, or via a communication link to an external computer. The "Teach-in" process required jogging the payout eye to the desired position and then storing it into the memory by an operator using the joystick and keypad. This positioning data can be easily edited from the pendant keypad. A personal computer can also provide equivalent operations through an external RS232 communication link. A special protocol (Chapter 5) was required to establish a standard message syntax between the robot computer processor and the personal computer. The robot computer can only perform one task at a time which idles the robot manipulator during an external data link. Therefore, the robot controller supervises the joint motors and can be programmed by "Teach-in" or through an external communication link.

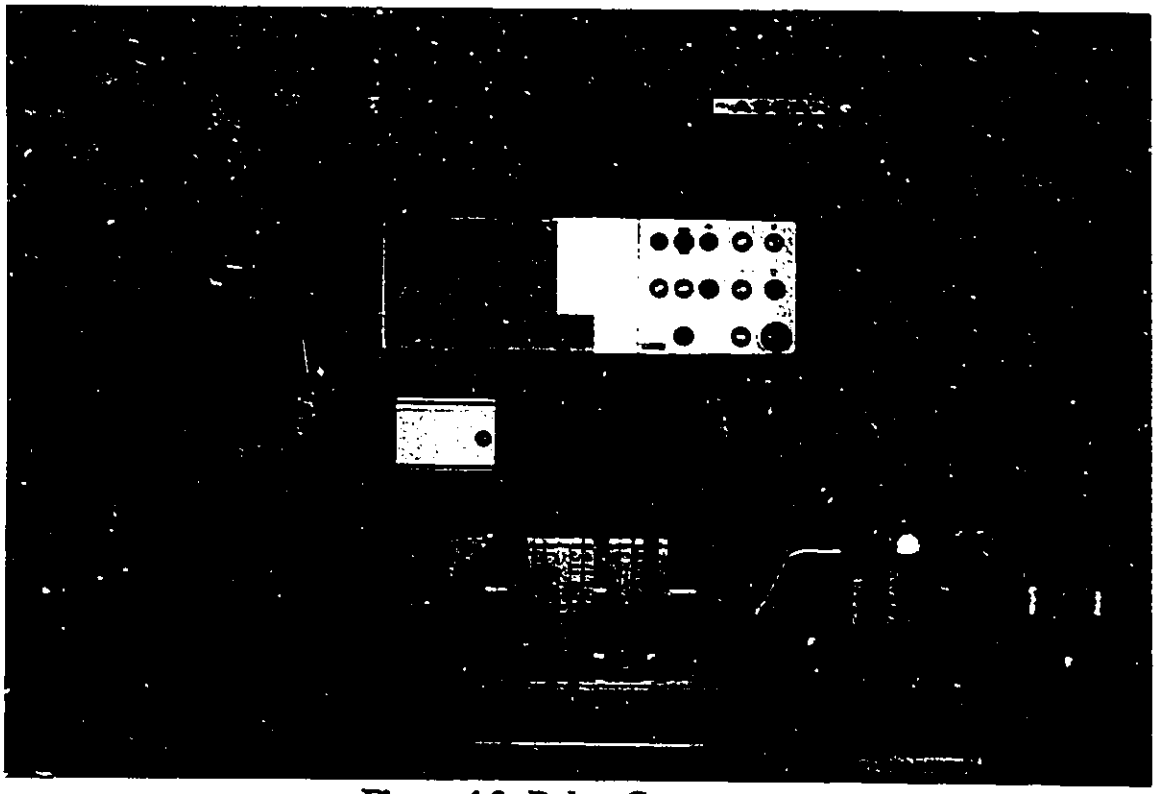

Figure 4.2: Robot Computer

4.1.3: Fibre Spool, Tensioner and Payout Eye Mechanism

Fibres were supplied from a single fibre spool. The spool is located on link 2 of the robot and rotates on a shaft that is attached to an electric brake (Figure 4.3). The fibre travels from the spool and through many guide rollers to the payout eye mechanism. The payout eye mechanism has a spring loaded rocker arm to take up any slack in the fibre (Figure 4.4) and is positioned on the same axis as the roll axis of the wrist.

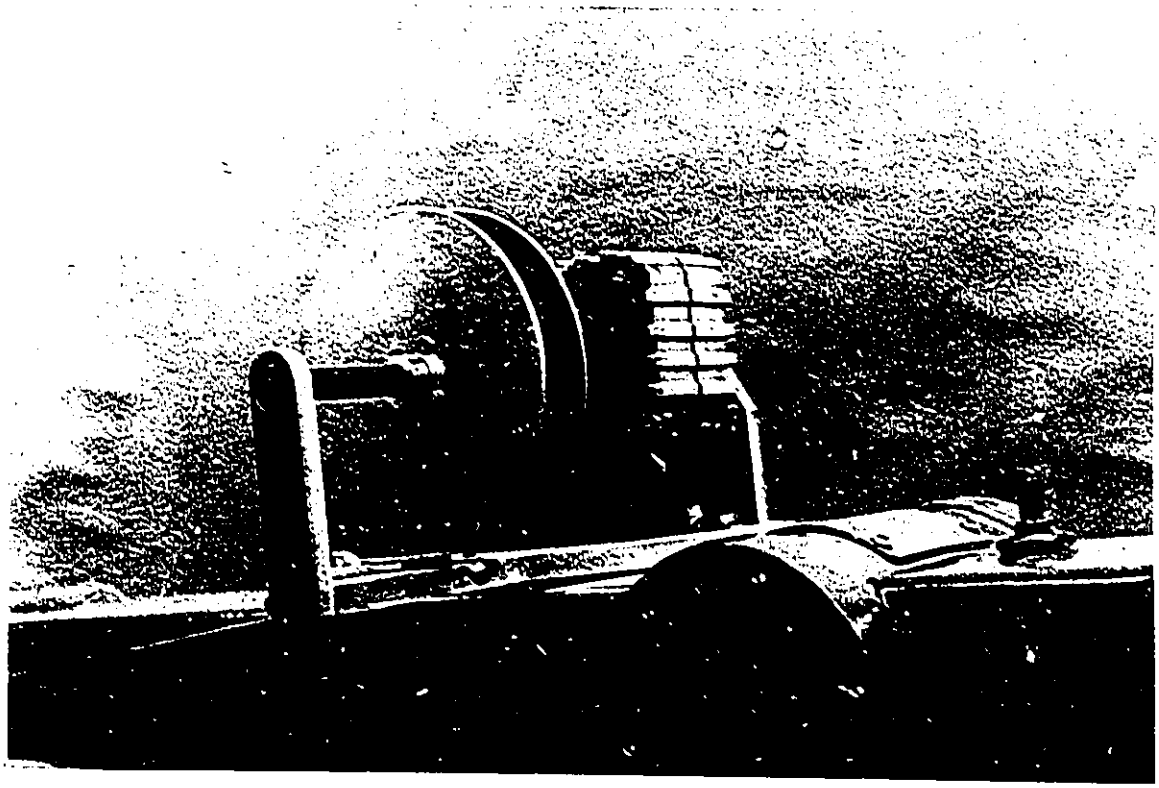

Figure 4.3: Tension Brake and Fibre Spool

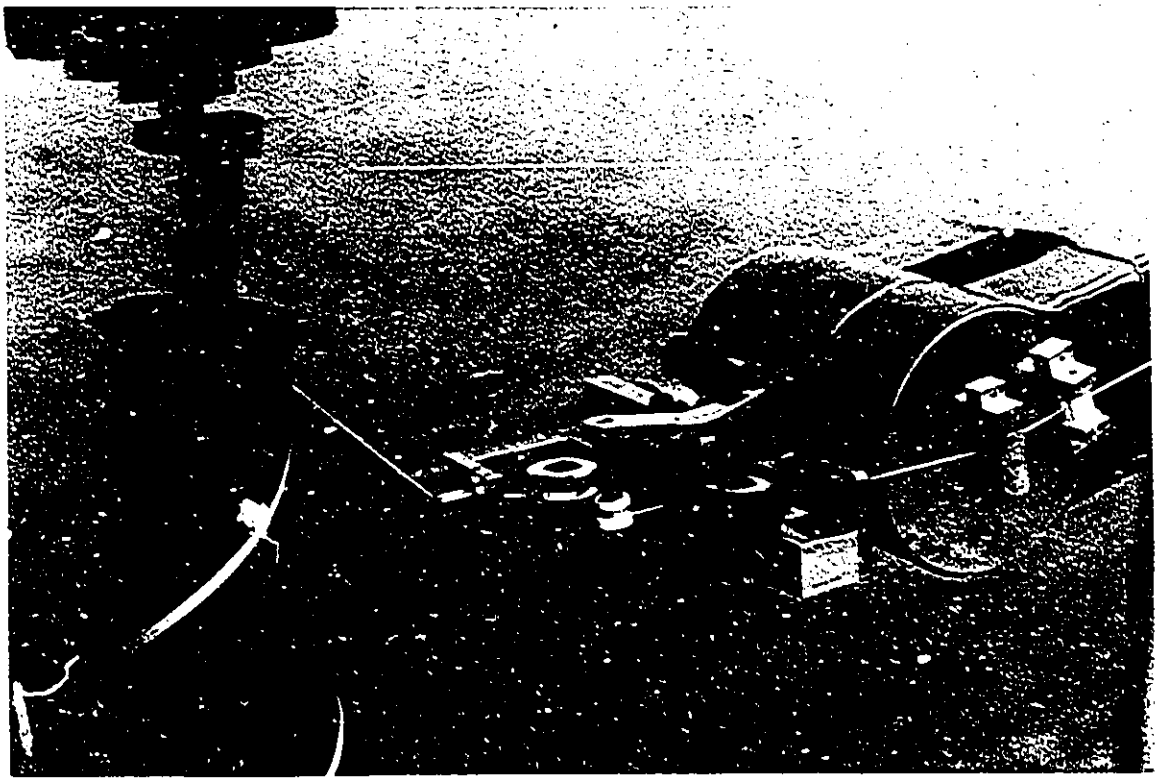

Figure 4.4: Payout Eye Mechanism

4.1.4: Mandrel Drive Unit

The drive unit consists of a steel rectangular frame, two adjustable chucks, and a gear train (Figure 4.5). The chucks are mounted vertically and are used for holding the mandrel in a vertical posture. The top chuck rotates freely on a bearing and the bottom chuck is connected to a gear train. The gear train has a ratio of 13 teeth for the gear sprocket on the drive shaft to 60 teeth for the chuck gear sprocket. A timing belt was used to transmit power to the gear train from the stepper motor. This unit can accommodate a mandrel of 550 mm in length and 230 mm in diameter.

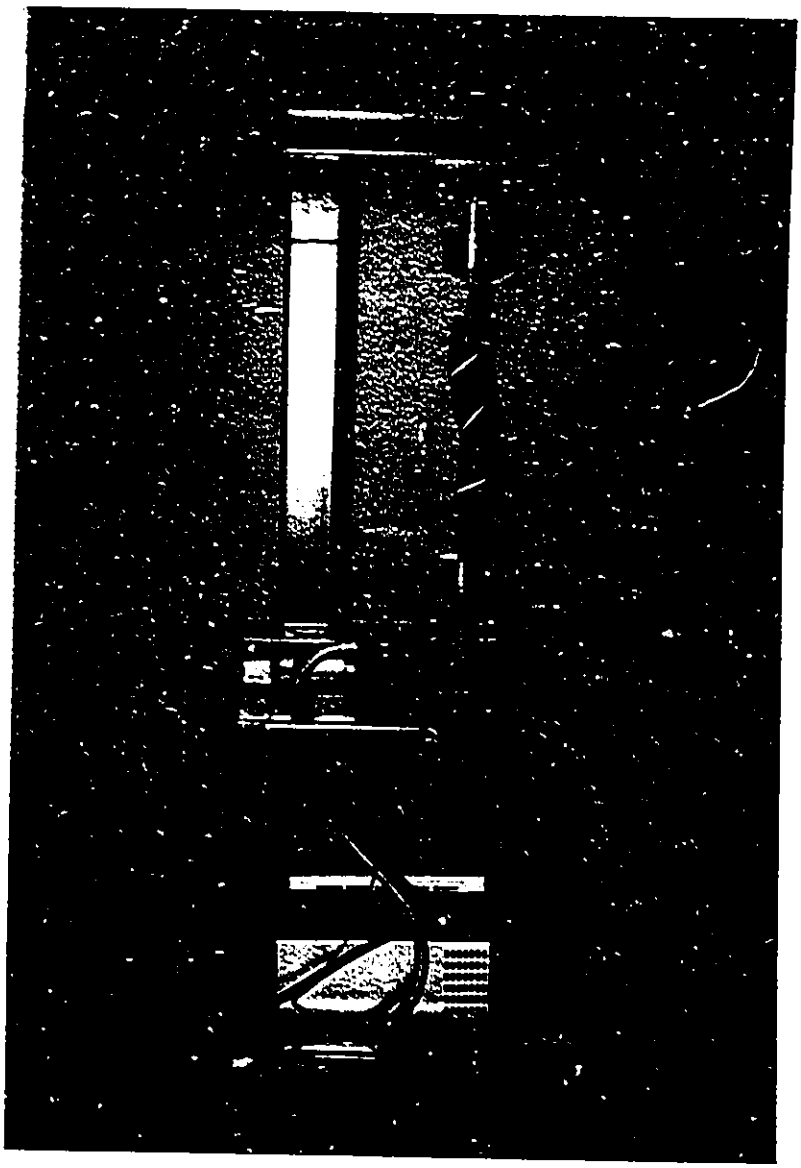

Figure 4.5: Mandrel Drive Unit

4.1.5: SLO-SYN TM600U Translator

The translator converts the electrical pulses into the switching sequence needed to drive a SLO-SYN stepper motor (Section 4.1.6). An SLO-SYN TM600U operates from

a DC power supply and is capable of producing up to 10,000 pulses per second. The electrical pulses can be from a personal computer or a dedicated indexer card. An internally mounted indexer card in a personal computer was used to provide pulses for the translator (Section 4.1.8).

4.1.6: SLO-SYN M112 FD25 Stepper Motor

An SLO-SYN stepper motor provides 840 oz-in torque to the mandrel drive and consumes 12.7 amperes at 1.75 DC volts. It can be configured for full stepping giving 200 steps per revolution or half stepping with 400 steps per revolution. The resolution in the full step mode is 1.8° or 0.9° for the half step mode. In this research, the half step mode was utilized to obtain higher resolution.

4.1.7: A Micro Personal Computer

A 386 personal computer with four megabytes of random access memory (RAM) and a 120-megabytes hard disk was used for this experiment. It was equipped with two communication serial ports and one parallel port. Communication port, COM1, was utilized for the serial link with the robot computer. COM2 was used for the mouse interface. The parallel port was configured to handle the input and output signals between the robot and the personal computer. Microsoft Quick C version 2.5 was utilized for

writing the robot and mandrel control software programs. AutoCAD version 10.2 was used for graphical display of the simulation results. Calculations on the personal computer were performed to obtain the fibre paths and the payout eye positions, and to supervise the robot and the mandrel movements.

4.1.8: PC21 Compumotor Indexer Card

A microprocessor based indexer card, PC21 Compumotor, was mounted in the personal computer. The indexer card can command the stepper motor to rotate to a precise position and stop; rotate at constant velocity; alternate back and forth between two angular positions; or use a combination of the above moves.

CHAPTER 5

ROBOTIC FILAMENT WINDING MACHINE SOFTWARE

5.1: Robotic Filament Winding Cell Controller

Filament winding requires that many fibre paths are used to cover the entire mandrel surface. Each fibre path has corresponding robot and mandrel control files. There are two methods for inputting the control files data into the winding machine's controller memory. The "Teach-in" mode allows the individual points to be entered manually when the payout eye is positioned by the operator. The second method is to have an off-line technique. The second method was incorporated and specific software written to control the robot. An intuitive user interface was created to simplify the operation.

Prior to this work the payout eye positions were entered manually into the robot's controller in "Teach-in" mode. The following sections will discuss the subsequent additions i.e. the aspects of the communication link, data specifications, and user interface of the robotic filament winding cell software.

5.2: Communication Between Personal Computer and Robot

The robot was purchased without the communication software, due to the high cost of that software. The communication protocol was therefore determined by exchanging commands between the robot and a computer, and then through observation decipher the code for that command. Communication between the robot computer and the personal computer are established through the following protocols. There are four phases in the communication protocol.

(1) Establish connection

(2) Transfer the telegram or message

(3) Verify transmitted message and

(4) Terminate the transmission.

Before any communication between any machines can take place, the connection must be established. In this phase the host station will transmit an ENQUIRE command to the slave computer to verify a correct computer link. If the correct link is found, the slave computer will answer with an ACKNOWLEDGE message back to the host machine. If the communication link is faulty, the host computer will receive no message and a time out (exceeded the time limit given for answering the enquiry) will occur. Therefore, the communication between the robot computer and personal computer has to wait until a correct link has been made.

After the correct link has been accomplished, messages can be sent between the robot computer and the personal computer. Messages are utilized for entering commands

into the robot memory. These messages involve three main parts. Each message contains a start of text transmission, the telegram, and the end of text transmission. The start of text transmission indicates the beginning of the text in the telegram. A telegram consists of a header, to identify the following command with the telegram length, and the command description. There are 26 commands that can be sent from the personal computer to the robot computer. After the telegram has been transmitted, the end of text transmission byte is sent to the slave computer. Following the end of transmission byte, the host computer will send a byte containing the sum of the message bytes to verify the accuracy between transmitted and received message. This value will be compared with the sum of the bytes received by the slave computer. If the values do not match, a negative acknowledgement will be sent by the slave computer to the host computer. This will make the host station repeat the message transmission. In the case of no difference between the two values, the slave station will send an acknowledgement to indicate a successful communication. After the verification is done, the transmission can be terminated by sending the end of transmission. Therefore, a message can contain various telegrams which includes detection for transmission errors. The details of the communication protocols are described in a separate proprietary document [21].

5.3: Controller Software

The controller software developed in this work is a menu driven program and was written in Microsoft C language [22]. This software has been modified to accommodate more user functions and adapted to accept external accessories. It uses graphical screens and menus to interact with the operator. This software is called Robot Control Communication Software (RCCS) [22]. Extensive error checking was used to maintain the integrity of the data link. Assembly coded routines were used to ensure maximum data throughput and minimize any handshaking delays. The entire program is made up of many modules. Each module represents a main command. There are four main commands.

(1) Mode

(2) Manual Control Mode

(3) File Control Mode

(4) Program Control Mode

5.3.1: Mode

The robot has to be in the appropriate mode for it to execute any commands. The robot will be in either standby or operate mode. While it is in standby mode, the robot will execute the given commands from memory without the participation of the robot

arm. In the robot operational mode, the given commands are executed in memory along with the robot arm. Standby mode permits verification of the syntaxes and coordinates of the robot instructions. If there are any errors in the syntax or invalid command positions, the robot will stop executing and display the error. This error checking function will find most errors before executing in the operate mode. A continuous check of the communication link is possible with the ENQUIRE command. The robot may also be synchronized to the home position. The home position allows the robot to rest in a balanced posture.

5.3.2: Manual Control Mode

In the past, robot movements were taught to the robot memory by using the "Teach-in" mode. This mode requires the robot to be jogged to the desired positions by the operator using a joystick and storing the desired positions. In the manual control mode, jogging with a joystick is now replaced with position coordinates provided by the personal computer. Figure 5.1 shows the manual control display screen and a flow chart is shown in Figure 5.2. All command positions are entered using the Cartesian coordinate system in absolute or relative terms.

The starting point must be established before the robot can be commanded manually. A typical robot instruction consisted of: (a) the robot's base speed, (b) rectangular or robot (revolute) movements, (c) the program number, (d) the instruction

number and (e) the Cartesian position. The robot's base speed is defined as the reference speed. A percentage of the base speed is used by the robot instructions for movements. The rectangular movement uses a straight line to move from point to point. The robot (revolute) movement uses the shortest path in joint space to move from point to point and thus results in an unpredictable path. To complete the robot instruction, the wrist's pitch and roll angles have to be specified (Appendix A).

The mandrel instruction set consists of: (a) angular acceleration, (b) start and stop limit angular velocity, (c) maximum constant angular velocity, and (d) the angle of rotation. The acceleration input determines the time needed to reach constant velocity. This value is also used for deceleration. Correct start and stop velocities will prevent the mandrel drive motor from stalling. The stepper motor will start to operate if the velocity has reached the start velocity, and stop operating when it reaches the stop velocity. The maximum constant velocity value governs the maximum constant rotation velocity of the mandrel. The mandrel travel is set by the angle of rotation value.

The combination of the robot instructions with the mandrel instructions form the complete instruction for controlling the robot and mandrel necessary to wind one segment of a fibre path. These instructions are stored into a robot and mandrel control files to be used in the future.

The robot instructions and mandrel instructions are sent simultaneously when a transmit command is executed (Figure 5.2). The robot and mandrel will respond to the given instructions.

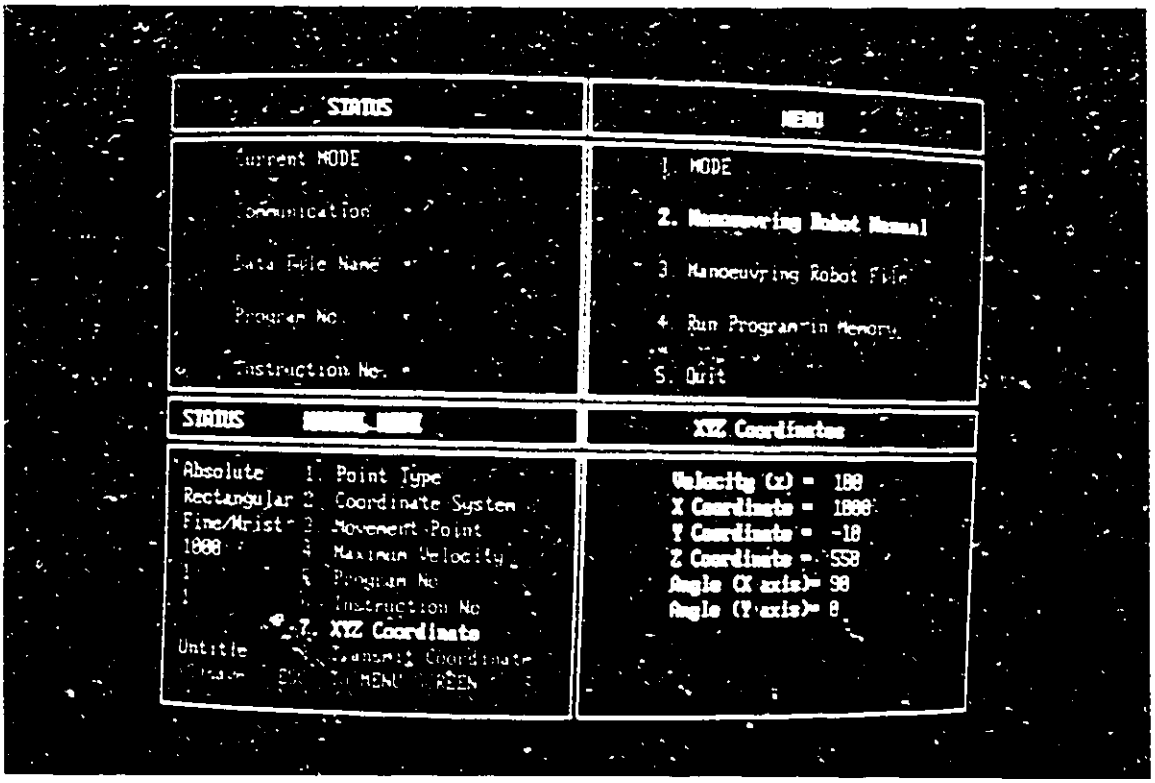

Figure 5.1: Manual Mode Screen

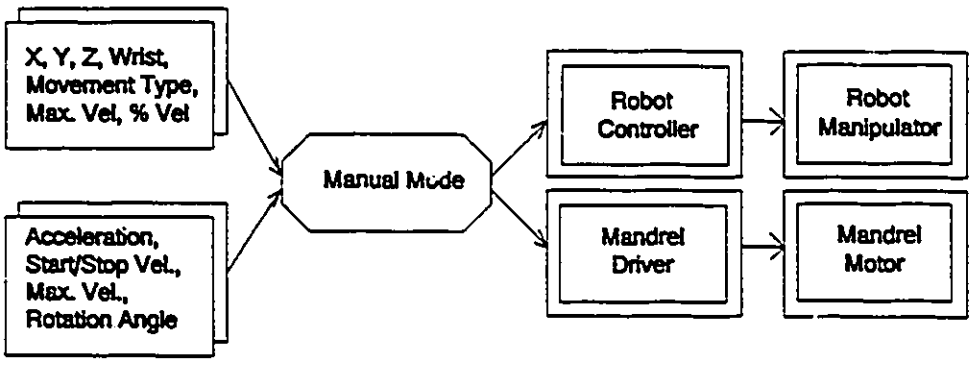

Figure 5.2: Manual Mode Flow Chart

5.3.3: File Control Mode

This control method is similar to the manual control mode with the difference being the point positions coming from the control files rather than an operator. These commands are sent to the robot computer and the mandrel driver in sequential form. When a given command has been executed, the next command is then read and executed from the data file. The entire mandrel can be wound without operator interaction, as long as there are path files to supply the robot and mandrel positions.

The file display screen is shown in Figure 5.3. This sequence file (Figure 5.4) contained the names of the fibre path file to be sequentially wound. Manual transmit coordinate command is replaced with an auto-transmit command (Figure 5.3). The auto-transmit command is used to send instructions to the robot and to the mandrel automatically, until the sequence file is exhausted. In addition, the command stop, auto-transmit has been added to terminate the winding at any desired position. The TOOL command (Section 5.6) can also allow the operator to generate control files without leaving the program environment.

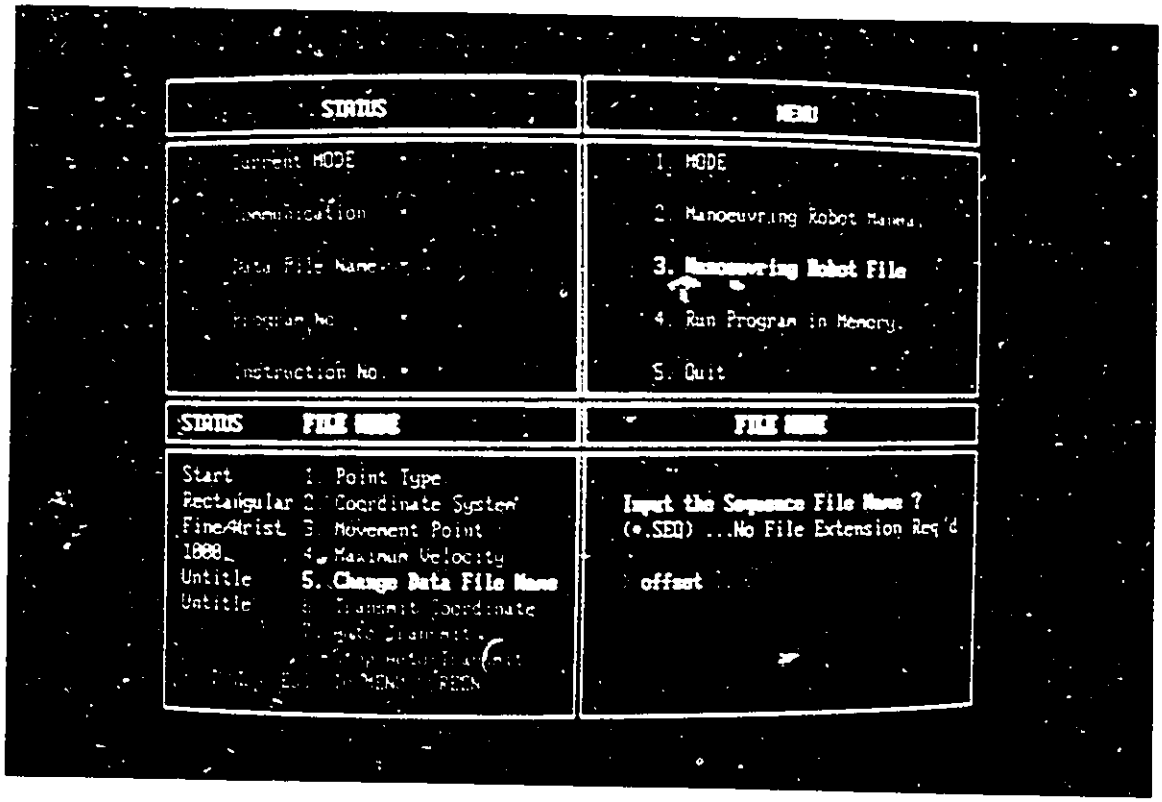

Figure 5.3: File Mode Screen

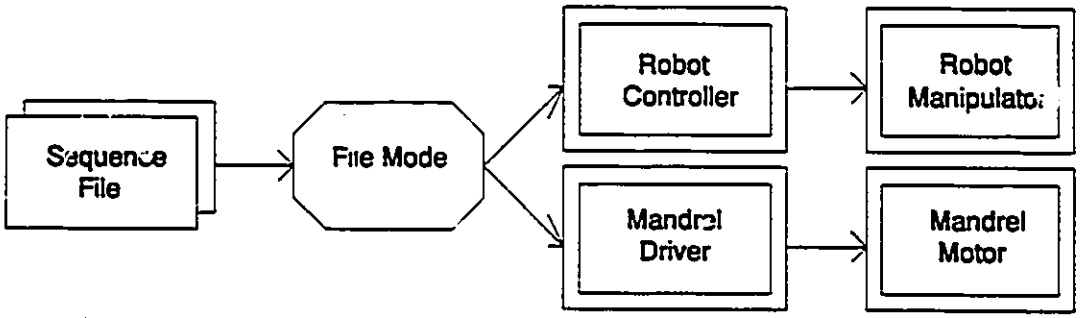

Figure 5.4: File Mode Flow Chart

5.3.4: Program Control Mode

Data throughput from the personal computer to robot computer is limited by the RS232 hardware. This creates transmission delays which result in slow robot movement. To prevent delays, data transmission can be executed in non real time by storing robot instruction into the robot computer memory before running the sequences. This minimizes any delays and ensures smooth continuous fibre windings. The TOOL module (Section 5.6) or manual control mode creates the control files. The program control mode screen is shown in Figure 5.5. This screen illustrates how the robot control files can be loaded into the robot memory and how program can be randomly executed. To load the robot control files to the robot computer memory, the position and the control instructions in the data file must be converted into the proper format for the robot computer [22]. Since the robot computer does not identify data files with names, the control files are stores under different program numbers. The robot control filenames to be loaded into the robot memory are retrieved from the sequence file (Figure 5.6). Once all the robot control files are loaded into in the robot controller memory, the entire mandrel can be wound without any time delay or interruption from the personal computer. To begin a winding, a run file is required (Figure 5.6). A Run file consists of a series of program numbers that were to be sequentially executed (Section 5.6.3). In this mode the robot computer signals the personal computer to synchronize the robot and mandrel. The personal computer will sent a signal to the robot computer and the mandrel driver to begin winding after the synchronization. It will remain in idle state until the

winding is complete.

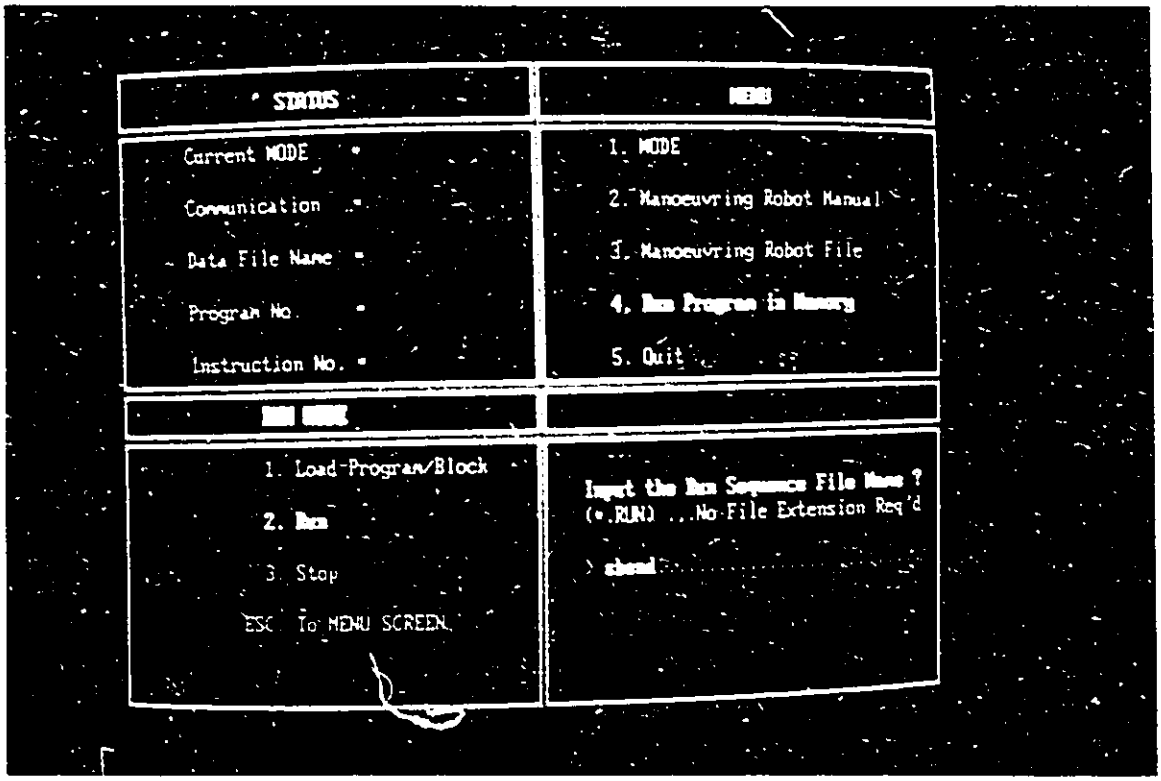

Figure 5.5: Program Control Mode Screen

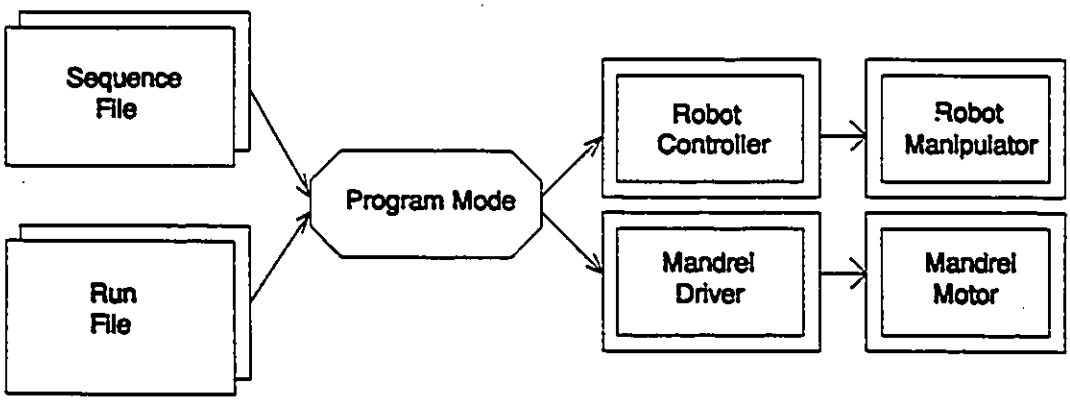

Figure 5.6: Program Control Mode Flow Chart

5.4: Description of Robot Commands

The robot requires that all command positions be available during the execution. These positions are sent to the robot in a telegram (Section 5.2). There are two methods for sending the telegram to the robot computer: (a) discrete movement mode, and (b) fine, medium and coarse movement modes.

5.4.1: Discrete Movement Mode

In the manual and file mode, positions are sent one at a time to the robot. When the robot and mandrel receives the instruction, they will execute immediately without storing the position. This discrete movement type has the robot and mandrel reaching desired location and stopping after execution of each instruction.

The velocity of the robot is given as a percentage of the specified base velocity. This base speed is used as a reference speed for the robot motions. For example, if the base speed was set to 1000 mm/s, and the robot was required to moved at 750 mm/s, then the required input will be 75% of the base speed. A maximum velocity input is required to limit the robot from achieving any higher speeds. The robot design includes a scale factor of 1/8192 for the speed input values. The base and maximum speed inputs are therefore multiplied by the scale factor.

The tool centre point in Cartesian coordinate has a scale factor of 0.0625. The coordinates are described in x, y and z axis. The x, y, and z coordinates must be

multiplied by this scale factor before sending them to the robot computer. The wrist of the robot is defined in a quaternion coordinate system (Appendix A). The wrist configuration can be changed by modifying the angle in the pitch axis and roll axis.

A complete position instruction is comprised of the point coordinates, speed, and the wrist geometry. The necessary protocol instructions are then attached to the position instructions to form a message (Section 5.2) ready to be sent to the robot computer.

5.4.2: Fine and Medium Movement Mode

The fine and medium movement modes require a different type of telegram, but has similar data as the discrete movement mode. In this approach the entire robot control file of commands or instructions are sent down in the form of machine language in one process [22]. These telegrams do not need further interpretation to be stored in the robot computer memory.

There are three movement types. The first is the fine accuracy movement, where the robot will reach the specified point with a zone radius of 1 mm accuracy before moving on to next position. The second is the medium accuracy movement, where the robot will move to within a zone radius of 10 mm accuracy to the specified point before moving on to the next given position. The third is the coarse accuracy movement, where the robot movement is outside the 10 mm zone radius accuracy before moving towards the next position. The best accuracy can be achieved by using the fine movement, but

total execution time is greatest. The medium movement type is faster in execution, but has poorer accuracy then the fine movement. The worst accuracy is given by the coarse movement, but it has the fastest time of execution. All three movement types display a decrease in accuracy as the speed increases. Coarse movement type is not considered useful for filament winding.

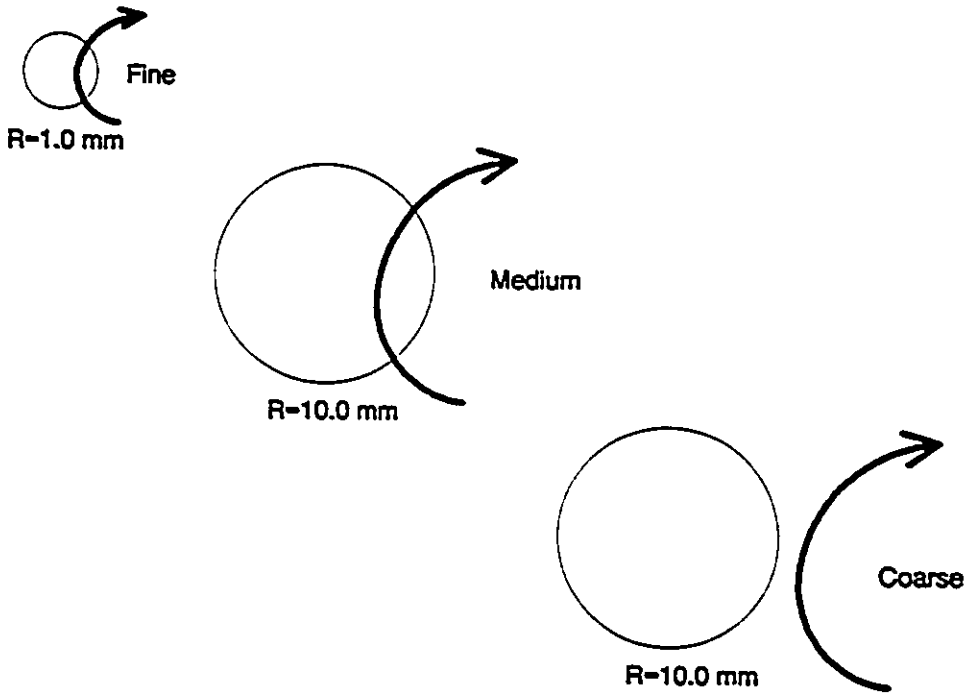

Figure 5.7: Accuracy of Robot Movement Types

The robot tends to smooth out the corners (coming close to the desired position) when there is insufficient time given to achieved a full acceleration and deceleration

period (Figure 5.7). This produces a smoothing effect on the payout eye paths and introduce errors to the robot positions. This smoothing effect will reduce the distance between two points, thus reducing the total. The accuracy decreases proportionally with the speed of the winding process.

Once the points are loaded into the robot memory, individual programs can be selected for execution. All the paths are identified by individual program numbers and can be recalled and run sequentially or randomly depending on the strategy to cover the surface of the mandrel.

5.5: Data Extraction from AutoCAD

Payout eye positions were generated by using the fibre path geometry. Paths were extracted from the AutoCAD drawing files and calculations were performed to determine the payout eye positions.

The fibre paths for the S-mandrel were generated by using the program developed by E. Bernard [7], using triangular patches to model mandrel surfaces. This introduce some irregularities in the generated paths which were smoothed out by spline fitting in AutoCAD. The paths were then divided into equal length segments where each segments' length dictated the speed of the robot. Once the paths were equally divided, AutoCAD automatically determined the end points of the segments (Figure 5.8) which were stored in a .DXF file format. These points represent the locations on the mandrel surface onto

which the robot will place the fibre.

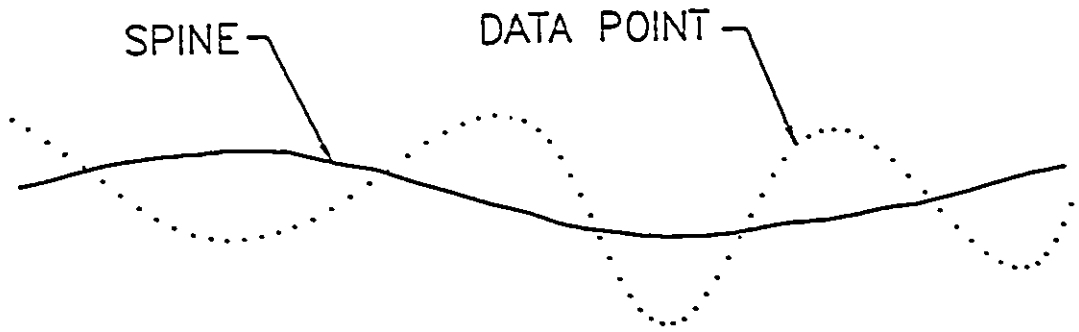

Figure 5.8: Data Points of a Path on AutoCAD

5.6: Creation of Robot and Mandrel Cont· ı Files

Using the .DXF file of the path and the spine profile, the TOOL program was invoked to produce the robot and mandrel control files. This TOOL program is incorporated in the winding cell control program (RCCS) and written in Microsoft C language [22]. Using the data given in the .DXF file and the spine profile, the tangent positions of the robot can be found (Section 3.2). These tangent positions are then used to find the mandrel rotation angle.

The tool program requires the following:

(a) .DXF and spine profile filenames

(b) program number (used for identifying the individual path name)

(c) distance from the robot pedestal to the rotational axis of the mandrel

drive unit (Section 3.2)

(d) starting point height (needed to initiate the first position of the payout eye)

(e) speed of the mandrel (entered in revolutions per second to calculate the speed of the payout eye)

(f) length of the payout eye mechanism and

(g) offset distance from the mandrel surface to the payout eye.

The TOOL program produced robot and mandrel control files using the above inputs. These control files are identified by attaching the program number to the end of the .DXF filename. The robot control file has the file extension of .ROB and mandrel control file has the file extension .IND. For example, the .DXF filename is SBEND.DXF, and the generated fibre path program number as 1, then the robot and mandrel control files will have the following name SBEND_1.ROB and SBEND_1.IND, respectively.

5.6.1: Robot Control File

This file alone is sufficient to control the robot and mandrel under the discrete movement type. The robot control file consists of three sections. The first section is used for initializing the robot base velocity, maximum velocity, and instruction to synchronize the mandrel to the robot. The second section contains instructions for the

robot and mandrel. The robot instruction contains the percentage of maximum velocity to be used to travel to next position, the coordinate of the next position, the instruction number, the program number, the type of coordinate system, relative or absolute movements and the mandrel instruction. The mandrel instruction consists of angular acceleration, the start/stop angular velocity, the maximum operating angular velocity, and the number of steps to rotate corresponding to the robot movements. The third section is used for terminating the communication link between the robot and the personal computer.

5.6.2: Mandrel Control File

The mandrel control file consists of three instructions. The first instruction initializes the indexer card. The second instruction contains the angular acceleration, the start and stop limit angular velocity, maximum angular velocity, and number of steps need to wind a complete filament path on the mandrel. The third instruction resets the indexer card. This file is only necessary in the program control mode.

5.6.3: Sequence and Run File

Many paths are required to fully cover the mandrel surface. These paths can be duplicated in various sequences to produce a desired thickness and coverage of the

composite shell. This is accommodated by the sequence file which is used for the discrete movement. It contains the control filenames without file extensions to be executed in sequential form. This sequence file is also used for indicating which path file will be enter into the robot computer memory (Figure 5.6). The content of the sequence file to wind paths name 1, 2, 3, 2, etc.., is as follow:

SBEND_1

SBEND_2

SBEND_3

SBEND_2

etc...

The run file is used exclusively by the program control mode. This file contains the fibre path program number in sequence to be executed under fine or medium movements. As an example, to run the above sequence of control files as in sequence file, the run file will be as follow:

1

2

3

2

etc...

The content of both files can be changed to accommodate the repetition of path files. An axis-symmetrical cylindrical mandrel requires only one fibre path. This path

is indexed to cover the entire mandrel surface. This indexing of fibre paths can be achieved by entering the corresponding control filename as many time as required to achieve the entire surface coverage. For cases where some area on the mandrel needs extra reinforcement, the fibre path that covers the required area can be repeated by entering the corresponding co ıtrol filename as many time as needed.

Therefore, the sequence and run file make the winding procedure very flexible. Fibre paths can be wound in any order and as many times as required to satisfied the component requirement.

5.6.4: Discrete, Fine and Medium Movement Mode Control File Logic

The discrete movement mode has the following flow of logic.

(1) the sequence file is opened and the first control filename is read

(2) the file extension .ROB is attached to the filename

(3) the robot control file is opened

(4) the header of the robot control file is executed

(5) the mandrel position is synchronized with the robot position

(6) the robot and mandrel instruction are read and executed until the robot control file is exhausted

(7) communication link between the robot and the personal computer is terminated and both the robot and the personal computer become idle.

The fine and medium movement mode has the following flow of logic.

(1) the sequence file is opened, and the control filename is read

(2) file extension .ROB is attached to the control filename

(3) the robot control file is converted to the assembly language and written to the robot computer memory until the robot control file is exhausted

(4) step 1 to 3 are repeated until the data in the sequence file is empty

(5) the run file is opened and the program number to be executed is read

(6) the run command is sent by the personal computer with the program number to the robot computer

(7) the program header is executed by the robot computer

(8) the mandrel position is synchronized with the robot position

(9) the first and second instructions in the mandrel control file is executed by the personal computer

(10) the start signal is sent to both the mandrel and the robot simultaneously

(11) the personal computer wait in idle until the robot computer signal again to indicate completion of winding

(12) the last instruction of the mandrel control file is read by the personal computer and executed

(13) steps from 5 to 12 are repeated until the data in the run file is exhausted

(14) the communication between the robot and the personal computer is terminated.

5.7: Verification of Robot Position Relative to Mandrel Surface

Verification of collision avoidance is important to avoid damage to the equipment and for safety. This verification is performed by plotting the tool position relative to the mandrel using the AutoCAD. The tangent positions, payout eye positions, tow paths (line between the tangent position on the mandrel surface to the payout eye position) and the mandrel surface can be seen in 3D on the graphical screen (Figure 5.9). Figure 5.9 illustrates the tool path in the upward winding, downward winding, the mandrel spine and the circular cross-section of the mandrel. Each circular cross-section is located at a point on the desired fibre path. A collision is detected if any of the circular cross-sections contact the tool paths. If any erratic motion or collision is found, it can be corrected through a change in the robot or mandrel control programs. Figure 5.9 can also be used for displaying how far the payout eye is situated from the mandrel surface. This information can be used for optimizing the distance between the mandrel and the payout eye.

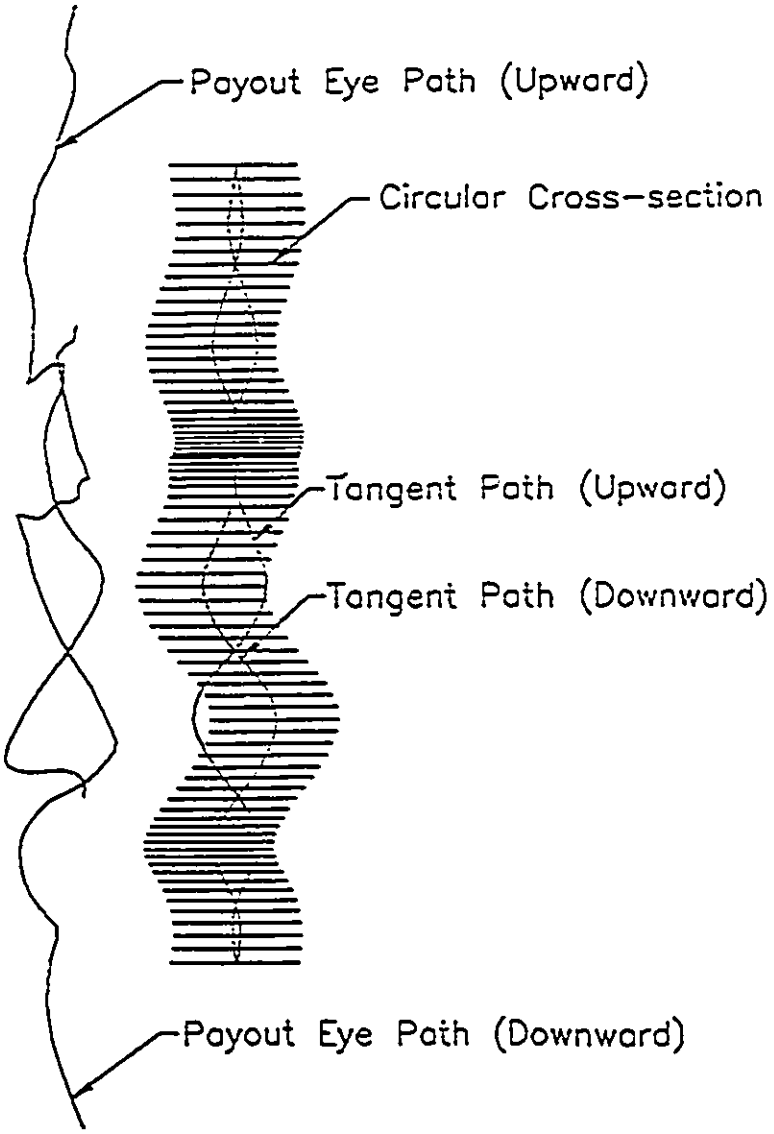

Figure 5.9: Payout Eye Collision Avoidance

CHAPTER 6

EXPERIMENTAL PROCEDURES, RESULTS and DISCUSSION

The details of the hardware and software developments for the robotic filament winding cell have been given in the previous two chapters. It is essential that the robotic filament winding cell's equipment and, concepts be evaluated experimentally. It is particularly important to determine the accuracy versus speed relationship for the different movement modes (discrete, fine and medium) using different mandrels (cylindrical and s-shaped). The following sections describe the procedures and results of the experimental work.

6.1: Accuracy and Repeatability

Accuracy is defined as the error in achieving a theoretically commanded location. For high performance components, the desired accuracy of fibre placement in wet filament winding is $\pm$ 2.0 mm, while for prepreg tape winding, the desired accuracy is + 0.5 mm. These are practical values that are used in industry. Middleton, et. al. [8]

reported that the accuracy of the fibre placement must be kept within the fibre band width in order to prevent slippage when the fibres are laid on the mandrel. This was reported in the order of 2 mm.

Repeatability is defined as the error in reproducing the same results time after time. The mandrel can repeatedly reproduce the same result within 0.2 degrees while the robot has a repeatability of $\pm$ 0.004 mm.

The filament winding cell is made up of hardware (mandrel drive, robot manipulator, and controller) and software. They are generally very accurate and have high repeatability; however, these devices have to work together in a cell. Therefore, the accuracy and repeatability depends on all the individual accuracies plus the accuracy in coordinating the individual items.

6.2: General Sources of Errors

It is appropriate to discuss the possible sources of error for the experiment as it may assist in the setup and procedures. Some sources of error are correctable and some are not. The correctable sources of error include the sources that were controlled in this research and some that are out of the scope of this thesis. Hence, errors for the fibre placement in a filament winding cell which can be due to the configuration, setup, hardware and software are discussed using these subheadings in the next section.

6.2.1: Correctable Sources of Error

Within the Scope of Thesis

The following sources of error were measured and controlled.

1) Definition of mandrel geometry

The accuracy of the filament winding cell is as good as the definition of the mandrel geometry. The geometry of the mandrel is produced in the AutoCAD either by explicitly using AutoCAD entities, or by interpolating amongst data measured from a model. For the model subsequently generated in AutoCAD there is no consideration of imperfections in the mandrel shape and surface or from measurement errors when digitizing the mandrel. Therefore, the computer will generate a theoretical model of the mandrel shape. When the fibre path is generated for this model, the path may be in error due to the assumptions of exact mandrel shape, perfect cross-section roundness, and imperfections on the surface. This type of error can be reduced by having a known geometry shape and precisely made mandrel. The tolerances for the mandrels will be discussed in Section 6.4.

2) Mandrel position relative to robot

The payout eye position is on a tangent to the mandrel surface. The calculation of the position involves the use of the relative position and orientation

between the mandrel and the robot. Any change in the relative position or orientation between the two machines can introduce errors in the position of the payout eye. This deviation of the payout eye can cause the fibre to be placed on a path different from the desired one. Also the orientation of the rotational centre of the mandrel drive with respect to the axis of link 1 is important. For the payout eye position calculations, the two axes are assumed to be aligned. These errors can be reduced by having the mandrel drive aligned and them permanently fixed relative to the robot. The alignment of the two axes was determined using a dial gauge attached to the end effector of the robot. The absolute deviation along the length of a 178 mm cylindrical mandrel was 0.1 mm in the x-z plane and 0.15 mm in the y-z plane.

3) Fibre tension

Tension is very important in all forms of filament winding. If the fibres are highly tensioned this may cause slippage of the fibre on the mandrel and deflection of the payout eye mechanism which would result in misplacement of the fibres on the mandrel. For this study the tension was limited to 10 Newtons.

4) Initial position setup

Initial conditions are very important in filament winding. Since, for example, geodesic paths depend only on the geometry of the mandrel, any

deviation in the starting position will cause placement of the fibre on a path different from the desired one.

Each experiment setup has different mandrel shapes and orientations. The changes in the orientation is accommodated by brackets holding the mandrel in different positions. When the mandrels are installed in the mandrel drive errors can be due to slight misalignments. These inaccuracies will cause the mandrel to follow a different path than the predicted one thus causing the fibre to be misplaced on the mandrel during the filament winding. The accuracy of the mandrel placement will be discussed in Section 6.4.

Out of the Scope of Thesis

The following sources of errors can be controlled but they are out of the scope of this thesis.

1) Linear Cartesian between points

Paths on the mandrel are divided into many segments; each segment has a start and end position. The robot will move from the start to the end positions in a straight line. The linear segments are an approximation to the calculated curvilinear path. The approximations will introduce errors to the filament winding path. This error can be reduced by dividing the path into shorter segments, but

the winding process will be slower and the memory required to store the positions will be large. This is a fundamental problem with all robots and cannot be solved in this thesis.

2) Lack of positional feedback for the robot and mandrel

The robotic winding cell operates under open loop control since the payout eye and the mandrel positions are not determined using a feed back sensors. This is a very complex problem which is well beyond the scope of this thesis.

3) Timing between the robot and mandrel drive

The robot and mandrel have their own controllers which operate autonomously. The lack of communication between the robot and mandrel drive causes mistiming. This problem can be solved by having an integrated controller for mandrel and robot, which will monitor the robot and mandrel positions and eliminate any mistiming.

4) Geometry and size of the payout eye opening

The fibres are guided onto the mandrel surface by the payout eye. The fibres exit the payout eye mechanism through an opening. The geometry of the opening is important as, for example, if the eyelet diameter is too small, the fibre will be damaged. On the other hand if the eyelet is too large then there is a loss

of fibre positional control.

The exit position of the fibres is assumed to be the centre of the opening in theory. However, the fibres are always situated at the edge of the opening in reality. Thus, the fibre can move around the edge of the opening during the winding. These unpredictable fibre movements causes error in the placement of the fibres on the mandrel. The hole diameter of the payout eye in this research was 3 mm.

5) Balancing

Robots are generally balanced using a fixed counterweight equal to half its load carrying capacity. For payloads larger than half the load carrying capacity of the robot, the net force on the linkages is downward. For payload less than half the load carrying capacity, the net force on the linkages is upward. The ASEA robot used in this study has a load carrying capacity of 6 kg. For this experiment the end effector is a very light payout eye mechanism attached to the wrist. In addition, the tension applied to the fibre was less than 10 newtons. Therefore, the robot is overbalanced and the robot's motors are working against the weight of the counterweight. This results in less effort being used in the upward direction motions.

6) Calibration

Joint alignment is important in achieving good accuracy. If the joints are misaligned, errors can result in the placement of the fibre as the robot will reach the given position with some error. Since the robot is a revolute type, the magnitude of the error will depend on the configuration of the robot's arms. This type of error can be eliminated by calibrating the robot or having an adaptive robot which can learn the magnitude of errors in different configurations. Both solutions were beyond the scope of this thesis.

7) Robot movement modes

The robot computer can command the robot to move in discrete, fine or medium modes. In discrete movement mode the robot positional accuracy is high since it is allowed to reach the given position before it is commanded to move to the next position. In fine movement mode, the robot has the liberty of coming within an accuracy zone of 1 mm radius of the given point. The medium movement mode is similar to the fine movement, except the radius of the accuracy zone is 10 mm. The smaller the accuracy zone, the slower will be robot, hence the filament winding process. One solution would be to develop an in-house controller.

8) Mandrel drive resolution

The auxiliary mandrel is rotated by a stepper motor drive. The stepper motor itself has a resolution of 400 steps per revolution which gives a resolution of 0.9 degree for each step. The rotation of the stepper motor is transmitted to the mandrel through a timing belt drive with a ratio of 13 to 60. This further reduces the resolution to 0.2 degree per step. Since the mandrel driver operates using integer values for the number of steps, the best accuracy of the mandrel driver is 0.2 degree. Since the winding paths are divided into many segments, they each have a calculated non-integer number of steps for the mandrel rotation. These values are rounded to nearest integer as mentioned above. Due to the large number of segments, the accumulation of round off error can be significant in the fibre placement. This error can be reduced by using a stepper motor with a higher steps per revolution, micro stepping motors or a DC servo motor with an encoder.

6.2.2: Others Sources of Error

The following sources of errors were not correctable.

1) Number of axis involved in winding

Simple shape mandrels have simple winding paths. These simple paths

need only two degrees of freedom of the robot to position the payout eye. Complex shape mandrels have complicated paths for the payout eye which requires at least six degrees of freedom. Each degree of freedom will contribute error in the winding. If large number of degrees of freedom are operating, the total error from the motors will be a combination of the errors of the individual motors. In addition, for a revolute type robot the errors of the degree of freedom are magnified by the length of the robot's arms. This error can be reduced by using the least number of axes as possible.

2) Inability to reach constant velocity

Movement between points involve acceleration, constant velocity, and deceleration phases. The duration of each phase depends on the speed and the distance between end points and the mode of operation. If the speed is high and length is short, the following will occur. In the beginning, the robot will try to accelerate to the desired speed; however, the short distance will require that the robot decelerate before reaching the desired speed. This causes the robot to come out of synchronization with the mandrel that is rotating at a constant angular velocity and will result in errors. The robot can be made to reach the desired speed by reducing the speed; however, this will make the winding process slower. Another solution is to increase the segment length between points, though, this could result in a loss of definition for the fine changes in geometry of the

mandrel.

6.3: Procedure for Robotic Filament Winding

The existing algorithm for 3-D asymmetric filament winding utilizes the concept of a 2-D generatrix closed curve representing the cross-section of the mandrel, that traverses a 3-D directrix curve. Figure 6.1 shows a schematic of the procedure for robotic filament winding. With reference to Figure 6.1, the surface of the mandrel and the stable fibre paths are found by using TRIASYM program developed by E. Bernard[7]. From these paths, selected coordinate points can be extracted and stored in a .DXF file format. This file contains the coordinate points used to calculate the payout eye positions.

Payout eye position is defined by the tangent to the path on the mandrel surface and the offset distance from the mandrel surface. The program TOOL creates the payout eye file and the associated mandrel position file. A sequence and run file is required for the Robot Control Communication Software (RCCS) program. These files contain the names of the path file to be executed in a sequential manner. The robotic filament winding cell will filament wind the mandrel until all the file names in the sequence and run file have been executed.

6.4: Experimental Setup

After the control structure was completed, experiments were conducted to determine the accuracy and repeatability of the complete system. Accuracy of the winding cell was tested for discrete, fine and medium movement types in both the up and down directions. A distance of 100 mm was used between the payout eye and the mandrel surface. The fibre paths were divided into 50 equal length segments. Three different winding speeds for each movement type were used to evaluate the effect on accuracy. For each speed three tests were carried out to assess the repeatability of the results. Therefore, a total of 378 tests were carried out to assess the accuracy and repeatability of the robotic filament winding cell. The results are presented in Appendix B and are plotted in the corresponding configuration sections.

Four configurations were used for testing the winding cell. The first three configurations involved the basic mandrel orientations that constitute many winding situations. The fourth can be considered as a combination of the previous three setups. The detail of the individual configurations are as follows:

1) Axis-symmetric Cylindrical Mandrel

This configuration uses a cylindrically shaped mandrel with a diameter of 63.5 mm and length of 178 mm. The tolerance for the diameter of the cylindrical mandrel was $\pm$ 0.05 mm. It has a 19 mm diameter shaft on each end of the mandrel. The mandrel was placed at the centre of rotation of the mandrel drive (Figure 6.2). Therefore, the accuracy of the winding cell was examined for the

case of a mandrel simply rotating. The mandrel is wound at an angle of 48.3 degrees to the axis of the mandrel which corresponds to two revolutions over the length.

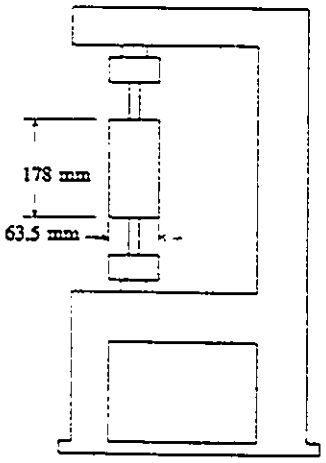

Figure 6.2: Axis-symmetric Cylindrical Mandrel Setup

2) Offset Axis-symmetric Cylindrical Mandrel

This configuration used the same mandrel as the axis-symmetrical cylindrical mandrel. However, the mandrel was offset from the centre of rotation of the mandrel drive. Mandrel centre-line offsets of 1, 2, and 3 times the radius of the mandrel were used for testing the ability of the winding cell to wind a

mandrel moving in an eccentric motion (Figure 6.3). The location of the mandrel in the mandrel drive using brackets was within $\pm$ 0.5 mm. As in the first configuration, the mandrel was wound at an angle of 48.3 degrees to the axis of mandrel.

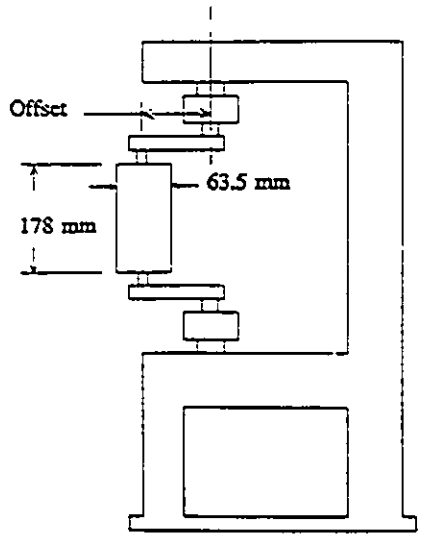

Figure 6.3: Offset Axis-symmetric Cylindrical Mandrel Setup

3) Axis-asymmetric Cylindrical Mandrel

The same mandrel from the previous tests was used in this configuration. In this experiment, the mandrel was eccentric as in configuration 2, except that

it was also at an angle to the rotational centre of the mandrel drive (Figure 6.4). The angle was created with unequal offsets at the top and bottom of the mandrel. Differences of mandrel centre-line offset of 1, and 2 radii of the mandrel were used to provide the angle (Figure 6.4). The location of mandrel in the mandrel drive using the brackets was within ± 0.5 mm. This configuration made the mandrel trace a conical shape. The mandrel was wound at an angle of 48.3 degrees to the axis of mandrel.

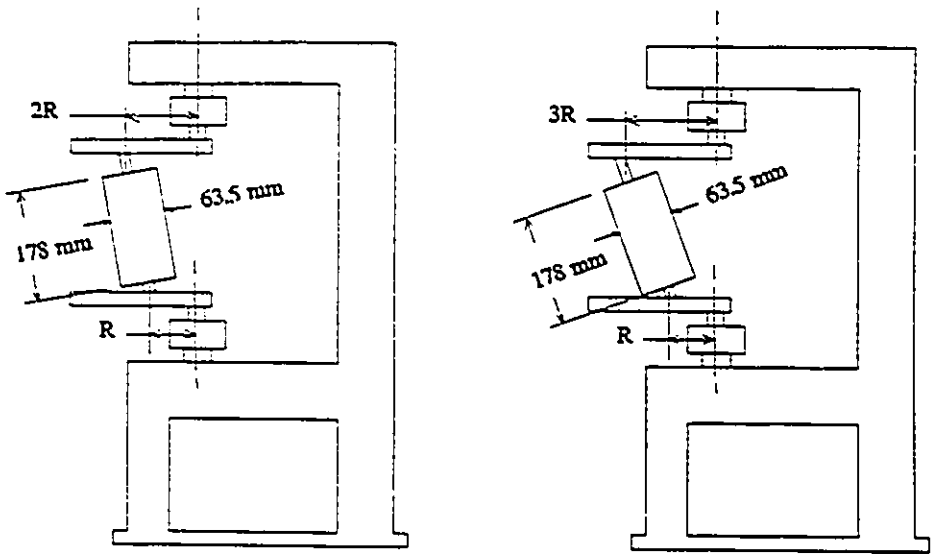

Figure 6.4: Axis-asymmetric Cylindrical Mandrel Setup

4) Axis-asymmetric S-bend Mandrel

The asymmetric mandrel used in this configuration had an S-shaped geometry with 57 mm diameter and 350 mm length (Figure 6.5a). The maximum diametrical difference between the X axis and Y axis was $\pm$ 1.3 mm (Appendix C). The measured spine geometry is described in Table 6.1 by offset distances from the rotation axis with accuracy of $\pm$ 0.5 mm. It has an offset shaft on each end of the mandrel for fastening to the mandrel drive. The centre of rotation of the mandrel was aligned with the centre of rotation of the mandrel drive. The shape of this mandrel can be considered as a combination of the previously tested geometries. The mandrel was wound at fibre angle of 45 degrees to the mandrel spine. The initial position was tangent to mandrel at a position 90 degree to the mandrel circumference (Figure 6.5b). The fibre path is for the case of a geodesic path.

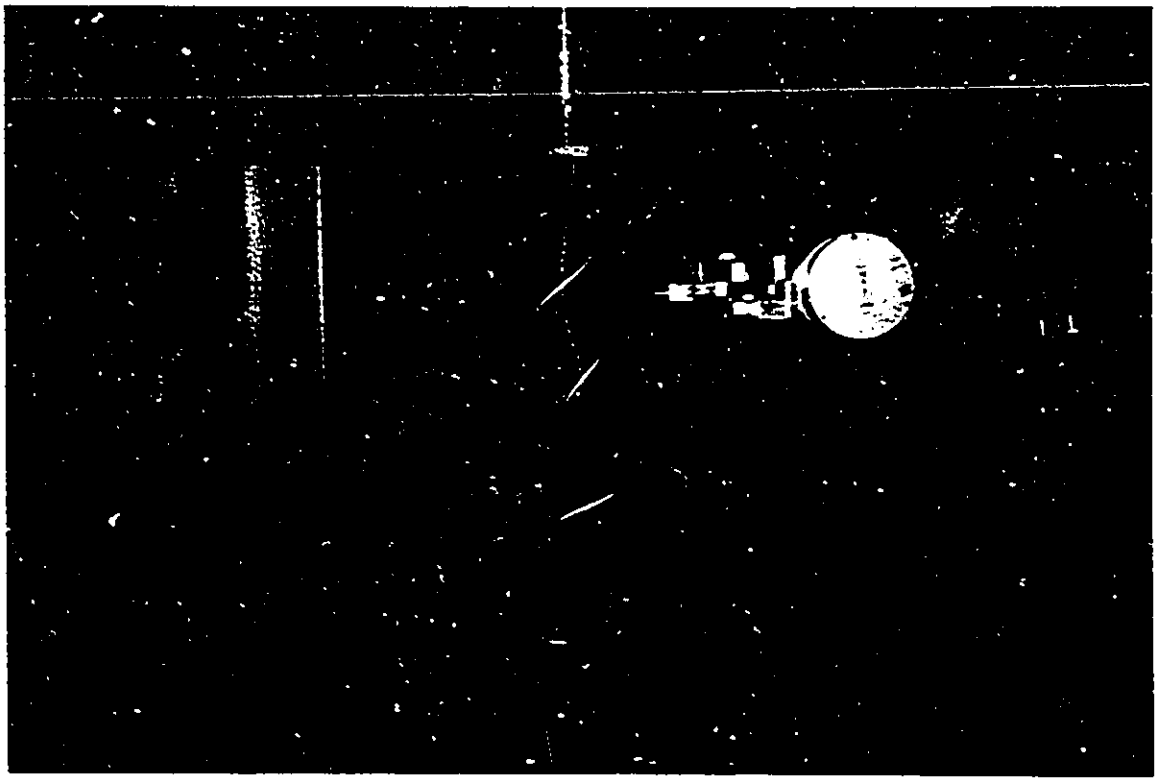

Figure 6.5a: Axis-asymmetric S-bend Mandrel

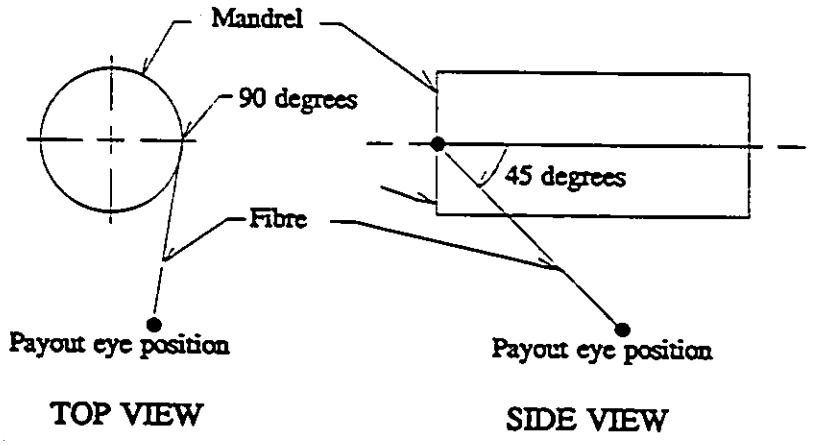

Figure 6.5b: The Initial Position of the Fibre

Table 6.1: S-bend Mandrel Spine Geometry

Distance (mm)	Offset distance (mm from centre of rotation of mandrel (mm)	Distance (mm)	Offset distance from centre of rotation of mandrel (mm)
0	0.0	180	15.0
10	2.5	190	17.0
20	4.0	200	18.0
30	6.0	210	19.0
40	7.5	220	20.0
50	8.5	230	20.0
60	9.0	240	19.0
70	10.0	250	17.5
80	10.0	260	16.0
90	9.5	270	15.5
100	7.0	280	14.0
110	5.0	290	12.0
120	3.0	300	11.0
130	0.0	310	9.0
140	5.0	320	7.0
150	6.0	330	4.5
160	9.0	340	2.0
170	11.5	350	0.0

6.5: Experimental Data Collection

The experimental mandrel paths were determined using small diameter (0.25 mm) hard twine. Ink was impregnated onto the twine by a foam roller (Figure 4.4) which had

been soaked in ink. A sheet of paper on which the desired path had been drawn was taped to the cylindrical mandrel. In all cases the ink from the twine created a distinct line on the mandrel covering (Figure 6.6a). For the s-shaped mandrel a white line is drawn on the mandrel surface (Figure 6.5a).

6.6: Path Error Estimation

In the experiments the actual path always de iated from the desired path in a bow shape. The accuracy can be judged by the maximum deviation between the desired and the experimental paths or the area between the two paths (Figures 6.6a and 6.6b). These two methods were evaluated to determine which is a more appropriate estimate of path error.

The area between the two paths can be approximated by a parabola, which is made up of the height (maximum deviation distance) times 4/3 of the base (length of fibre path) [23]. Since the base is common to all test that is conducted, the only difference is the variable height. Therefore, the area between the desired and experimental paths and the maximum deviation differ by a scale factor of 4/3, hence the area between the two paths or the maximum deviation distance can be use for indicating the error. In this research, the maximum deviation distance between the two paths was recorded as the error of the test.

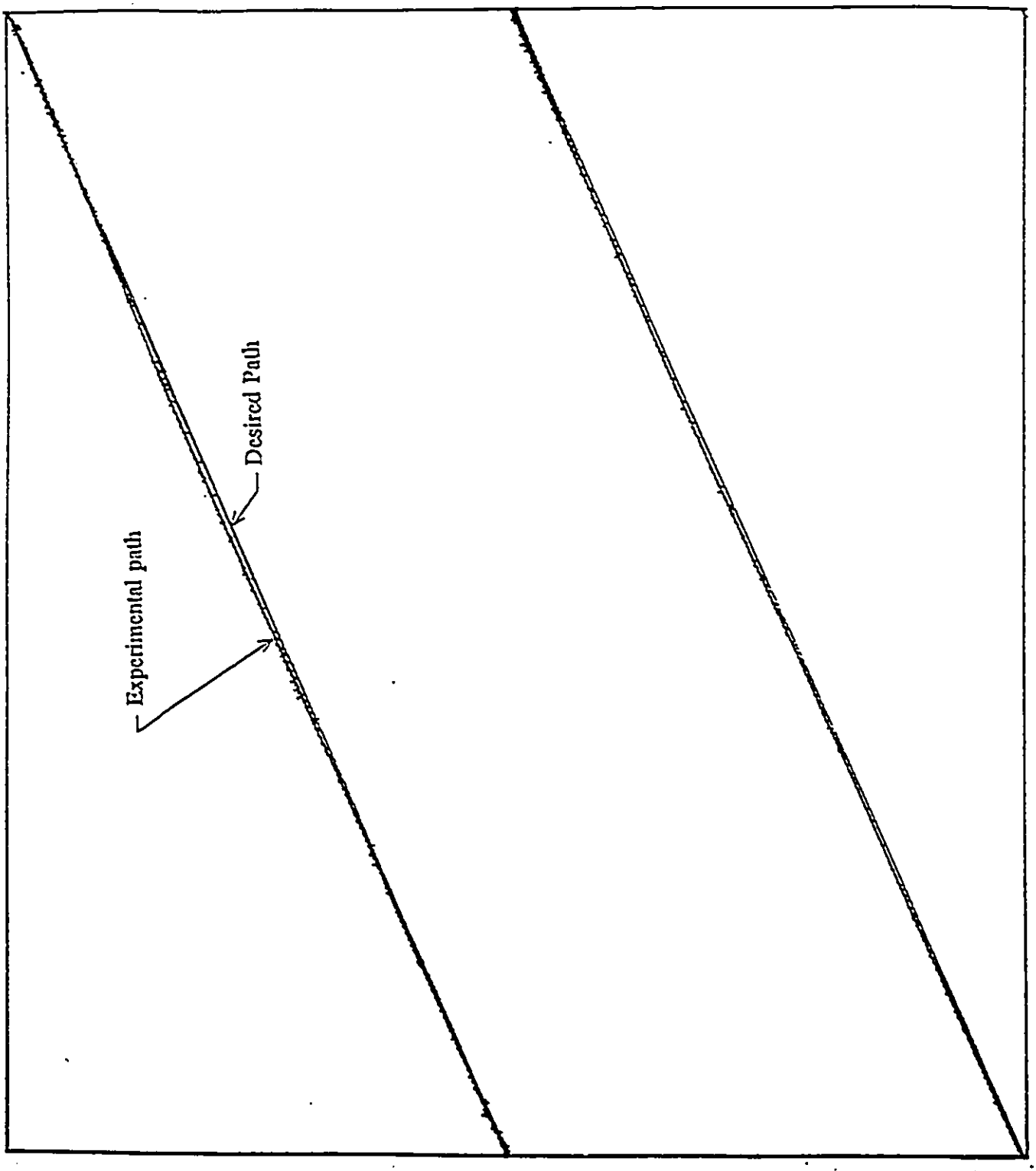

Figure 6.6a: Typical Tracing for Cylindrical Mandrel

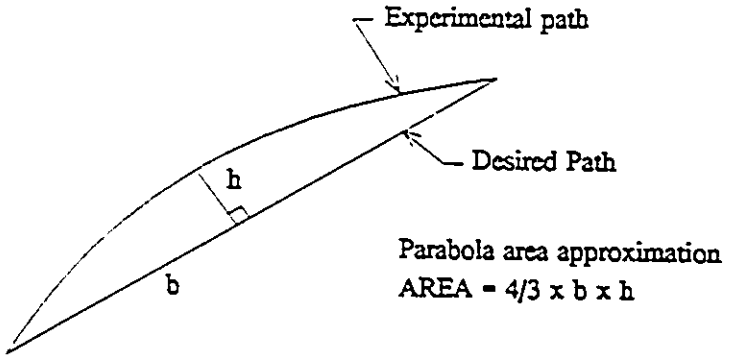

Figure 6.6b: Area Between Desired and Experimental Path

The accuracy of the winding process is measured by determining the deviation between the wound path and the desired path as discussed in previous section. Since the measuring device (a vernier caliper) is graduated to 0.5 mm, the errors were read to the nearest 0.25 mm. This is reasonable as the twine used in the experiment has a diameter of 0.25 mm. Thus, the measured accuracy of 0.25 mm is very similar to the maximum industrially achievable accuracies of 0.25 and 0.5 mm.

6.7: Segment Length Versus Robot Speed

As the distance for the robot to travel decreases the time taken to complete the movement also decreases. Even when the distance reaches a zero length, the robot will still require some time. This time is needed for interpreting and executing the

instructions. An experiment was carried out to determine a critical segment length for which this is negligible. This experiment involved the robot travelling various vertical distances using fine and medium movement modes. A micro computer was used for recording the time by determining where it started and stopped the timer on the signal from the robot computer (Table 6.2). Figures 6.7a and 6.7b present the total time required to complete the move versus the segment length (distance travelled). The slower velocity of 100 mm/s shows a linearly increasing curve and has an intersect of 550 msec. Figure 6.7b shows a plateau at 710 msec and 550 msec for fine and medium modes, respectively. Speeds of less than 500 mm/s do not have a plateau; the total time increases with segment length. The plateau represents the time that is needed by the robot to interpret and execute the instruction plus the time needed to control the servo motors so no large oscillations will occur at the robot linkages. This time needed for the robot computer to control the motors depends on the maximum velocity given. Therefore, the medium movement mode has a lower plateau time than the fine mode.

The existence of a plateau region means that the actual time will be greater than the theoretical time (segment length/robot speed) due to the acceleration and deceleration phase. As the times associated with these phase becomes small compared to the total time, the actual time will approach the theoretical time. Figure 6.7c is a plot of the ratio of actual time to theoretical time versus segment length. Figure 6.7d shows that even for slow speed (100 mm/s) of medium movement mode, ratio is still above 2 for segment lengths equal to length of mandrels. Therefore, no realistic critical segment length exist.

Table 6.2: Time Taken for the Robot Payout Eye to Move Various Vertical Segment Lengths

Distance (mm)	Robot Speed							
	2000 mm/s		1000 mm/s		500 mm/s		100 mm/s	
	Fine (ms)	Medium (ms)	Fine (ms)	Medium (ms)	Fine (ms)	Medium (ms)	Fine (ms)	Medium (ms)
300	1050	930	1100	930	1260	1210	3620	3520
250	1050	880	1050	930	1210	1090	3130	2960
200	930	820	930	880	1100	980	2680	2530
150	880	710	880	770	990	880	2140	1970
100	820	710	830	770	880	770	1630	1480
80	820	660	830	710	770	660	1430	1270
60	770	660	770	660	770	660	1210	1100
50	770	600	770	660	770	660	1100	990
45	770	600	770	610	770	610	1040	940
40	770	600	770	610	770	610	980	880
35	710	600	720	610	770	600	930	820
30	710	600	710	610	710	600	930	770
25	710	540	710	600	710	600	880	710
20	710	540	710	550	710	600	820	660
15	710	540	710	550	710	600	820	600
10	710	540	710	550	710	600	770	600
5	710	540	710	550	710	600	660	550
2	710	540	710	550	710	600	660	550

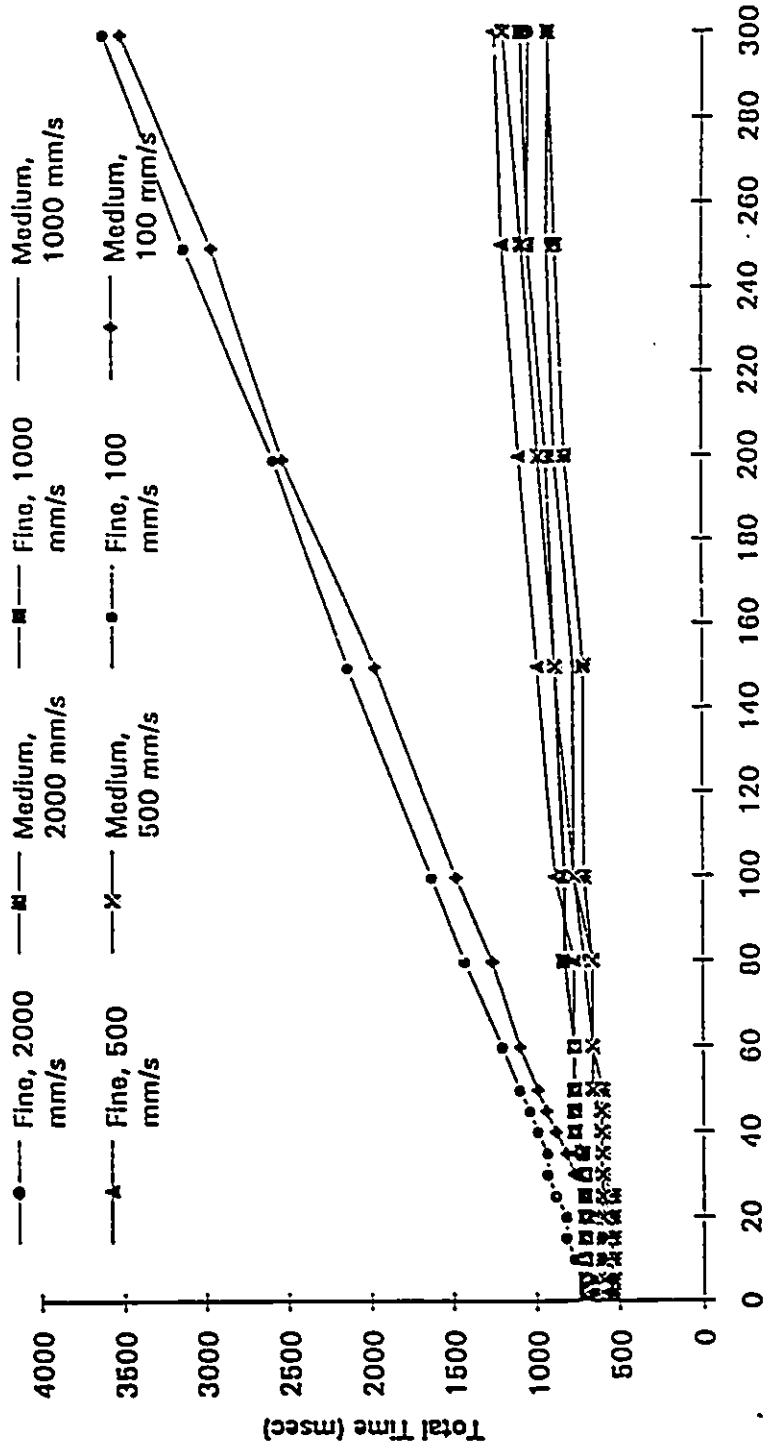

Figure 6.7a: Total Time Versus Segment Length at Various Robot Speed

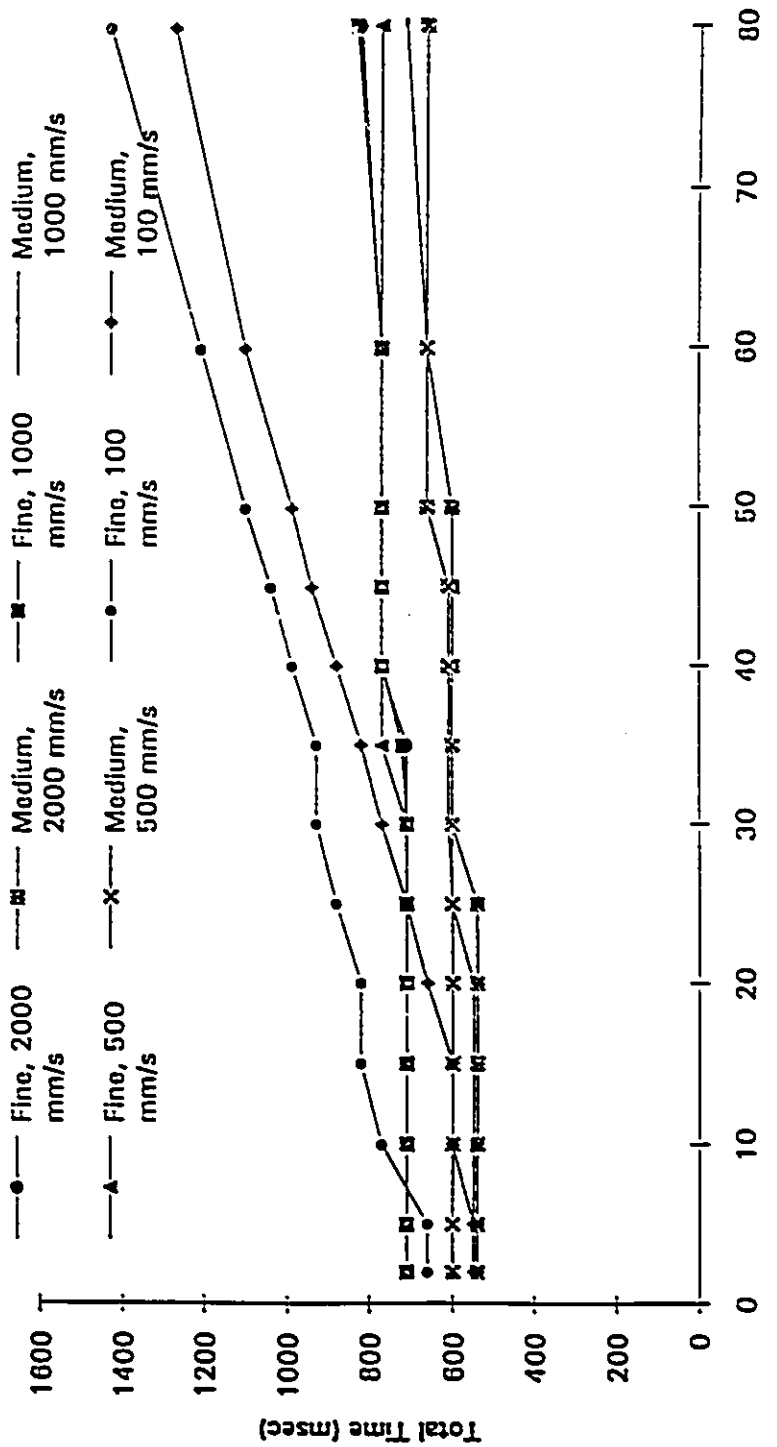

Figure 6.7b: Exploded View of Total Time Versus Segment Length at Various Robot Speed

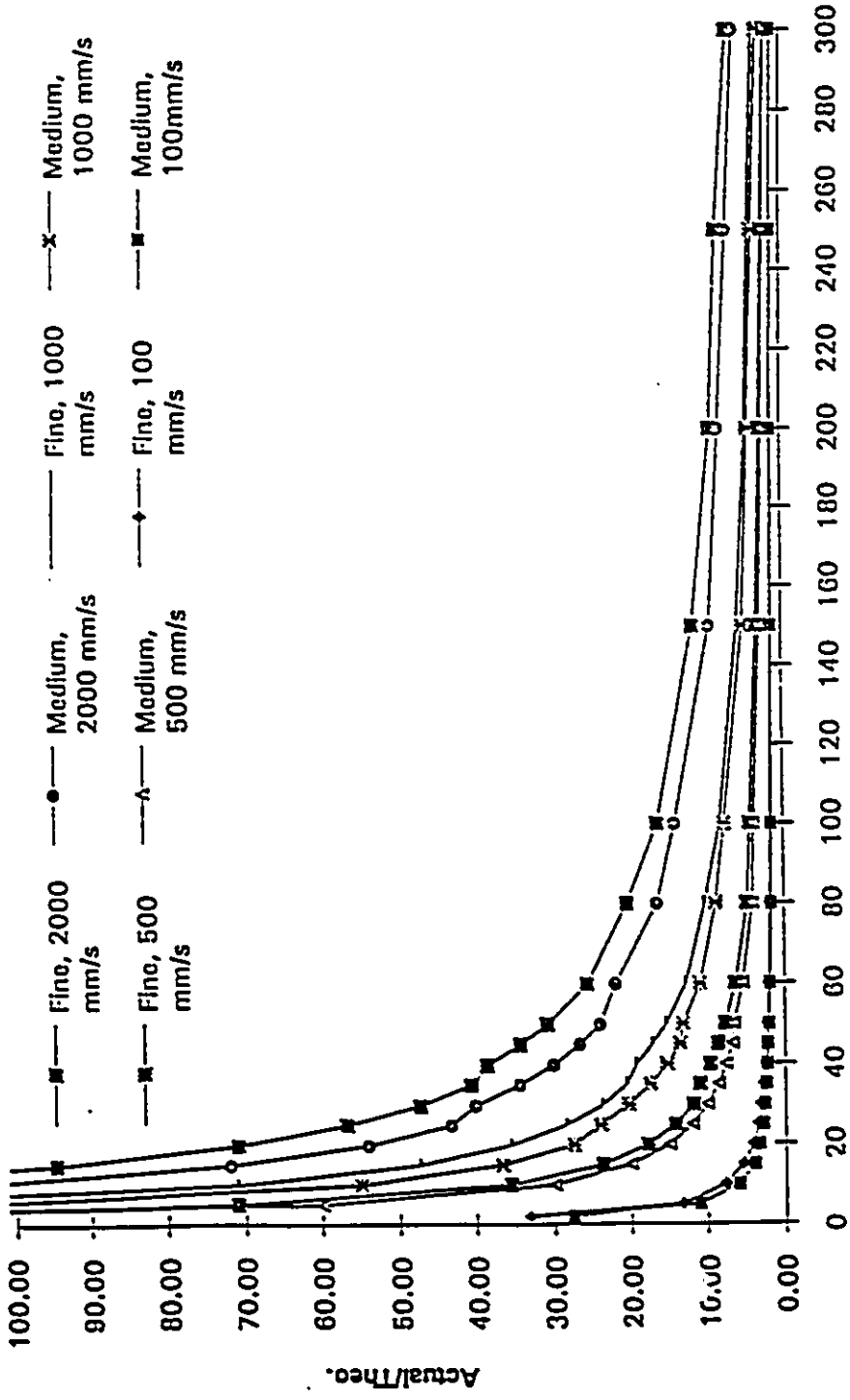

Figure 6.7c: The Ratio of Actual Time to Theoretical Time Versus Segment Length at Various Robot Speed

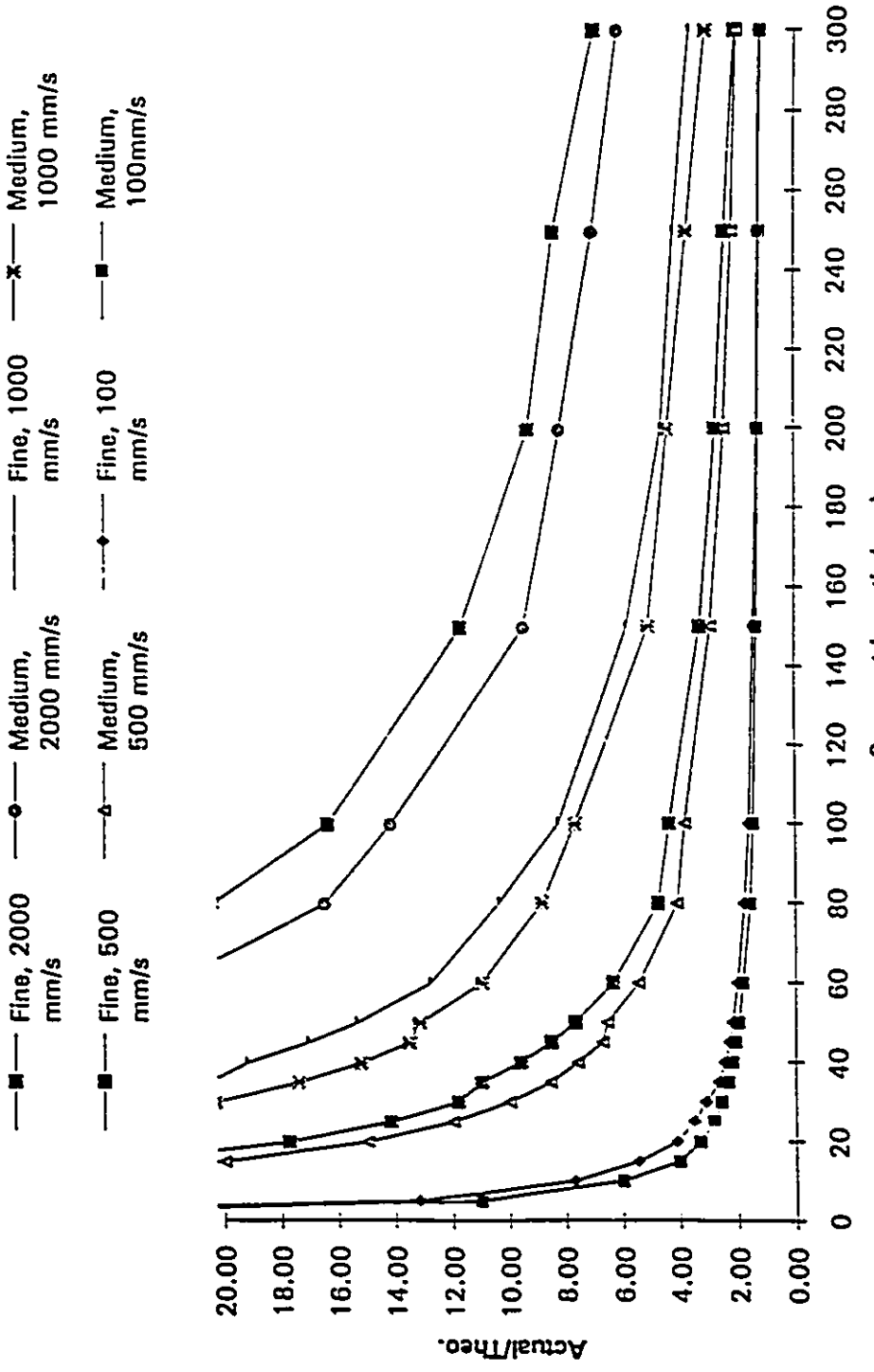

Figure 6.7d: Exploded View of the Ratio of Actual Time to Theoretical Time Versus Segment Length at Various Robot Speed

6.8: Interpretation of Results

All the graphs in the following chapters show discrete, fine and medium movement modes using different line types. They also present the three speeds at which the three modes were tested. Since, three tests results carried out at each of those speeds, the range of values are also shown. For comparison purposes, the upward winding direction and the corresponding downward winding direction results are plotted side by side.

6.8.1: Discrete Movement Mode Tests

Discrete movement mode was tested for 3 winding speeds (see mandrel speed in Appendix B). At each winding speed 3 experimental runs were carried out. The TOOL program (Section 5.6) used the winding speed to calculate the robot positions and speeds. These data were stored into a file. After the robot and mandrel were placed at the initial setup position, they were commanded simultaneously by sending data from the file by a personal computer. The personal computer sent the data through the communication link for the robot and mandrel. These data were sent one at a time, and executed without storing the data by the robot and mandrel. The next data was sent only when the robot and mandrel has come to a stop. This tests assumed simultaneous start and stop, eliminating the acceleration and deceleration effect of the robot and mandrel.

The errors between the experimental and desired paths for different winding speeds were collected (Appendix B). When these errors were plotted (for example,

Figure 6.8), it showed a larger error for the faster winding speed and lower error for the slower winding speed. At the slower winding speed the magnitude of the errors are found to be very similar. These errors were due to the positioning and accuracy in the initial setup. The faster winding speed has a larger error than the slower speed because of the errors are magnified by the delay in the robot response to the command. The delay is caused by the time taken for the message from the personal computer to transmit through the communication link and the time to interpreted the message by the robot computer. This delay caused the robot to start later than the mandrel and to loose coordination between the robot and mandrel. Therefore, larger errors are found in the faster winding speeds.

6.8.2: Fine and Medium Movement Modes Tests

Fine and medium movement modes were tested for 3 winding speeds (see mandrel speed in Appendix B). At each winding speed 3 experimental runs were executed. With the winding speed, the TOOL program calculated the robot positions and speeds. These data were stored in a file. These files were sent to the robot memory. The robot computer used the data from the robot memory. In these experimental runs the robot and mandrel were moved to the start position and run under the control of the robot computer. This eliminated the need for constant communication link and the consequent delay problem. In these tests the robot acceleration and deceleration are assumed negligible.

The robot speed was based on a constant speed in each segment. In the test the mandrel was given a constant angular velocity to keep the start and final point of winding.

The error were found to be larger for the faster winding speed and smaller for the slower winding speed. At slower winding speed the errors are found to be similar. The errors were caused by the positioning and accuracy in the initial setup. In these tests the mandrel rotates at a given constant angular velocity and the robot was following the predetermined payout eye path by accelerating and decelerating. Thus, the faster winding speed magnified the coordination errors higher than the slower winding speed. In addition, the fine movement mode has a tolerance zone of 1 mm radius and the medium movement mode has a 10 mm radius. These zones causes the smoothing of the robot path (Section 5.4.2). The extent of the smoothing is dependent of the robot movement speed. When the speed of the robot movement increases, the smoothing of the robot path increases. Therefore, the errors are more prominent at the faster winding speed.

6.8.3: Transition Point

The curve for each movement mode shows the error decrease with the decrease in winding speed and then a plateau region as the total time increases. This inflection point indicates the most significant point called the transition point. The transition point represents the smallest error for the smallest total time (or least amount of error for the highest speed) for that movement mode.

Therefore, the transition point value will be used for discussion in the following sections.

6.9: Cylindrical Mandrel

In this section, the results of the axis-symmetric, offset axis-symmetric, and the axis-asymmetric configuration experiments using a cylindrical mandrel will be discussed. For each configuration the results will be discussed in term of repeatability, winding time and path deviation errors.

6.9.1: Axis-symmetric Cylindrical Mandrel

This experiment tested the ability of the winding cell to wind a simple mandrel rotating about its centre of rotation. The accuracy and the total time to complete a winding are plotted in Figures 6.8. Figure 6.8 shows the results of winding in the downward and the upward direction plotted side by side.

These two figures show the maximum difference between the three repeated tests at each winding speed (Appendix B) was approximately 0.2 mm for discrete movement mode and 0.5 mm for fine and medium movement modes. Thus, the repeatability of the results in robotic filament winding for this mandrel configuration is within the accuracy that is required by industry (Section 6.1).

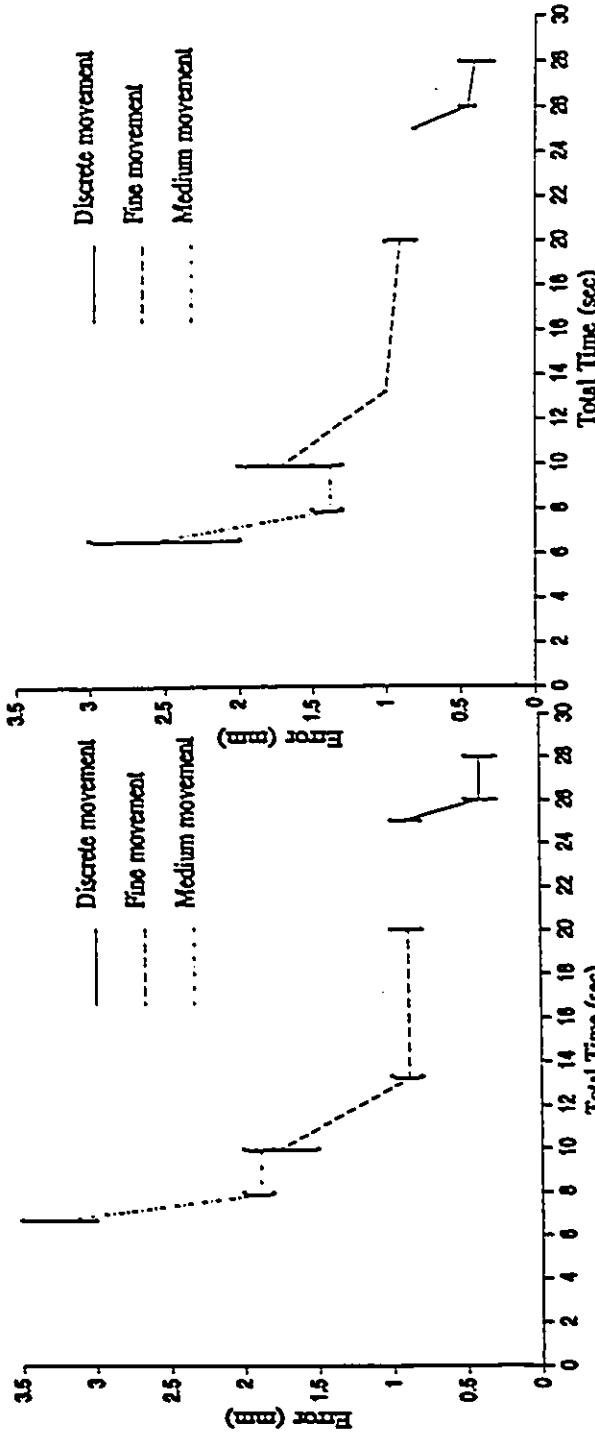

Figure 6.8: Downward and Upward Winding of An Axis-symmetric Cylindrical Mandrel

The results show that the total time taken to complete a winding in the up and down directions are the same. The discrete movement mode has the longest total time of 26 seconds while the fine movement mode took 13.3 seconds (0.5 times) of the total time of the discrete movement mode. The medium movement mode experiment required 8.0 seconds, approximately one-third of the total time of the discrete movement mode. The discrete movement mode total time was longest because of the winding cell has to stop at every given point for communication between the robot and the micro computer and the micro computer and the PC-21 indexer card. The fine and medium movement modes do not stop between points but move on a continuous basis.

The discrete mode had the best accuracy, while the fine movement mode had approximately twice the error of the discrete movement mode. The medium movement mode had the largest error, approximately four times the error of the discrete mode. Hence, the errors increased as the movement mode changed from discrete, fine to medium. Peters, et. al., [24] published an error of 0.75 mm in their conventional modified lathe winding machine. This value compared favourably to the result of the 0.4 and 0.5 mm of the discrete mode in up and down directions, respectively.

For both upward and downward winding directions there was no change in accuracy observed. This is because motion of two arms only is required to guide the payout eye along a straight line. Thus, only the two joints involved are sources of error. The upward and downward winding direction gave a similar accuracy for the discrete and fine mode. However, the accuracy is higher in the upward direction for the medium mode. Since this project utilized a overbalanced robot, the upward motion will have less strain on the robot motor and result in a higher accuracy. The error in the discrete movement mode which is typically very small (0.5 mm) is probably due to the error in the setup and the robot. Any misalignment or error in the initial conditions in the setup will cause a difference in the values from the theoretical model. This error is very near the minimum value expected and therefore could be very difficult to improve. The errors for the fine and medium movement modes are due to the robot not reaching the desired positions (ends of segments). In the fine mode, the robot computer has a 1 mm error radius zone while the medium mode has a 10 mm error radius zone. These error zones gave the robot the liberty of reaching the desired position or just coming within these zones (Section 5.4.2) depending on the previous speed and direction. Furthermore the lack of coordination of motion between the robot and the mandrel contributed to the errors in the results. The other source of error is the assumption of constant velocity movement by the robot without the acceleration and deceleration portion.

Therefore, the winding accuracy on a simple axis-symmetrical cylindrical mandrel was found to be very high for the discrete movement, but has the longest total time. The accuracy and total time decreases as the movement types change from fine to medium mode. If the product application is of this form requires high precision fibre placement, the discrete mode should be utilized. If precision is not required, the fine and medium modes can be used to save manufacturing time.

6.9.2: Offset Axis-symmetric Cylindrical Mandrel

A cylindrical mandrel moving in an eccentric motion is the next configuration that was studied. Three offset distances of 1, 2 and 3 times the mandrel radius were used; each case was tested in the up and down directions (Figure 6.3). The results are plotted in Figures 6.9 to 6.11. Figure 6.9 presents the results for the downward and upward winding of the mandrel with a 1 radius offset. Figure 6.10 shows the results for the downward and upward winding of the mandrel with a 2 radius offset. The results for the downward and upward winding of the mandrel with a 3 radius offset are given in Figure 6.11.

As before, the error results of three repeated tests at each speed give a difference of approximately 0.2 mm for the discrete and 0.5 mm for the fine and medium movement modes (Appendix B). This demonstrates again that the robotic filament winding has a very good repeatability.

The results again show that the total time for each experiment in the up and down direction is the same. With reference to Figure 6.9, the graphs show that the discrete mode had the highest total time of 28.00 seconds, the fine mode had 15.40 seconds (0.55 times the discrete mode), and the medium mode had 11.10 seconds (0.39 times the discrete mode). Figure 6.10 shows that the discrete mode has the lowest total time of 32.00 seconds, the fine mode had 20.00 seconds (0.63 times the discrete mode), and the medium mode had 13.30 seconds (0.42 times the discrete mode). Again, Figure 6.11 shows the winding results of a 3 radii offset of the mandrel.

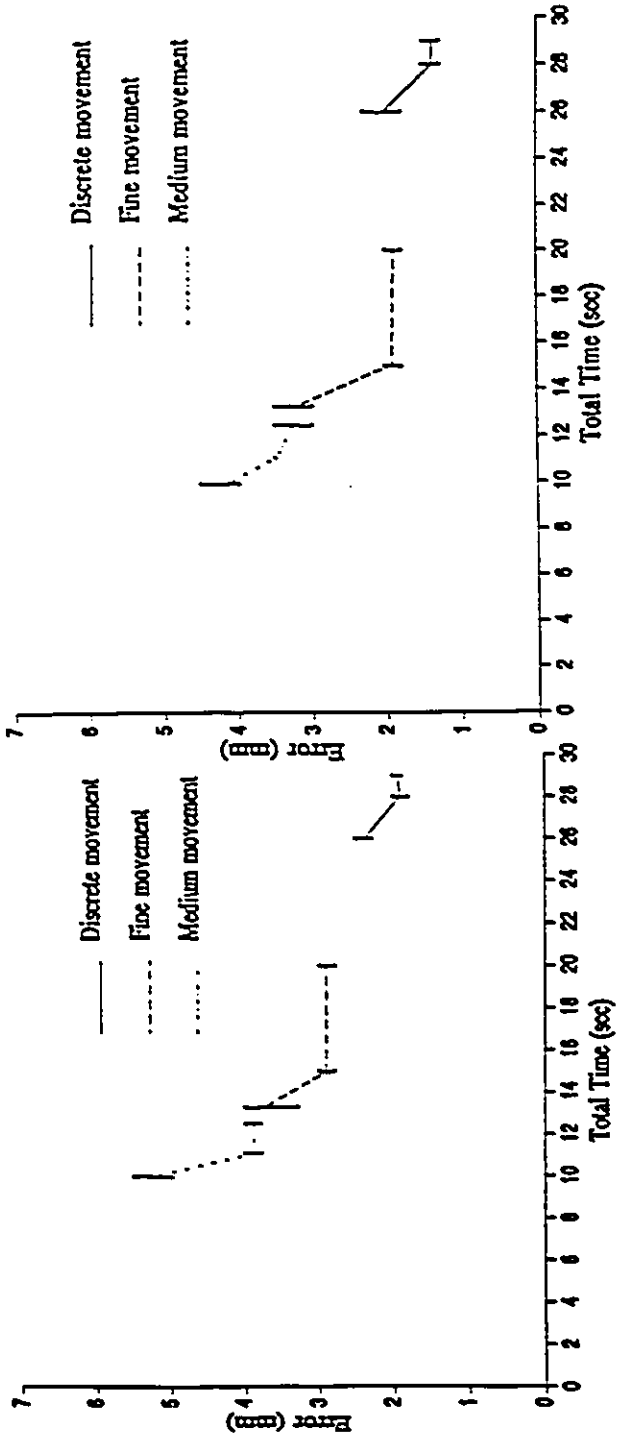

Figure 6.9: Downward and Upward Winding of a 1 Radius Offset Axis-symmetric Cylindrical Mandrel

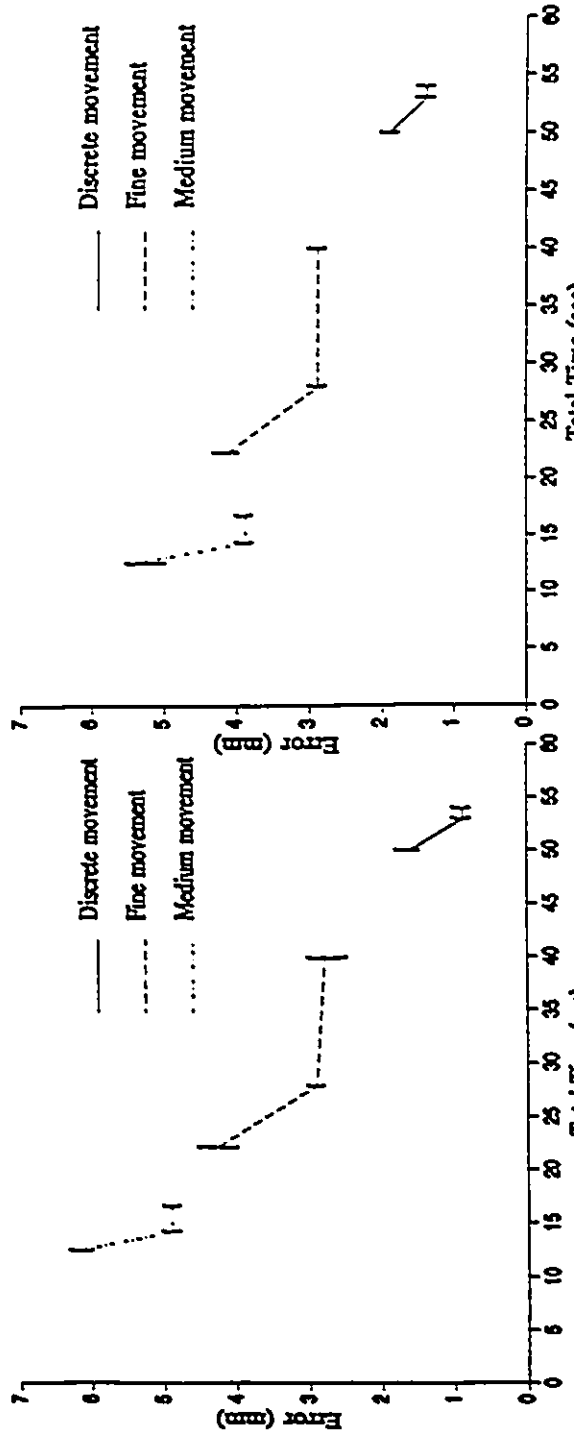

Figure 6.10: Downward and Upward Winding of a 2 Radius Offset Axis-symmetric Cylindrical Mandrel

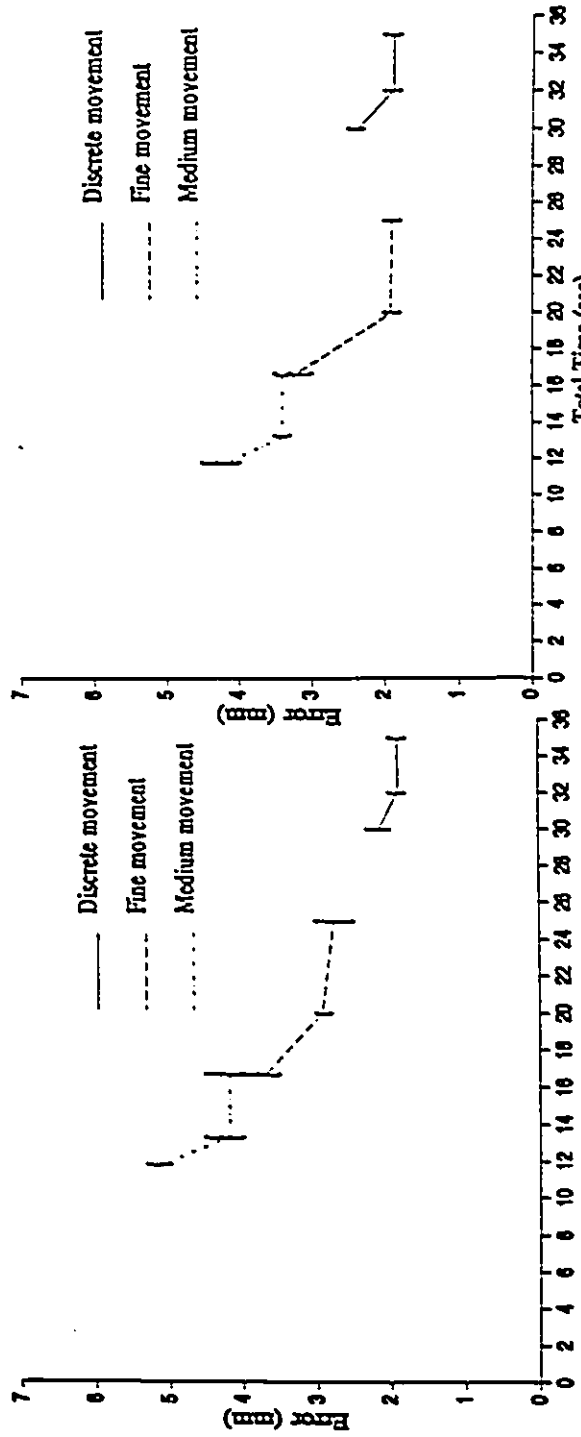

Figure 6.11: Downward and Upward Winding of a 3 Radius Offset Axis-symmetric Cylindrical Mandrel

Similarly, the discrete mode had a highest total time of 53.00 seconds, the fine mode had a 28.60 seconds (0.54 times the discrete mode), and the medium mode had 14.30 seconds (0.27 times the discrete mode). The discrete mode always had the longest total time because the discrete mode makes the system stop at each segment end point. The fine and medium modes do not stop at the segment end points but come within the tolerance zone of the end points of the path, thus achieving a higher speed.

The results show that the total time increased as the offset distance changed in the discrete mode. The total time increased from 28.00 seconds for the 1 radius offset to 53.00 seconds (1.90 times) for the 3 radius offset due to the stops at segment end points and greater movement of the robot. In fine mode there was an increase from 15.40 to 28.60 seconds (1.86 times) for the geometry change. In the medium mode the increase was from 11.10 to 14.30 seconds (1.27 times), which is the least effect of the geometry change in this group of tests. Therefore, it has taken longer time to complete the winding as the degree of offset increased; however, the degree of offset had the least effect on the total time of the medium mode. The effect is less for the fine and medium due to the smoothing (reducing the distance travelled by the robot) of the payout paths and moving on a continuous basis.

The comparison of the errors is presented in tabular form (Tables 6.3 to 6.5) in which the values are normalized using the error of the axis-symmetric cylindrical mandrel discrete movement mode (0.5 mm). This was considered as the best accuracy achievable with the present robotic winding cell.

Table 6.3: Results of Downward and Upward Winding of a 1 Radius Offset

Modes	Downward Winding Error (mm)	Normalized to Discrete mode	Upward Winding Error (mm)	Normalized to Discrete Mode
Discrete	1.8	3.6	1.5	3.0
Fine	2.8	5.6	1.8	3.6
Medium	3.8	7.6	3.5	7.0

Table 6.4: Results of Downward and Upward Winding of a 2 Radius Offset

Modes	Downward Winding Error (mm)	Normalized to Discrete mode	Upward Winding Error (mm)	Normalized to Discrete Mode
Discrete	2.0	4.0	1.8	3.6
Fine	2.8	5.6	2.0	4.0
Medium	4.3	8.6	3.5	7.0

Table 6.5: Results of Downward and Upward Winding of a 3 Radius Offset

Modes	Downward Winding Error (mm)	Normalized to Discrete mode	Upward Winding Error (mm)	Normalized to Discrete Mode
Discrete	1.0	2.0	1.5	3.0
Fine	2.8	5.6	2.8	5.6
Medium	5.0	10.0	4.0	8.0

Tables 6.3 to 6.5 show that the normalized error increases with the change in the movement modes. The normalized values of the upward winding direction are found to be generally lower than the downward direction (Figures 6.9, 6.10, 6.11). The discrete mode had the lowest error, while the fine mode has an error larger than discrete, and the medium mode had twice the error magnitude of the discrete mode. The upward winding direction gives a better accuracy than the downward direction. This can be accounted for by the fact that the robot is overbalanced which will reduced the strain on the motors as the robot moves in the upward direction.

From Tables 6.3 to 6.5, the error of each movement mode increases as the configuration is changed from 1 to 3 radii offset. Except for the 3 radii offset cases, the discrete movement shows a decrease in the error (Figure 6.11). The error is expected to increase as the offset distance increases because the errors are magnified. The larger offset required the mandrel move in a larger circle which makes the robot follow longer distances with complex paths. This involves a higher number of degrees of freedom in motion with longer distances to travel. These factors will magnify the error in the

movements. This increase in distances between points will increases the error due to the approximation of a curvilinear path with straight paths. The straight path of the robot is shorter than the curve path from the theoretical model making the robot and mandrel lose synchronization. In addition, the accuracy from the setup and initial conditions becomes very critical. Any setup or starting condition error will also be magnified in the winding process. Again, the discrete mode has the least error due to the payout eye reaching the desired positions and coming to a stop before moving onto next position. However, the fine and medium modes have large errors because of smoothing the corners (reducing the distance travelled by the robot) to reach a higher speed.

Therefore, the winding accuracy on an offset axis-symmetrical cylindrical mandrel was found to be very high for the discrete movement, but has the longest total time. The accuracy and total time decreases as the movement types change from fine to medium mode. If the product application is of this form and requires high precision fibre placement, the discrete mode should be utilized. If precision is not required, the fine and medium modes can be used to save manufacturing time.

6.9.3: Axis-asymmetric Cylindrical Mandrel

This test involved the winding of mandrel rotating in a conical shape. Two configurations were used in assessing the accuracy and the total time to complete the winding process. The first setup used a 1 radius difference between the top and bottom fixtures. The second setup had a 2 radii difference between the top and bottom fixtures (Figure 6.4). Each setup was tested in the up and down winding directions. The results of the two setups are collected and plotted in the Figures 6.12 and 6.13. Figure 6.12 present the downward and upward winding of the mandrel with the first setup. Figure 6.13 indicate the results for downward and upward winding of the mandrel with the second setup.

Similar to the previous set of experiments, three repeated tests at each winding speed show a difference of approximately 0.2 mm for the discrete and 0.5 mm for the fine and medium movement modes (Appendix B). These results indicate that the robotic filament winding cell has a high repeatability.

The results show that the total time of winding in up and down direction was similar for each movement mode. Figure 6.12 shows that the discrete mode had the highest total time of 43.00 seconds, the fine mode had 25.00 seconds (0.58 times the discrete mode), and the medium mode had 16.70 seconds (0.39 times the discrete mode). Figure 6.13 shows that the discrete mode have the highest total time of 43.00 seconds, the fine mode had a 25.00 seconds (0.58 times the discrete mode), and the medium mode had a 15.40 seconds (0.36 times the discrete mode).

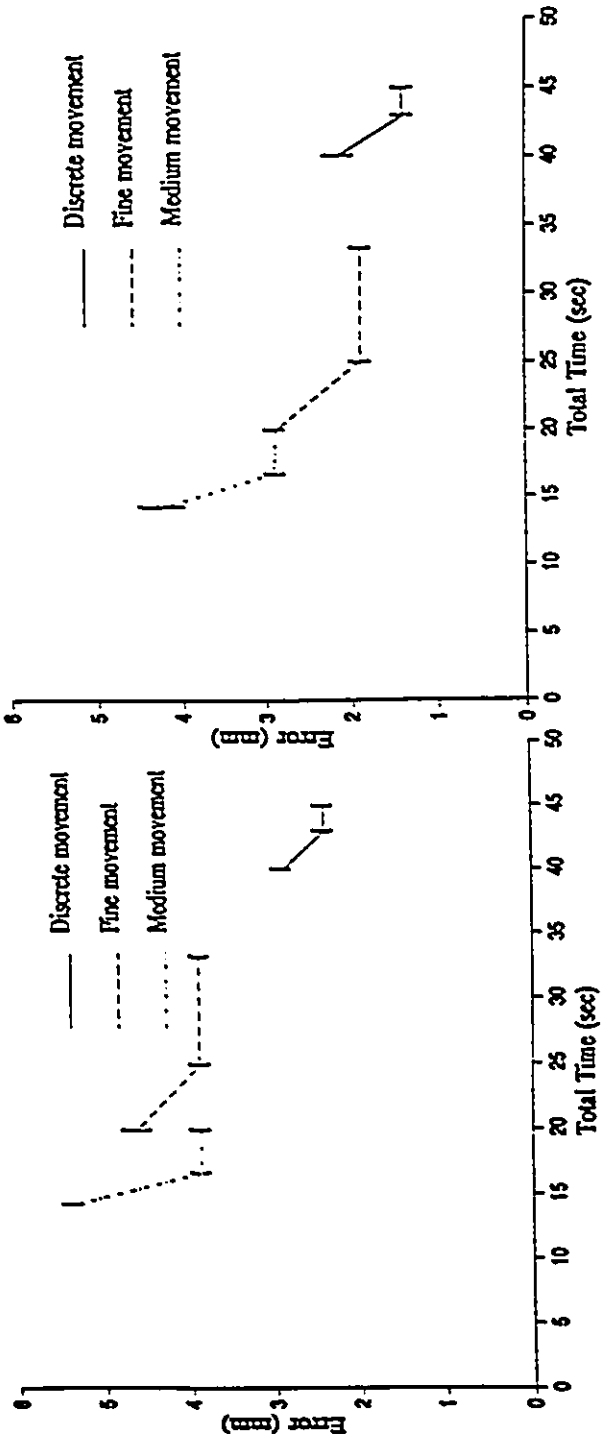

Figure 6.12: Downward and Upward Winding of a 1 Radius Offset Axis-asymmetric Cylindrical Mandrel

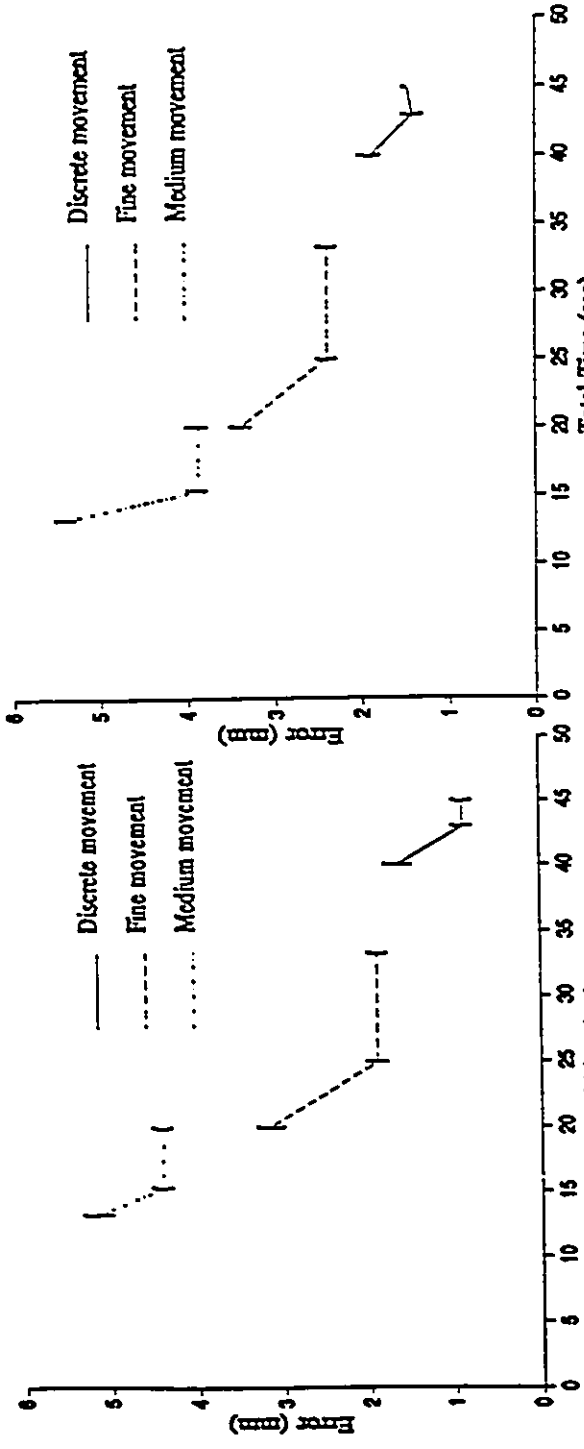

Figure 6.13: Downward and Upward Winding of a 2 Radius Offset Axis-asymmetric Cylindrical Mandrel

There was no significant change between the two geometric configurations in the total time of the movement mode. Since the geometry changes were not very drastic, the total time for the discrete, fine, and medium movement modes did not change by very much.

The comparison of the errors is presented in tabular form (Tables 6.6 and 6.7) in which the values are normalized using the error of the axis-symmetric cylindrical mandrel discrete movement (0.5 mm).

Table 6.6: Results of Downward and Upward Winding of a 1 Radius Axis-asymmetric

Modes	Downward Winding Error (mm)	Normalized to Discrete mode	Upward Winding Error (mm)	Normalized to Discrete Mode
Discrete	2.5	5.0	1.5	3.0
Fine	3.8	7.6	2.0	4.0
Medium	4.0	8.0	2.8	5.6

Table 6.7: Results of Downward and Upward Winding of a 2 Radius Axis-asymmetric

Modes	Downward Winding Error (mm)	Normalized to Discrete mode	Upward Winding Error (mm)	Normalized to Discrete Mode
Discrete	0.8	1.6	1.5	3.0
Fine	2.0	4.0	2.5	5.0
Medium	4.3	8.6	4.0	8.0

Tables 6.6 and 6.7 show that the lowest error is given by the discrete mode, the fine movement mode has a higher error than the discrete mode and the medium has twice the error of the discrete (Figures 6.12). The normalized values of the upward winding direction are generally lower than the downward winding direction. Thus, the normalized values of the upward winding direction are closer to the discrete movement mode than the downward winding direction. The errors of the medium movement mode increases with the change from 1 radius to 2 radii offset in geometry. The discrete and fine movement modes' error both decreased with the change from the first to the second configuration. The error in winding in the upward direction (Figures 6.13) is lower than the downward direction for 1 radius axis-asymmetric mandrel configuration because of the overbalanced robot. This has made the robot easier to move in the upward direction. This reduces the strain on the motors and gives better accuracy. For the 2 radius axis-asymmetric mandrel configuration (Figure 6.13), the error increases in the upward direction as compared to the downward direction. This is due to the large angle to the rotational axis of the mandrel driver. This angle made the mandrel rotate in complex motion and creates a complicated path for the robot to follow. The large angle causes the mandrel to pull the fibre onto its surface, instead of fibres laid down by the robot. This results in error on the placement of the fibres. Another source of error is caused by the robot moving along a complex path. This involves the use of multiple degrees of freedom of the robot to manipulate the payout eye. Therefore, an increase in the number of degrees of freedom increased the sources of error. The error is also magnified with

the errors in the setup and initial conditions. The discrete mode had a better accuracy than fine and medium mode due to the payout eye reaching the desired position and coming to a stop. The other fine and medium modes do not come to a stop at the segment end points.

Therefore, the winding accuracy on an axis-asymmetrical cylindrical mandrel was found to be very high for the discrete movement, but has the longest total time. The accuracy and total time decreases as the movement types change from fine to medium mode. If the product application is of this form and requires high precision fibre placement, the discrete mode should be utilized. If precision is not required, the fine and medium modes can be used to save manufacturing time.

6.10: Axis-asymmetric S-bend Mandrel

This last experiment tested a mandrel composed of previously tested configurations. This mandrel was called an s-bend mandrel due to its shape which resembles the letter s in the alphabet (Figure 6.5a). Downward and upward tests were carried out to determine the accuracy and the total time it takes to complete a winding process. The results are presented in the Figure 6.14.

Again, the two figures show the results of three tests carried out at each speed differ approximately by 0.2 mm for the discrete mode. The fine and medium modes have higher error than the discrete mode. Consequently, when the magnitude of the error increases, the magnitude of the error between each test at each speed proportionally increases. However, the error of the discrete mode is well within the accuracy required by the industry. Therefore, the robotic filament winding cell can reproduce the experimental results using the discrete mode.

The total time of each movement mode in the upward and downward winding directions are very similar. Figure 6.14 shows that the discrete mode had the highest total time of 47.00 seconds, the fine mode had a 20.80 seconds (0.44 times the discrete mode), and the medium mode had a 13.20 seconds (0.28 times the discrete mode). The discrete mode has the highest total time due to the stop at the segment end points. The fine and medium modes had a shorter total time because of the smoothing the corners and smoothing the payout eye path to achieve a higher speed.

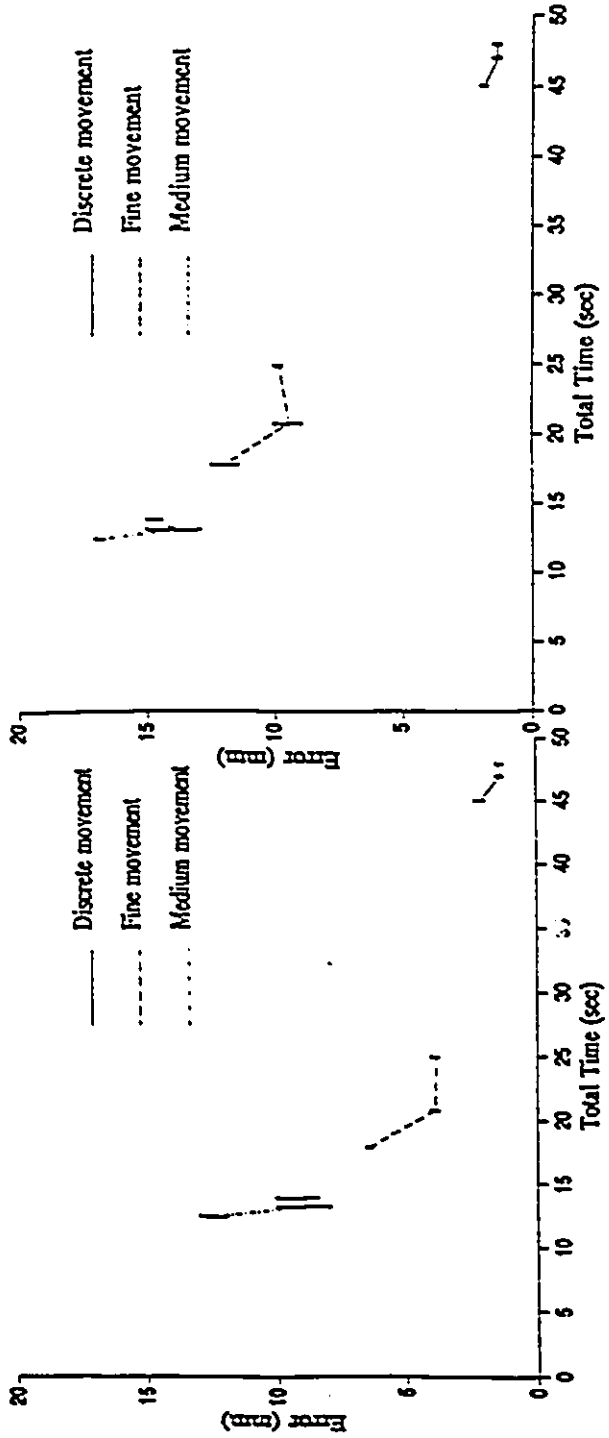

Figure 6.14: Downward and Upward Winding of a S-head Axis-Asymmetrical

Figure 6.14 shows the discrete mode had an error of 1.5 mm and 1.3 mm in the downward and upward winding directions, respectively. The fine mode had a 4.0 mm (2.67 times the discrete mode) and 9.5 mm (7.31 times the discrete mode) in downward and upward winding, respectively. The medium mode had a 8.0 mm (5.33 times the discrete mode) and 14.0 mm (10.76 times the discrete mode) in downward and upward directions, respectively. The accuracy of the discrete mode is higher than the other two modes because the payout eye come to a stop at each segment end points. The fine and medium modes do not stop at the segment end points but cut the corner of the payout eye path and move on the continuous basis. The discrete movement accuracy suffered less in up and down directions. However, the change in winding direction cause the fine and medium movement modes accuracies to suffer greatly. The upward direction gave a higher error than the downward direction because of the drastic change of mandrel geometry in the upward direction. This phenomena is similar to the 2 radius axis-asymmetric mandrel. This geometry changes in the upward direction has a higher angle than the downward direction. As describe in the axis-asymmetrical mandrel configuration, the fibres are tends to be pulled on to the mandrel surface and will effect the up coming winding fibre position. If the geometry changes from a valley to crest in a very short distance, the up coming fibre will be pushed down to the valley. In the case of a crest to a valley geometry change will cause the fibre to be pull into the valley. Also the complex paths made the robot move in very complex motions. Consequently, all the motors of the robot will be in motion. This introduces the error of robot configuration

to the fibre path. The errors of the robot configuration magnified from the base of the robot to the wrist. Since the robot path is approximated with straight line segments, the robot positions will have e.rors. In addition, the accuracy of the winding process is as good as the accuracy of the definition of the mandrel geometry. Since the geometry of the mandrel is found from tracing the mandrel shape, errors are introduced into the calculation of the fibre paths on the mandrel surface.

Therefore, the winding accuracy on a s-bend axis-asymmetrical mandrel was found to be very high for the discrete movement, but has the longest total time. The accuracy and total time decreases as the movement types change from fine to medium movement. If the product application require high precision fibre placement, the discrete movement should be utilized. If precision is not required, the fine movement can be used to save manufacturing time. The medium movement mode accuracy does not come close to the required value of the industry, hence, it should not be used for winding.

6.11: Summary Discussion

In this research four configurations were tested to assess the accuracy and repeatability of the filament winding cell. The first three configurations used the cylindrical mandrel that was positioned on centre (Figure 6.2), offset (Figure 6.3), and angled (Figure 6.4) to the rotation centre of the mandrel drive. The last configuration using the s-bend mandrel (Figure 6.5a), is the combination of the previous three configurations. For each configuration, upward and downward winding directions were tested to examine the effect of the winding direction. Discrete, fine and medium movement modes were used for assessing the movement mode on the accuracy. Three tests were carried out at each speed of the movement mode to check the repeatability of the system.

Figures 6.15 and 6.16 present plots of the errors of the four configurations against the total time for downward and upward winding direction, respectively. They show the plot of transition points, which is the value of the best accuracy with the least amount of total time. The axis-asymmetrical S-bend mandrel results are enclosed with a circle to differentiate them from the other setups.

Generally, the upward winding direction has a lower error than the downward direction. This is shown in the axis-symmetric, offset axis-symmetric, and 1 radius axis-asymmetric mandrel configurations. The opposite is shown in the 2 radius axis-asymmetric and the s-bend mandrel configurations. The large angle or drastic changes in the geometry of the two latter cases caused the fibre to be pull onto the mandrel

surface instead of laid down by the robot. This introduced errors in the placement of fibre onto the mandrel surface.

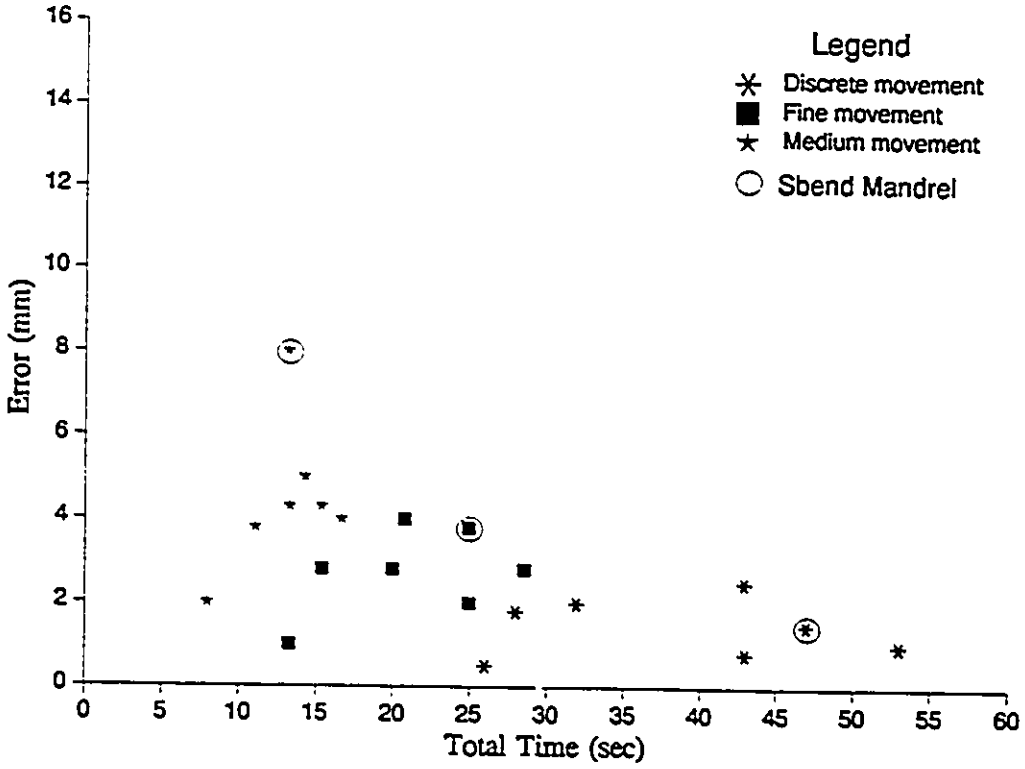

Figure 6.15: Downward Winding Errors of Four Configurations

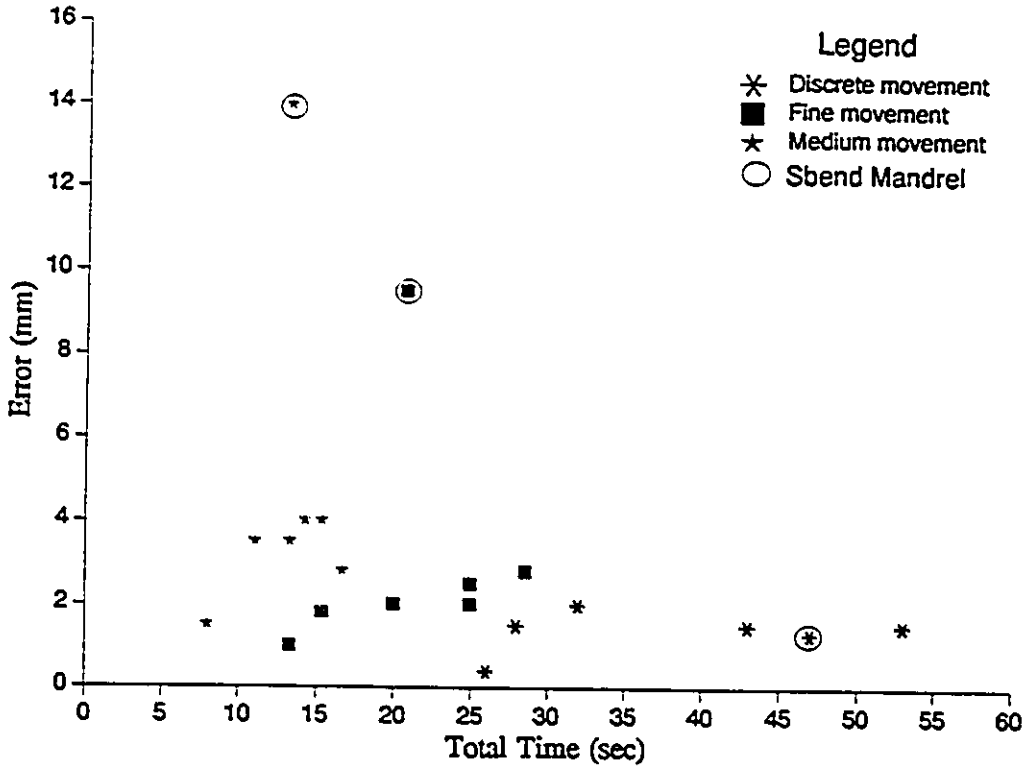

Figure 6.16: Upward Winding Errors of Four configurations

The results of the experiments show that the discrete movement was the most accurate movement mode, the fine mode was the second best, and the worst accuracy was given by the medium movement. The discrete mode results are very close to the x-axis with a low error while the medium mode had the highest error. Therefore, the accuracy of the robotic filament winding cell suffers from the change of movement mode but does not suffer severely from changes in configuration. The only disagreement is for the result of the medium mode of s-bend mandrel. It had approximately two to three times the error of the other configurations medium mode results because of the complex payout path. Hence, the effect of smoothing corner (reducing the distance travelled by the robot) increases.

From the Figures 6.15 and 6.16, the fastest winding is achieved by the medium movement type while the second fastest is for the fine movement. The slowest winding is given by the discrete movement. As the geometry changes, from a simple to complex shape, the total time increases. The wide spread of the discrete mode results in the Figures 6.15 and 6.16 show that the total time of discrete movement type is most affected by the change in geometry. Geometry changes affected the total time of fine movement; however, the effect is less than the discrete movement. The total time of the medium movement mode does not spread very much, hence, it is not very sensitive to changes in configurations. However, the medium movement total time is only slightly effected.

The results show that the axis-symmetrical cylindrical mandrel setup gives the best accuracy and longest total time. As the configurations change from a simple to a complex

shape, the error of winding and the total time increases. The worst winding inaccuracy and shortest total time was found in the winding of the s-bend mandrel using the medium mode.

The s-bend mandrel is made up of the combination of other three tested configurations. Therefore, it is fitting to see how the magnitude of error on the s-bend mandrel related to the other three configuration errors. This comparison will be done through the discrete movement mode. The geometry of the s-bend mandrel can be divided into 5 cylindrical sections (Figure 6.17). The first, third and fifth section are similar to the axis-asymmetric cylindrical mandrel while the second and fourth sections resemble the offset axis-symmetric mandrel. The errors of each section for different movement types are listed in the Table 6.8.

Table 6.8: Maximum Error Recorded at Each S-bend Mandrel Sections

Section Number	Discrete Mode	Discrete Mode	Fine Mode	Fine Mode	Medium Mode	Medium Mode
	Down (mm)	Up (mm)	Down (mm)	Up (mm)	Down (mm)	Up (mm)
1	1.5	1.5	1.3	1.5	1.8	1.3
2	1.5	1.5	2.8	3.8	3.5	4.8
3	1.8	2.0	3.0	10.0	8.5	15.0
4	1.5	1.5	4.0	5.5	10.0	6.0
5	1.3	1.3	1.3	1.5	1.3	1.5

Table 6.8 shows the section 3 has the highest error and section 4 has the second highest error. These results are due to the highest error found in the cross-sectional dimension of the mandrel at the third and fourth sections. The cross-sectional dimensions are listed in the Appendix C. Other contributing sources of error are discussed in the Section 6.10.

The results show that for the discrete mode, the experimental path on the first section, axis-asymmetric cylindrical mandrel, had a maximum deviation of 1.5 mm from the desired path. The angle of the first section is less than the tested angle of 1 radius offset angle. This magnitude of error is similar to the error of 2.5 mm from 1 radius offset axis-asymmetric mandrel. The difference of 0.5 mm is quite small. The second section, offset axis-symmetric cylindrical mandrel, had an error of 1.5 mm. This section has a less offset than the 1 radius offset axis-symmetric cylindrical mandrel that is tested. The error of a 1 radius offset axis-symmetric cylindrical mandrel tested had an error of 1.8 mm. These two errors values are very close to each other with the difference of 0.3 mm. The difference is within the accuracy that is required by the industry. Therefore, the error on the s-bend mandrel can be predicted, but due to the other sources error (Section 6.2) the magnitude of the error for the s-bend mandrel can be higher. Finally, the results for the s-bend mandrel are surprisingly good considering the large variation in mandrel diameter (Section 6.4).

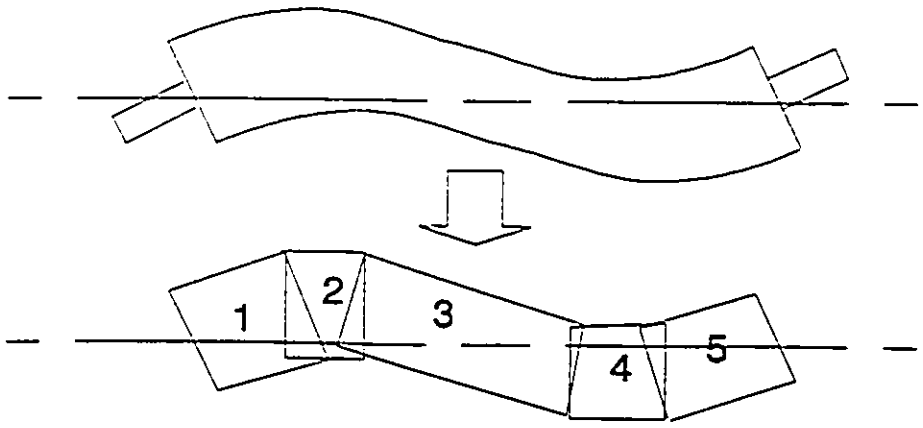

Figure 6.17: Decomposition of the S-bend Mandrel to Basic Geometry

CHAPTER 7

CONCLUSIONS AND RECOMMENDATIONS

This research shows that all the objectives of the research were accomplished. The complete controller software and hardware were established. The payout eye position program is written. They were tested on both simple cylindrical and the complex shape of the s-bend mandrel.

The accuracy and the repeatability of the robotic filament winding is high. The discrete movement gives the best accuracy and second is the fine movement. The worst accuracy is the medium movement. In discrete movement, geometry of the mandrel does not affect the accuracy. The higher the complexity in the mandrel shape resulted in larger errors for the fine and medium movement modes.

The cylindrical mandrel can use discrete and fine movement modes for accurate winding. For complex shapes the discrete movement is recommended. The medium movement should be used for very simple shape mandrel cases with no complicated motions for the payout eye to track.

Tension and slack in the fibre does affect the accuracy in the placement of the fibres. However, without these factors under control, the results are very reasonable. The accuracy can be increased by having the tensioner to give constant tension and slack

control device to remove any slack in the fibre.

Another recommendation is to produce a feedback system between the robot and mandrel to keep them synchronized. This will remove most of the error from the filament winding. Also the out of the scope sources of error (Section 6.2) can be examined and possibly evaluated to reduce the error from the winding process. The easiest error to correct would be the inaccuracy caused by the low number of steps of the stepper motor.

It has been shown that controlling the robot through the manufacturer supplied robot controller introduced some limitations and sources of error. Bypassing the existing controller and controlling the robot using a customize controller which will oversee the robot servo motors will decrease the error.

Therefore, the research reveals that the existing off the shelf ASEA industrial robot can be used in the filament winding of complex mandrels with reasonable accuracy.

REFERENCES

[1] James V. Kelly, "A Method for Computer Generated Paths for Off-Line Programming of Filament Winding Patterns", 32nd International SAMPE Symposium, April 6-9, 1987. pp. 974-973.

[2] Brian A. Wilson, "Filament Winding - Past, Present, and Future", 34th International SAMPE Symposium, May 8-11, 1989. pp. 2429-2439.

[3] William D. Callister, Jr., "Materials Science and Engineering", John Wiley and Sons, Inc., New York, New York, 1985.

[4] E. Kafrissen, M. Flephanf, "Industrial Robot and Robotics", Princeton Hall Publishing, Reston, Virginia, USA, 1984.

[5] Phillip John Mckerrow, "Introduction to Robotics", Addison-Wesley Publishing Company, New York, New York, 1991.

[6] J. Scholliers, H. Van Brussel, G. Van de Bruaene, "Robotic Filament Winding of Asymmetric Parts", Society of Manufacturing Engineers, 1990. Paper No. EM90-662.

[7] E. Bernard, "Path Generation for Filament Winding of Asymmetric Fibre Composite Components", Master Thesis, University of Ottawa, Ottawa, Canada, 1992.

[8] V. Middleton, K. W. Young, D. G. Elliman and M. J. Owen, "Software for Filament Winding", First International Automated Composites, The Plastics and Rubber Institute, Nottingham, England, 1986. pp. 9/1-9/6.

[9] G. M. Wells and G. C. Eckold, "Computer Aided Design and Manufacture of Filament Wound Composite Structures", First International on Automated Composites, The Plastics and Rubber Institute, Nottingham, England, 1986. pp. 6/1-6/16.

[10] M. Munro, "Review of Manufacturing of Fibre Composite Components by Filament Winding", Polymer Composites, Vol. 9, No. 5, october 1988. pp. 352-359.

[11] D. E. Shaw Stewart, "Integrated Modwind Systems", First International on Automated Composites, The Plastics and Rubber Institute, Nottingham, England, 1986. pp. 8/1-8/14.

[12] V. Middleton, M. J. Owen, D. G. Elliman and M. Shearing, "Developments in Non-Axisymmetric Filament Winding", Second International Automated Composites, The Plastics and Rubber Institute, Noordwijkerhout, Netherlands, 1988. pp. 10/1-10/15.

[13] Freddy Y. C. Boey, "Simple Automated Continuous Filament Winding System for Fibre Reinforced Composites", Polymer Testing, Vol. 9, 1990. pp. 45-52.

[14] S. Kurt Olofsson, Peter Gudmundson, L. Anders Strombeck, "Process Simulation of Wet Filament Winding and Curing of Thick-Walled Cylinders", 37th International SAMPE Symposium, March 9-12, 1992. pp. 1132-1145.

[15] Kenneth B. Bubeck, "Robotic Winding: Continuous Fibres in Complex shapes", Composites in Manufacturing, Fall 1987. pp. 2-4.

[16] Sanjeev Seereeam and John Ting-Yung Wen, "An All-Geodesic Algorithm for Filament Winding of a T-Shaped Form", IEEE Transactions on Industrial Electronics, Vol. 18, No. 6, December 1991. pp. 484-490.

[17] Joachim Hummler, Sang Kwan Lee, and Karl V. Steiner, "Recent Advances in Thermoplastic Robotic Filament Winding", 36th International SAMPE Symposium, April 15-18, 1991. pp. 2142-2156.

[18] W. Braun, "A Control System for Filament Winding Equipment as a Prerequisite for Automation", First International Automated Composites, The Plastics and Rubber Institute, Nottingham, England, 1986. pp. 11/1-11/11.

[19] E. Bernard, "Fibre Composite Pressure Vessel Winding Using a Robotic Arm", University of Ottawa, 1986.

[20] ASEA Service Manual, CK 09-1501E, January, 1984.

[21] S. K. Chan, "Robot Control Communication Software", Bachelor of Applied Science Thesis, University of Ottawa, Mechanical Engineering Department, Ottawa, Ontario, Canada, 1992.

[22] S. K. Chan, "Codes to Convert RCCS Data Files to Robot's Data Format", Internal report, University of Ottawa. 1992.

[23] Granino A. Korn, "Mathematical Handbook for Scientists and Engineers", McGraw-Hill Book Company, New York, New York, 1968.

[24] S. T. Peters, W. D. Humpherey, R. F. Foral, "Filament Winding: Composite structure Fabrication", SAMPE Publication, 1991.

[25] Yoram Koren, "Robotics for Engineers", McGraw-Hill Book Company, New York, New York, 1991. pp. 117-125.

[26] ASEA Programming Manual, CK 09-1401E, June, 1984.

[27] Roger A. Ford, "Automated Fibre Orientation for Advanced Composites A Novel Approach to Continuous Processing", First International on Automated Composites, The Plastics and Rubber Institute, Nottingham, England, 1986. pp. 4/1-4/7.

[28] Hechmi Hamouda, Tae J. Kang and Aly El-Shiekh, "On the Mechanics of Filament Winding Part 1: A Generalized Model", 34th International SAMPE Symposium, May 8-11, 1989. pp. 1130-1142.

[29] Randall J. Philopt, Daniel K. Buckmiller, James E. Colegrove, "Design and Manufacturing of High Performance Recreational Product Via Filament Winding", 34th International SAMPE Symposium, May 8-11, 1989. pp. 2217-2228.

[30] Jack C. Vogt, "A Workstation for Off-Line Filament Winding Pattern Generation", 34th International SAMPE Symposium, May 8-11, 1989. pp. 1538-1544.

[31] Karl V. Steiner, "Development of a Robotic Filament Winding Workstation for Complex Geometries", 35th International SAMPE Symposium, April 2-5, 1990. pp. 757-766.

[32] Timothy S. Miller, Christopher J. Fortin, "Fabrication of Low Cost Composite Tooling for Filament Winding Large Structures", 37th International SAMPE Symposium, March 9-12, 1992. pp. 1160-1169.

[33] Randall J. Philpot, Daniel K. Buckmiller and David W. Erickson, "Commercial and Recreational Applications, Filament Wound Composites", 38th International SAMPE Symposium, May 10-13, 1993. pp. 320-333.

[34] Klaus D. Felderhoff, Karl V. Steiner, "A New Compact Robotic Head for Thermoplastic Fibre Placement", 38th International SAMPE Symposium, May 10-13, 1993. pp. 138-151.

[35] Shaiq A. Haq, "B-Spline Interpolation Improves Filament Winding Controller's Performance", 38th International SAMPE Symposium, May 10-13, 1993. pp. 163-169.

[36] Laurel M. Sheppard, "The Revolution of Filament Winding", Advance Materials and Process inc. Metal Progress, Vol. 7, 1987. pp. 31-41.

[37] D. G. Elliman, P. Sorenti, L. Brown, M. Shearing, V. Middleton, and M. J. Owen, "A Cell for the Manufacture of Composite Components by Filament Winding", Advance Manufacturing Engineering, Vol. 1, October 1988. pp. 15-20.

[38] E. Bernard, A. fahim, and M. Munro, "A CAD/CAM Approach to Robotic Filament Winding", University of Ottawa, 1991.

[39] C. L. Ma and Z. Q. Yang, "The Study on the Combination of CAD with CAM of Filament Wound Pressure Vessels and Pipes", First International Automated Composites, The Plastics and Rubber Institute, Nottingham, England, 1986. pp. 16/1-16/7.

[40] Jeffery A. Ziegel, Timothy J. Sevener, "Filament Winding's Succession to Fibre Placement", Society of Manufacturing Engineers, 1989. Paper No. AD89-581.

[41] John Raymer, "Flexibility of the Filament Winding Process Improved Through a User-Friendly Interface", Society of Manufacturing Engineers, 1987. Paper No. MS87-127.

[42] Jeffery A. Ziegel, "Developing a Filament Winding Manufacturing Cell", Society of Manufacturing Engineers, 1990. Paper No. AD90-288.

[43] Brian E. Spencer, "Tooling Considerations for the Filament Winding Process", Society of Manufacturing Engineers, 1988. Paper No. MS88-800.

[44] Don O. Evans, "Robotic Seven Access Filament Winding", Manufacturing Engineered and Technologist, august 23-25, 1988.

[45] S. K. Mazumdar and S. V. Hoa, "On the Kinematics of Filament Winding on Non-Axisymmetric Cylindrical Mandrel. Part I. A Generalized Model", 34th International SAMPE Symposium, May 8-11, 1989. pp. 1130.

[46] S. K. Mazumdar and S. V. Hoa, "On the Kinematics of Filament Winding on Non-Axisymmetric Cylindrical Mandrel. Part II. For Convex Polygonal Cross-section", 34th International SAMPE Symposium, May 8-11, 1989.

[47] Yocan Koren, "Robotic for Engineers", McGraw Hill, New York, New York, 1985.

[48] P. Sinrken, H. Van Brussel, S. Serrien, S. Bryon, "Generating Off-line Robot Programs with Geometrical Data from a CAD-database", 18th International Symposium on Industrial Robot, Lausanne, Switzerland, 26-28 April, 1988.

[49] G. Menges, E. Neise, "Use of Industrial Robots for Filament Winding", 40th Annual Conference, Reinforced Plastics/Composite Institutes, SPI, Jan. 28-Feb. 1, 1985.

[50] G. Menges, M. Effing, "CADFIBER - A Software Tool for Composite Engineering", Second International Automated Composites, The Plastics and Rubber Institute, Noordwijkerhout, Netherlands, 1988. pp. 11/1-11/21.

[51] K. K. Chawla, "Composite Materials", Springer-Verlag, New york, New York, 1987. pp. 30.

[52] James H. Campbell and Jeff L. Kittelson, "Winding the Tape", Aerospace Composites and Materials, Volume 3, Number 6, Nov.-Dec. 1991. pp. 21-25.

[53] G. S. Bolmsjō, "Programming Robot Systems for Arc Welding in Small Series Production", Robotic and Computer-Integrated Manufacturing, Volume 5, No. 2/3, pp. 199-205, 1989.

[54] Glenford J. Myers, "Software Reliability, Principles and Practices", A Wiley-Interscience Publication, New York, New York, 1976.

[55] Funsho Ajibade, "Successful Marriage of Textiles and Composite Technology", Second International Automated Composites, The Plastics and Rubber Institute, Noordwijkerhout, Netherlands, 1988. pp. 2/1-2/13.

[56] K. W. Kirberg, W. Michaeli, G. Menges, A. Seifert, "Process Simulation in Filament Winding - New Insights Show the Way to Cost Effective Component Development", Second International Automated Composites, The Plastics and Rubber Institute, Noordwijkerhout, Netherlands, 1988. pp. 16/1-16/15.

[57] D. G. Lloyd-Thomas, G. C. Eckold and G. M. Wells, "Asymmetric Filament Winding", Second International Automated Composites, The Plastics and Rubber Institute, Noordwijkerhout, Netherlands, 1988. pp. 12/1-12/12.

APPENDICES

APPENDIX A

Quaternion Wrist Coordinate

The orientation of the wrist is given in quaternion. The quaternion is based on the Euler's theorem which states that a displacement of a rigid body with one fixed point can be described as a rotation about some axis. Quaternion is a four elements vector, Equation A.1, three of which are components of a spatial vector and define the direction of the common rotation axis, and the fourth component provides information about rotation angle [25].

$$q = q_0 + \hat{q} = \cos(\frac{\theta}{2.0}) + \hat{e}\sin(\frac{\theta}{2.0}) \qquad (A.1)$$

where

q_0=scalar

$$\hat{q} = q_1\hat{i} + q_2\hat{j} + q_3\hat{k}$$

$\hat{e}$ = unit vector

θ = $\angle$ of Rotation

The wrist of the robot has only the pitch and roll degree of freedoms. This requires two successive rotations, which are describe by two quaternions g and g' (Figure A.1), to be represented as a single rotation describe by one quaternion. Each of the quaternioins g and g' in the Equation A.2 is resolved in its local coordinate system in which the rotation is taking place. In the Figure A.1, the vector undergoes two successive rotations. The first is defined by the quaternion g, rotates the vector and a reference coordinate system O' attach to the vector through an angle of 90 degrees about Z axis, and creates the new vector. The second quaternion g', in the O' frame, rotates the new vector and a frame O'' attached to it through 90 degree about X' axis into the final position. The following Equation A.2 can be used to find the components of the vector at its final position.

$$q = g * g' = (g_0, \hat{g}) (g_0', \hat{g}') \tag{A.2}$$

$$q = (g_0 g_0' - \hat{g} \cdot \hat{g}', g_0 \hat{g}' + g_0' \hat{g} + \hat{g} \times \hat{g}') \tag{A.3}$$

where

g = first rotation

g' = second rotation

g_0 = first rotation(Scalar)

$\hat{g}$ = first rotation(Vector)

g_0' = second rotation(scalar)

$\hat{g}'$ = second rotation(Vector)

Since there are only pitch and roll degree of freedom in the wrist (Figure A.2), the following set of equations are derived for the robot.

The first rotation, pitch degree of freedom, about the Y axis gives the scalar component (Equation A.1) as follow:

$$g_0 = \cos(\frac{\theta}{2.0}) \qquad (A.4)$$

Since the rotation is about Y axis (Figure A.1), the unit vector in the Equation A.1 will equal to [0,1,0]. This gives the following 3D space vector components.

$$g_x = 0.0 \qquad (A.5)$$

$$g_y = \sin(\frac{\theta}{2.0}) \tag{A.6}$$

$$g_z = 0.0 \tag{A.7}$$

The second rotation, roll degree of freedom, about the X axis gives a scalar component as follow:

$$g_0' = \cos(\frac{\Phi}{2.0}) \tag{A.8}$$

Since the rotation is about X axis (Figure A.1), the unit vector in the Equation D.1 will equal to [1,0,0]. This gives the following 3D space vector components.

$$g_x' = \sin(\frac{\Phi}{2.0}) \tag{A.9}$$

$$g_y' = 0.0 \tag{A.10}$$

$$g_z' = 0.0 \tag{A.11}$$

The final result of two consecutive rotations about Y axis and then X axis gives

the following result.

$$\therefore q = (g_0 g_0', g_0 g_x' + g_y g_0' - g_y g_x') \tag{A.12}$$

Therefore, scalar component of the quaternion coordinate is given as:

$$Q1 = g_0 g_0' \tag{A.13}$$

The first vector component is:

$$Q2 = g_0 g_x' \tag{A.14}$$

The second vector component is:

$$Q3 = g_y g_0' \tag{A.15}$$

The third vector component is:

$$Q4 = - g_y g_x' \tag{A.16}$$

The symbols in the above equations represent for the following:

θ = ∠ Rotation (Y axis)

Φ = ∠ Rotation (X axis)

Q1 - Q4 = Components of Robot

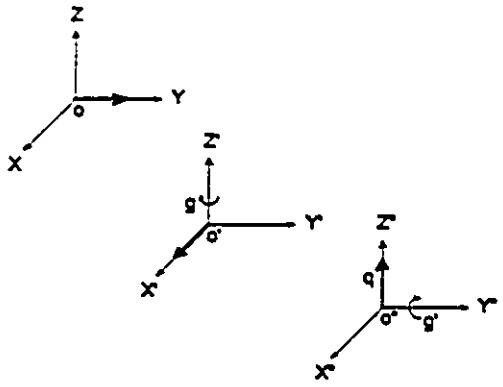

Figure A.1: Two Consecutive Rotations Quaternion

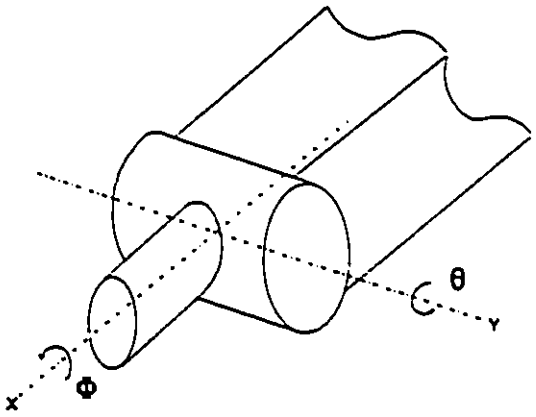

Figure A.2: Wrist in Quaternion Definition

APPENDIX B

Experiment Results Tables

Table 1: Axis-Symmetric Cylindrical Mandrel (Downward)

Movement Type		Error (mm)			Mandrel Speed (rev/sec)	Total Time (sec)
		1	2	3		
Discrete	v1	0.5	0.5	0.3	1.00	28.00
	v2	0.5	0.5	0.3	2.00	26.00
	v3	0.8	1.0	0.8	3.00	25.00
Fine	v1	0.9	0.8	1.0	0.10	20.00
	v2	1.0	1.0	0.8	0.15	13.30
	v3	2.0	1.5	1.8	0.20	10.00
Medium	v1	2.0	2.0	1.8	0.20	10.00
	v2	2.0	2.0	1.8	0.25	8.00
	v3	3.0	3.5	3.5	0.30	6.70

Table 2: Axis-Symmetric Cylindrical Mandrel (Upward)

Movement Type		Error (mm)			Mandrel Speed (rev/sec)	Total Time (sec)
		1	2	3		
Discrete	v1	0.3	0.5	0.5	1.00	28.00
	v2	0.5	0.4	0.4	2.00	26.00
	v3	0.8	0.8	0.8	3.00	25.00
Fine	v1	1.0	0.8	0.8	0.10	20.00
	v2	1.0	1.0	1.0	0.15	13.30
	v3	1.5	2.0	1.8	0.20	10.00
Medium	v1	1.5	1.3	1.3	0.20	10.00
	v2	1.5	1.5	1.3	0.25	8.00
	v3	2.5	3.0	2.0	0.30	6.70

Table 3: Offset Axis-Symmetric Cylindrical Mandrel (Downward)(1 Radius Offset)

Movement Type		Error (mm)			Mandrel Speed (rev/sec)	Total Time (sec)
		1	2	3		
Discrete	v1	2.0	2.0	1.9	1.00	29.00
	v2	2.0	1.8	1.8	2.00	28.00
	v3	2.3	2.5	2.3	3.00	26.00
Fine	v1	2.9	3.0	2.8	0.10	20.00
	v2	3.0	2.8	2.8	0.13	15.40
	v3	4.0	3.3	3.3	0.15	13.30
Medium	v1	4.0	3.8	4.0	0.16	12.50
	v2	3.8	4.0	3.8	0.18	11.10
	v3	5.0	5.5	5.3	0.20	10.00

Table 4: Offset Axis-Symmetric Cylindrical Mandrel (Upward)(1 Radius Offset)

Movement Type		Error (mm)			Mandrel Speed (rev/sec)	Total Time (sec)
		1	2	3		
Discrete	v1	1.3	1.3	1.5	1.00	29.00
	v2	1.5	1.5	1.3	2.00	28.00
	v3	1.8	2.0	2.3	3.00	26.00
Fine	v1	2.0	1.8	1.8	0.10	20.00
	v2	1.8	2.0	1.8	0.13	15.40
	v3	3.0	3.5	3.3	0.15	13.30
Medium	v1	3.0	3.5	3.3	0.16	12.50
	v2	3.5	3.5	3.5	0.18	11.10
	v3	4.0	4.0	4.5	0.20	10.00

Table 5: Offset Axis-Symmetric Cylindrical Mandrel (Downward)(2 Radius Offset)

Movement Type		Error (mm)			Mandrel Speed (rev/sec)	Total Time (sec)
		1	2	3		
Discrete	v1	2.0	1.8	1.8	1.00	35.00
	v2	2.0	2.0	1.8	2.00	32.00
	v3	2.3	2.3	2.0	3.00	30.00
Fine	v1	2.5	3.0	2.5	0.08	25.00
	v2	3.0	2.8	2.8	0.10	20.00
	v3	3.5	4.0	3.8	0.12	16.70
Medium	v1	4.5	4.0	4.3	0.12	16.70
	v2	4.5	4.3	4.0	0.15	13.30
	v3	5.0	5.3	5.3	0.17	11.80

Table 6: Offset Axis-Symmetric Cylindrical Mandrel (Upward)(2 Radius Offset)

Movement Type		Error (mm)			Mandrel Speed (rev/sec)	Total Time (sec)
		1	2	3		
Discrete	v1	2.0	1.8	1.8	1.00	35.00
	v2	1.8	2.0	2.0	2.00	32.00
	v3	2.3	2.5	2.3	3.00	30.00
Fine	v1	2.0	1.8	2.0	0.08	25.00
	v2	2.0	2.0	1.8	0.10	20.00
	v3	3.3	3.3	3.0	0.12	16.70
Medium	v1	3.5	3.3	3.0	0.12	16.70
	v2	3.5	3.5	3.3	0.15	13.30
	v3	4.3	4.5	4.0	0.17	11.80

Table 7: Offset Axis-Symmetric Cylindrical Mandrel (Downward)(3 Radius Offset)

Movement Type		Error (mm)			Mandrel Speed (rev/sec)	Total Time (sec)
		1	2	3		
Discrete	v1	1.0	0.8	0.8	1.00	54.00
	v2	1.0	0.8	1.0	2.00	53.00
	v3	1.8	1.5	1.5	3.00	50.00
Fine	v1	3.0	2.8	2.5	0.05	40.00
	v2	2.8	3.0	2.8	0.07	28.60
	v3	4.5	4.3	4.0	0.09	22.20
Medium	v1	5.0	4.8	4.8	0.12	16.70
	v2	5.0	5.0	4.8	0.14	14.30
	v3	6.0	6.3	6.0	0.16	12.50

Table 8: Offset Axis-Symmetric Cylindrical Mandrel (Upward)(3 Radius Offset)

Movement Type		Error (mm)			Mandrel Speed (rev/sec)	Total Time (sec)
		1	2	3		
Discrete	v1	1.5	1.5	1.3	1.00	54.00
	v2	1.3	1.5	1.5	2.00	53.00
	v3	1.8	2.0	2.0	3.00	50.00
Fine	v1	2.8	3.0	2.8	0.05	40.00
	v2	3.0	2.8	2.8	0.07	28.60
	v3	4.0	4.3	4.0	0.09	22.20
Medium	v1	4.0	4.0	3.8	0.12	16.70
	v2	4.0	3.8	4.0	0.14	14.30
	v3	5.0	5.5	5.3	0.16	12.50

Table 9: Axis-Asymmetric Cylindrical Mandrel (Downward)(1 Radius Offset)

Movement Type		Error (mm)			Mandrel Speed (rev/sec)	Total Time (sec)
		1	2	3		
Discrete	v1	2.5	2.3	2.3	1.00	45.00
	v2	2.5	2.5	2.3	2.00	43.00
	v3	2.8	3.0	3.0	3.00	40.00
Fine	v1	4.0	3.8	4.0	0.06	33.30
	v2	3.8	4.0	3.8	0.08	25.00
	v3	4.8	4.8	4.5	0.10	20.00
Medium	v1	3.8	4.0	3.8	0.10	20.00
	v2	4.0	4.0	3.8	0.12	16.70
	v3	5.3	5.5	5.3	0.14	14.30

Table 10: Axis-Asymmetric Cylindrical Mandrel (Upward)(1 Radius Offset)

Movement Type		Error (mm)			Mandrel Speed (rev/sec)	Total Time (sec)
		1	2	3		
Discrete	v1	1.5	1.3	1.3	1.00	45.00
	v2	1.5	1.5	1.3	2.00	43.00
	v3	2.3	2.0	2.0	3.00	40.00
Fine	v1	2.0	1.8	1.8	0.06	33.30
	v2	2.0	2.0	1.8	0.08	25.00
	v3	3.0	2.8	3.0	0.10	20.00
Medium	v1	2.8	3.0	2.8	0.10	20.00
	v2	3.0	2.8	2.8	0.12	16.70
	v3	4.3	4.5	4.0	0.14	14.30

Table 11: Axis-Asymmetric Cylindrical Mandrel (Downward)(2 Radius Offset)

Movement Type		Error (mm)			Mandrel Speed (rev/sec)	Total Time (sec)
		1	2	3		
Discrete	v1	0.8	0.8	1.0	1.00	45.00
	v2	0.8	1.0	0.8	2.00	43.00
	v3	1.5	1.8	1.5	3.00	40.00
Fine	v1	1.8	2.0	1.8	0.06	33.30
	v2	2.0	2.0	1.8	0.08	25.00
	v3	3.3	3.3	3.0	0.10	20.00
Medium	v1	4.3	4.5	4.3	0.10	20.00
	v2	4.5	4.3	4.3	0.13	15.40
	v3	5.3	5.0	5.0	0.15	13.30

Table 12: Axis-Asymmetric Cylindrical Mandrel (Upward)(2 Radius Offset)

Movement Type		Error (mm)			Mandrel Speed (rev/sec)	Total Time (sec)
		1	2	3		
Discrete	v1	1.5	1.5	1.5	1.00	45.00
	v2	1.5	1.5	1.3	2.00	43.00
	v3	2.0	2.0	1.8	3.00	40.00
Fine	v1	2.5	2.5	2.3	0.06	33.30
	v2	2.5	2.3	2.5	0.08	25.00
	v3	3.3	3.5	3.3	0.10	20.00
Medium	v1	4.0	3.8	3.8	0.10	20.00
	v2	3.8	4.0	4.0	0.13	15.40
	v3	5.5	5.3	5.3	0.15	13.30

Table 13: Axis-Asymmetric S-bend Mandrel (Downward)

Movement Type		Error (mm)			Mandrel Speed (rev/sec)	Total Time (sec)
		1	2	3		
Discrete	v1	1.5	1.3	1.3	1.00	48.00
	v2	1.5	1.5	1.3	2.00	47.00
	v3	2.0	2.3	2.0	3.00	45.00
Fine	v1	4.0	4.0	3.8	0.10	25.00
	v2	4.0	4.0	3.8	0.12	20.80
	v3	6.5	6.5	6.3	0.14	17.90
Medium	v1	8.5	10.0	10.0	0.18	13.90
	v2	10.0	8.0	8.0	0.19	13.20
	v3	12.5	13.0	12.0	0.20	12.50

Table 14: Axis-Asymmetric S-bend Mandrel (Upward)

Movement Type		Error (mm)			Mandrel Speed (rev/sec)	Total Time (sec)
		1	2	3		
Discrete	v1	1.3	1.5	1.3	1.00	48.00
	v2	1.3	1.5	1.3	2.00	47.00
	v3	2.0	1.8	1.8	3.00	45.00
Fine	v1	10.0	9.8	10.0	0.10	25.00
	v2	10.0	9.0	9.5	0.12	20.80
	v3	12.5	12.0	11.5	0.14	17.90
Medium	v1	14.5	15.0	14.8	0.18	13.90
	v2	15.0	14.0	13.0	0.19	13.20
	v3	16.8	17.0	17.0	0.20	12.50

APPENDIX C

S-bend Mandrel Cross-sectional Dimensions

The s-bend mandrel cross-sectional dimension are listed in the following table.

Position	X-axis	Normalized to smallest dimension	Y-axis	Normalized to smallest dimension
0	57.63	1.008	57.35	1.009
10	58.20	1.018	57.34	1.009
20	58.29	1.020	57.16	1.006
30	58.04	1.015	57.08	1.004
40	58.02	1.015	57.44	1.004
50	57.90	1.013	57.15	1.011
60	57.96	1.014	56.94	1.005
70	57.92	1.013	56.95	1.002
80	58.00	1.015	57.07	1.002
90	57.97	1.014	57.44	1.004
100	57.87	1.013	57.61	1.011
110	57.65	1.009	57.60	1.014
120	57.13	1.000	57.61	1.013
130	57.41	1.005	57.88	1.013
140	57.55	1.007	58.01	1.018
150	57.41	1.005	57.79	1.021
160	57.70	1.009	57.59	1.017
170	57.60	1.009	57.75	1.017
180	57.65	1.008	57.76	1.016
190	57.74	1.010	57.28	1.008
200	57.76	1.017	57.32	1.008
210	58.12	1.016	57.40	1.009
220	58.06	1.013	57.40	1.009
230	57.88	1.020	57.14	1.005
240	58.29	1.019	56.84	1.000
250	58.22	1.019	56.84	1.000
260	58.26	1.022	57.10	1.004
270	58.39	1.009	57.62	1.013
280	57.66	1.007	58.12	1.022
290	57.33	1.009	58.24	1.025
300	57.62	1.022	58.87	1.036
310	58.41	1.042	58.24	1.024
320	59.52	1.009	58.87	1.036
330	57.62	1.008	58.60	1.031
340	57.63	1.009	58.50	1.029
350	57.50	1.006	57.80	1.017

APPENDIX D

Signal Processor

Signal Processor Between Robot and Mandrel Drive Unit

The robot is operated by the robot computer. The mandrel is controlled by the indexer card in the personal computer. Since the robot and mandrel do not sense each other, there is no feedback and, they need to be synchronized. After they are synchronized, they run in an open loop configuration. Thus, the emphasis is needed in the synchronization of the robot with the mandrel.

Currently the robot program contains instructions to signal the personal computer that the robot is in position to start the winding process and have the mandrel drive in according position. When the drive is in position, the personal computer will send a signal to robot computer and the mandrel driver simultaneously to begin the winding.

The signals from the robot computer to personal computer are sent through the output signal line from the robot computer to the parallel port of the personal computer. The parallel port is use because the existing two serial ports are occupied. Robot uses a 24-volt signal. The personal computer has a 5-volt logic circuit. The difference in the voltage must be eliminated. This is achieved by using a buffer made up of opto-isolators. Opto-isolator, similar to electronic relay, takes the signal and connect the other side contacts depending on the high or low input signal.

There are two opto-isolators used in the hardware (Figure D.1). One is for the input signal and the other for the output signal. There are two LEDs to indicate if the input or output line is under operation.

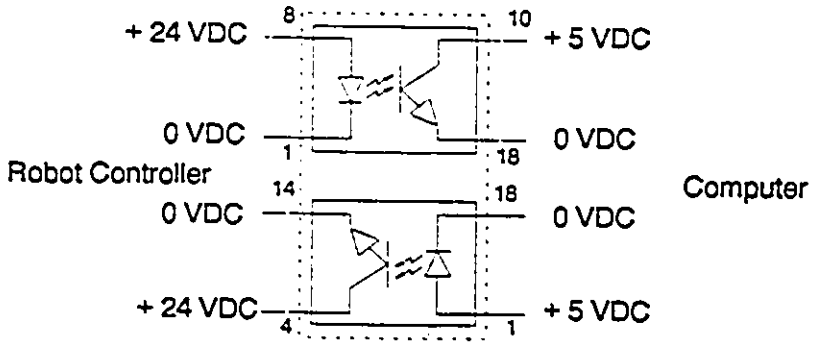

Figure D.1: Synchronization with Opto-Isolators

The above figure shows the arrangement of opto-isolators to prevent the different magnitude of voltage from crossing in the synchronizer. The setup consists of four connections for the robot controller and the same for the personal computer. Robot controller uses connection number 8 as the sender and 4 as the receiver. Connections 1 and 14 are used as ground. The connection numbers are corresponding to the robot controller's terminal unit D14.153 connection. The personal computer uses connection number 1 as sender and 10 as receiver. Connection number 18 is used as a ground. These connections numbers are corresponding to the parallel port's pin number of the personal computer.